QUANTUM DOT-FLUORESCENT PROTEIN PAIRS AS FLUORESCENCE RESONANCE ENERGY TRANSFER PROBES

A Dissertation
Presented to
The Academic Faculty

By

Allison Marie Dennis

In Partial Fulfillment
Of the Requirements for the Degree
Doctor of Philosophy in Bioengineering

Georgia Institute of Technology
December 2009

QUANTUM DOT-FLUORESCENT PROTEIN PAIRS AS FLUORESCENCE RESONANCE ENERGY TRANSFER PROBES

Approved by:

Dr. Gang Bao, Advisor
College of Engineering
Georgia Institute of Technology

Dr. Valeria Milam
College of Engineering
Georgia Institute of Technology

Dr. Shuming Nie
College of Engineering
Georgia Institute of Technology

Dr. Philip Santangelo
College of Engineering
Georgia Institute of Technology

Dr. James Powers
College of Sciences
Georgia Institute of Technology

Date Approved: September 16, 2009

ACKNOWLEDGEMENTS

First and foremost, I would like to gratefully acknowledge my advisor, Dr. Gang Bao. The confidence that he has expressed in me and the independence that he has fostered has made me a much more confident and competent researcher than I could have imagined otherwise. His support of me both in lab and in life has given me a secure environment in which I could thrive. His career advice will be a constant guide for me as I continue to make decisions about my future in science. I would also like to express my sincere appreciation for the members of my thesis committee: Drs. Valeria Milam, Shuming Nie, James Powers, and Phil Santangelo.

I am grateful to all of the members of the Bao Lab as they have been invaluable in their level of support. Many have acted as sounding boards for my ideas; others have at times acted as unofficial career (or life?) coaches. While all past and current lab members have been strong influences on my graduate school experience, several warrant a special mention. Dr. Phil Santangelo, Dr. Charles Glaus, Jeff Stirman, and Dr. Steven Dublin have all at different times been frequent and attentive discussion partners whose input undoubtedly positively influenced this thesis. Dr. Won Jong Rhee always had the perfect comment at the perfect time to inspire progress in my work and continues working wonders on the microscope to my benefit. Dr. Yiyi Zhang provided my introduction to molecular biology and fluorescent proteins. Dr Thanh Doan never failed to ask the right questions in any scientific discussion. The organizational help and lab management from Annie Zheng and Amy Tang have kept the gears grinding smoothly. My three undergraduate researchers, Marc Seaman, David Sotto, and Andrea Fernandez, have

proven themselves time and again to be interested, competent, consistent, and, most importantly, willing. I am very grateful that each of them chose to work with me for many semesters, keeping the protein machine moving. I know I learned more from them than I could have ever taught them.

I would like to acknowledge our collaborators at the Naval Research Laboratories in Washington, D.C. Dr. Bing Mei, Dr. Hedi Mattoussi, and particularly Dr. Igor Medintz have been supportive and interested discussion partners. Dr. Johnna Temenoff has also been of special help. Our frank conversations about career development and her teaching mentorship will shape my choices for some time.

Friends, particularly other graduate students, have provided a wonderful support system. From everyone in Regensburg to those who have come and gone here in Atlanta: it would not have been the same without you.

Above all, I am proud to acknowledge my family. My dad provided the inspiration for all of my endeavors and my mom the support for them. No other lay person has ever listened to so much stream of consciousness discussion about fluorescent proteins, FRET, or QDs! My dear husband Jesse has seen the good, the bad, and the ugly, and remains encouraging and supportive through it all. Finally, a few words of gratitude for the light of my life, Jack: he is my biggest motivation and my most persistent distraction and I would not have had this journey any other way.

This project was supported by funding from the Department of Energy and the National Institutes of Health (NHLBI PEN) as well as a National Defense Science and Engineering Graduate (NDSEG) Fellowship.

TABLE OF CONTENTS

LIST OF TABLES

LIST OF FIGURES

LIST OF ABBREVIATIONS

Amp	Ampicillin
BRET	bioluminescence resonance energy transfer
BSA	bovine serum albumin
Cam	chloramphenicol
cAMP	cyclic adenosine monophosphate
CdSe/ZnS	cadmium selenide-zinc sulfide core-shell QDs
DHLA	dihydrolipoic acid
DLS	dynamic light scattering
DNA	dioxyribonucleic acid
$DSPE\text{-}mPEG_{2000}$	1,2-distearoyl-*sn*-glycero-3-phosphoethanolamine-N-[methoxy(polyethylene glycol)-2000] (ammonium salt)
EDC	1-ethyl-3-(3-dimethylaminopropyl) carbodiimide
EDTA	ethylenediaminetetraacetic acid
FP	fluorescent protein
FRET	fluorescent (or Forster) resonance energy transfer
GFP	green fluorescent protein
IPTG	isopropyl-ß-D-thiogalactoside
LB	Luria Bertani
MAA	mercaptoacetic acid
MBP	maltose binding protein
mRFP1	monomeric red fluorescent protein (1)
NHS	*N*-Hydroxysuccinimide
NRL	Naval Research Laboratory
PBS	phosphate buffered saline
PCR	polymerase chain reaction
PEG	poly(ethylene glycol)
QD	quantum dot
S-NHS	Sulfo-NHS
TE	Tris EDTA
TOP/TOPO	trioctylphosphine/trioctylphosphine oxide

SUMMARY

Fluorescence resonance energy transfer (FRET)-based biosensors have been designed to fluorometrically detect everything from proteolytic activity to receptor-ligand interactions and structural changes in proteins. While a wide variety of fluorophores have demonstrated effectiveness in FRET probes, several potential sensor components are particularly notable. Semiconductor quantum dots (QDs) are attractive FRET donors because they are rather bright, exhibit high quantum yields, and their nanoparticulate structure enables the attachment of multiple acceptor molecules. Fluorescent proteins (FPs) are also of particular interest for fluorescent biosensors because design elements necessary for signal transduction, probe assembly, and device delivery and localization for intracellular applications can all be genetically incorporated into the FP polypeptide.

The studies described in this thesis elucidate the important parameters for concerted QD-FP FRET probe design. Experimental results clarify issues of FRET pair selection, probe assembly, and donor-acceptor distance for the multivalent systems. Various analysis approaches are compared and guidelines asserted based on the results. To demonstrate the effectiveness of the QD-FP FRET probe platform, a ratiometric pH sensor is presented. The sensor, which uses the intrinsic pH-sensitivity of the FP mOrange to modulate the FP/QD emission ratio, exhibits a 20-fold change in its ratiometric measurement over a physiologically interesting pH range, making it a prime candidate for intracellular imaging applications.

CHAPTER 1

INTRODUCTION

The development of fluorescent biosensors has provided a wealth of information to the biomedical community through their application in a wide range of modalities, including solution studies, flow cytometery and microfluidic devices, and fluorescence microscopy. Fluorescent indicators are typically more sensitive than their colorimetric counterparts and can be used in tandem for multiplexed analysis. The diversity of fluorochromes spans the visible wavelengths into the near-infrared, ranges in molecular weight from small molecule organic dyes to massive phycoerythrins and nanocrystals, and can be synthesized through organic chemistry, biochemical methodologies, or inorganic nanoparticle synthesis. Recent developments in nanobiotechnology have further enhanced the range of possibilities for fluorescent indicators, offering increased potential for multiplexing, sensitivity, and resistance to photobleaching.

The objective of this thesis research was to develop a novel quantum dot-fluorescent protein (QD-FP) probe platform that could be used to generate highly sensitive and specific fluorescent sensors. Integrating the customization of fluorescent proteins through genetic engineering with the unique optical properties of semiconductor QDs creates a unique inorganic-biomolecule hybrid that could be adapted to a number of sensing applications. It was hypothesized that, due to the exceptional brightness and photostability of quantum dots in comparison to organic dyes, the development of a switchable QD probe would produce indicators with heightened sensitivity and resistance to photobleaching. The rationale for this work was that the development of more sensitive

indicators would provide unique and important tools for both cellular biology studies and biomedical research. Such indicators could be adapted to monitor any number of environmental cues as well as small analyte concentration, enzyme activity, and ligand binding and could be applied in a range of sensing modalities. In particular, live-cell imaging studies could benefit from the development of fluorescence resonance energy transfer (FRET)-based ratiometric biosensors that resist photobleaching. The project entails developing FRET probes consisting of QD donors and fluorescent protein (FP) acceptors, investigating the properties of both the QD and FP that affect probe assembly and functionality, and producing a functional biosensor based on this probe platform, specifically a pH sensor.

To address the hypothesis, three specific aims were pursued.

SPECIFIC AIM 1: Investigate the self-assembly of QDs and His-tagged FPs using QDs with similar spectral properties and a variety of coating chemistries.

We hypothesized that histidines incorporated in a polypeptide tail chelate zinc ions in the ZnS capping layer of CdSe/ZnS quantum dots with sufficient affinities to produce stable, self-assembled probes when the polypeptide is able to access the ZnS surface. By using fluorescent proteins containing a His-tag as a FRET acceptor, the proximity-dependent change in the fluorescent spectra was used to assess the polyhistidine-QD interaction for eight different QD coating varieties. The distance between the donor and acceptor was estimated and correlated with measurements of various QD characteristics in order to compile information about the likely mechanisms

of the interactions between each of the QDs and the protein. In cases where defects in the organic coating appear to have left the ZnS shell accessible, direct binding of the His-tag to the nanocrystal surface resulted in self-assembly with reduced donor-acceptor distances and increased FRET efficiencies. In other cases, the organic coating effectively shielded the QD from direct binding of the polypeptide, but electrostatic interactions or the coordination of supplemented Ni^{2+} ions still facilitated associations between the QD and the protein, albeit with greater donor-acceptor distances. Finally, the presence of PEG chains on the surface of other QD varieties effectively blocked the self-assembly of proteins *via* steric hinderance. The results of this study give indications as to which QD varieties make the most successful FRET donors and what conjugation strategies may be most appropriate for each QD coating type.

SPECIFIC AIM 2: Examine the FRET efficiency of various QD-FP FRET pairs.

We hypothesized that a variety of QD and FP pairings could be used effectively if the spectral properties of the donor and acceptor were well matched. We analyzed a number of pairings, looking at the effect of the spectral overlap on the FRET efficiency as well as the influence of various properties of the fluorescent protein, such as the length of the polyhistidine tail, the molar extinction coefficient, quantum yield, and molecular weight. We observed that the optical properties of the protein, particularly its quantum yield, could dictate the most appropriate analysis techniques for a given FRET pair. Specifically, proteins with poor quantum yields, such as mCherry, can operate as effective protein quenchers, but are not desirable for ratiometric measurements because of their low sensitized emission. In contrast, FP acceptors with high quantum yields like

tdTomato show significant increases in their acceptor emission to donor emission ratios as the number of acceptor molecules per QD increases, making them good candidates for ratiometric FRET probe designs. These findings elucidate important parameters to consider when choosing the most appropriate FP for a given biosensor application.

SPECIFIC AIM 3: Design and evaluate a functional QD-FP FRET probe, specifically a ratiometric pH sensor.

We hypothesized that a ratiometric FRET-based biosensor could be designed using a fluorescent protein that showed the appropriate pH-sensitivity. The pH-specific spectral properties of two variants of the fluorescent protein mOrange were elucidated, while QDs and bioconjugation strategies were assessed for their stability over a range of pHs. The fluorescence spectra and FRET efficiency of two QD-mOrange hybrid probes were evaluated for their pH sensitivity. Each of these probes demonstrated a dramatic difference in the ratio of the acceptor emission to donor emission over a relatively short pH range. The probes' high signal-to-noise ratio and large, pH-dependent change in the FRET efficiency indicates that this probe has significant potential for intracellular imaging applications.

Collectively, these studies contribute to a better understanding of how to apply nanobiotechnology to biosensor design. The results herein shed light on how nanoparticle properties affect the formation of inorganic-biomolecule hybrid devices, reveal the utility of QDs and FPs as efficient FRET donor-acceptor pairs, and demonstrate the effectiveness of the QD-FP pairs as a biosensor, specifically as a ratiometric pH monitor.

As probe development continues, this and other QD-based FRET biosensors will enable the live-cell imaging of multiple parameters over extended periods of time.

CHAPTER 2

RESEARCH SIGNIFICANCE

The use of fluorescent biosensors has expanded precipitously in recent decades because of their high sensitivity, diversity, and simplicity (*1*). Probes that have been developed for a vast array of analytes, enzymes, and environmental cues can be utilized in conjunction with a variety of instruments, such as fluorescence microscopes, flow cytometers, fluorimeters, or multiplate readers. This versatility guarantees that optical sensing will continue to be a powerful tool in biomedical research. Driving the increased application of fluorescence-based biosensing has been the continued development of several relatively new and dynamic fluorophores. While traditional small molecule organic dyes continue to play a very important role in many sensing applications, the introduction of green fluorescent protein (GFP) and its analogues as genetically encodable fluorophores as well as optically active nanomaterials like semiconductor quantum dots (QDs) has transformed biosensor design (*2, 3*).

Many fluorescent biosensors utilize fluorescence (or Förster) resonance energy transfer (FRET) for signal transduction. FRET is the distance-dependent, non-radiative transfer of energy from one fluorophore (the donor) to an acceptor: either another fluorophore or a non-fluorescent quencher (*4*). FRET signals can be reversibly or irreversibly modulated in response to a biological stimulus or environmental cue. Both QDs and GFP-like fluorescent proteins (FPs) have been used as donors and acceptors in FRET-based biosensors. QDs have become a favorite FRET donor because their high quantum yield and the multivalancy of the nanoparticle platform increase FRET

efficiencies even as the high molar extinction coefficient of the QD results in bright signals that are ideal for fluorescence microscopy (*5*). Fluorescent proteins, in contrast, are heavily utilized in biosensor designs because they, by nature as biomolecules, interact with the biological environment in ways that make them innate biosensors. Cleavable polypeptides can be incorporated into their structure to create enzyme activity assays, protein transduction domains can be incorporated into the protein for localization to specific subcellular compartments, and molecular biology techniques can be used to coax cells into expressing the biosensors themselves, simplifying production and delivery of the fluorophores to an on-location event (*6, 7*).

While both of these fluorescent indicators have been garnering attention, and even a Nobel prize (*8, 9*), independently, no biosensors in the literature combine the unique optical properties of the QD with the inherent sensing versatility of fluorescent proteins. The work described in this thesis does exactly that.

First, the polyhistidine-mediated self-assembly of biomolecules to semiconductor QDs was examined and evaluated for a number of QD coating types. Although this form of protein-QD self-assembly had been described for dihydrolipoic acid (DHLA) coated QDs (*10, 11*), it was unclear whether this bioconjugation modality would be successful with other varieties of QDs. The demonstration of successful binding to QDs coated with several different approaches, including commercially available varieties, expanded the range of known options available for QD-biomolecule hybrids assembled *via* polyhisitinde-mediated self-assembly. Furthermore, the examination of what QD parameters determined whether or not self-assembly would be successful enables the

prediction of what other coating types are most likely to behave similarly. The straight-forward FRET assay that is described can be used to verify such predictions.

QDs have been described as FRET donors paired with organic fluorophores, organic quenchers, and gold nanoparticles as the acceptor (*12-14*). Although dye-labeled proteins have been used as FRET acceptors as well (*11*), the added complication of chemically labeling the protein with a fluorophore can be eliminated by adapting fluorescent proteins as FRET acceptors. In the first published study documenting the effectiveness of fluorescent protein acceptors (*15*), we demonstrate several successful FRET pairs. Analytical approaches focusing only on the donor emission and FRET efficiency are compared to ratiometric methods.

Finally, we demonstrate the effective utility of a QD-FP hybrid probe in the form of a FRET-based, ratiometric pH sensor. A very few reports of QD-based pH sensors have emerged in the literature (*16-18*), but none have exhibited a sufficient sensitivity that would make them promising candidates for intracellular imaging. Two different monomeric fluorescent proteins were evaluated for their pH-dependent optical properties and their effectiveness as FRET acceptors to a QD donor. With a 20-fold change in the acceptor emission to donor emission ratio over a pH range that is physiologically interesting, these probes hold promise as intracellular imaging agents. Potential applications include endosomal tracking or the elucidation of delivery pathways used by various cell-penetrating peptides with model nanoparticle-protein drug delivery devices.

By outlining and exploring a number of design parameters specific to the QD and the FP as well as detailing the interaction between the two, these studies provide a guide

for QD-FP hybrid biosensor design as well as demonstrating an example of a successful QD-FP FRET probe.

CHAPTER 3

LITERATURE REVIEW

FLUORESCENCE RESONANCE ENERGY TRANSFER

Fluorescence (or Förster) Resonance Energy Transfer (FRET) is the non-radiative transmission of energy from an excited donor molecule to an acceptor molecule in close proximity; the acceptor can subsequently radiatively emit this energy in the form of a lower-energy photon than was used to excite the donor (*4*). The energy transmission depends on several factors, most notably the spectral overlap between the donor emission and the acceptor absorbance and the proximity of the two molecules (*4*). FRET is inversely proportional to the distance between the donor and acceptor to the sixth power, making it highly sensitive to small changes in the distance between the donor and acceptor (*4*). This property has made FRET a valuable tool in a number of biophysical and biochemical studies, such as investigations into receptor-ligand interactions (*19*), protein phosphorylation (*20*), proteolysis (*21*), and nucleic acid hybridization (*22*). The fluorescence emission of the donor moiety can be modulated by either another fluorophore or a non-fluorescent quencher. The first results in sensitized emission of the acceptor fluorophore, while the second quenches the donor without emitting any photons (Figure 3.1). Typical FRET studies utilize either organic fluorophores or fluorescent proteins as the donor and one of these or an organic quencher as the acceptor, but the use of these molecules is accompanied by some inherent limitations, including susceptibility to chemical or photodegradation, photobleaching, and broad excitation and emission spectra, which can result in crosstalk between the two fluorophores during detection (*6*).

Fluorescent proteins have been used to develop an entire class of genetically-encoded FRET biosensors. Separately, fluorescent nanoparticles of semiconductor metals have been tested as both FRET donors and, more rarely, acceptors. Details of these types of FRET probes and specific examples of their application are included below.

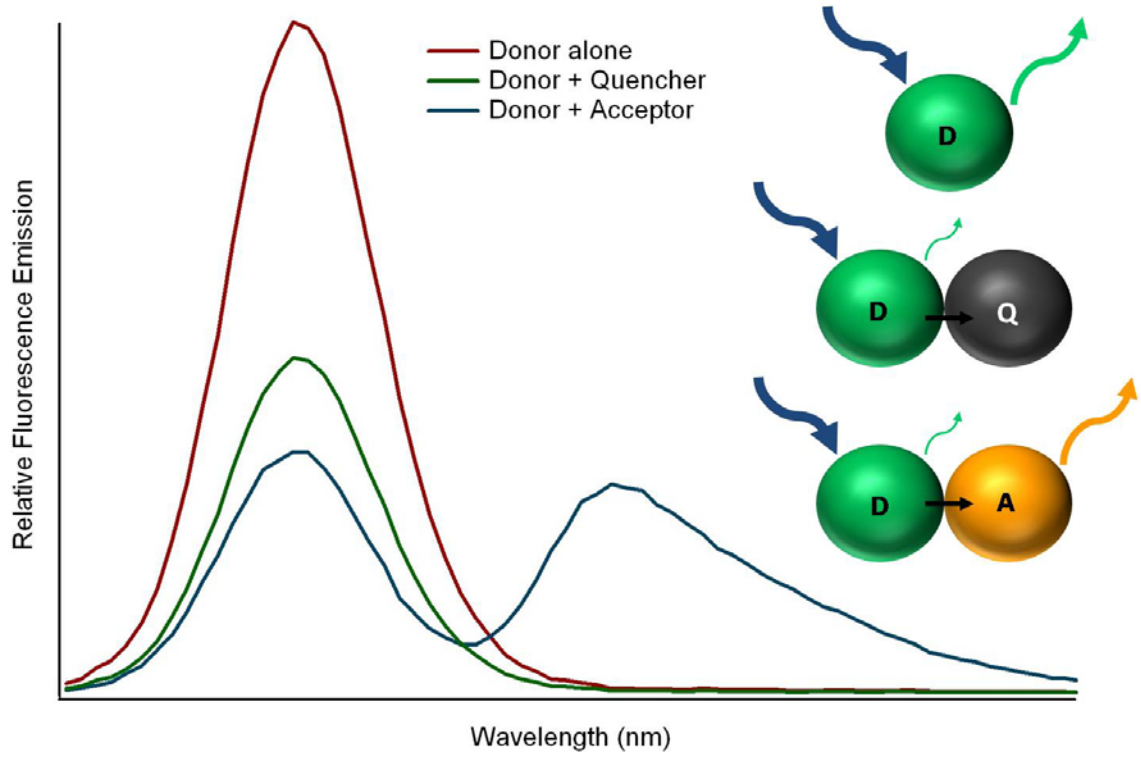

Figure 3.1: FRET modulation of the emission of a fluorescent donor.
In the presence of a quencher, the emission of the FRET donor fluorophore is decreased. In close proximity to a fluorescent acceptor, the emission from the FRET donor is decreased and sensitized emission of the acceptor is observed.

QUANTUM DOTS

Quantum Dot Crystal Properties

Semiconductor quantum dots (QDs) are crystalline nanoparticles often composed of group II-VI or III-V elements from the periodic table with diameters smaller than their exciton Bohr radius (*24*), typically just a few nanometers in diameter. Spherical CdTe QDs emitting visible wavelengths, for example, range in diameter from 1.5 to 4.2 nm (Figure 3.2) (*23*). Quantum confinement effects present at this size range give rise to distinctive optical and electronic properties that are not present in the bulk materials. QDs most commonly used in the visible wavelength range are CdSe/ZnS core-shell nanoparticles; the CdSe core confers the particle its unique optical properties, while the ZnS shell serves as a passivation layer, protecting the core from oxidation and enhancing the quantum yield (*25*, *26*).

High quality inorganic core/shell QDs are typically synthesized in a step-wise reaction using organometallic precursors (e.g., trioctylphosphine selenium (TOP:Se),

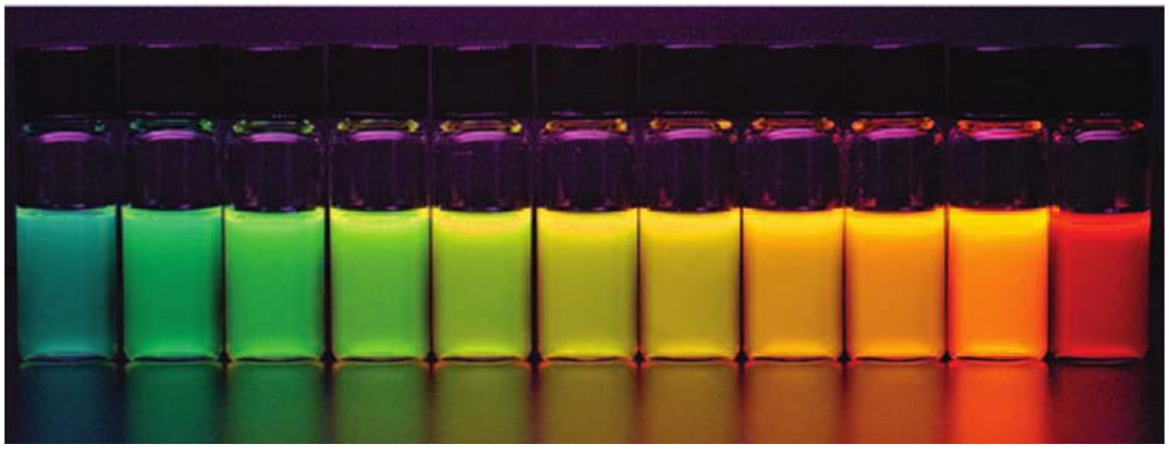

Figure 3.2: Series of CdTe QDs with fluorescence emissions from 515 to 655 nm. The QD color is tuned by modulating the size of the nanocrystal with larger particles exhibiting more red-shifted emission. Reproduced with permission from Kairdolf, Smith et al. 2008 (*23*).

cadmium acetylacetonate, diethylzinc and hexamethyldisilathiane) at high temperatures (*25-28*). Since these nanoparticles are grown and coated with a mixture of trioctylphosphine, trioctylphosphine oxide, and hexadecylamine, they are water insoluble and must be coated with an organic layer to be used in biological applications (see below).

The broad excitation range of QDs paired with narrow, symmetrical emissions make QDs an interesting option for fluorescence sensing applications. Excitation of QDs is possible with photons of higher energy than the semiconductor bandgap. Because a large number of energy states exist within the QD, a broad range of excitation wavelengths is possible, from the first exciton, or quantum-confinement, peak to shorter wavelengths with increasing molar extinction coefficients through the UV (Figure 3.3, top). QDs are optimally excited in the UV, but two-photon excitation can also be used to induce QD emission (*29*), a technique that reduces background autofluorescence and cell damage from UV irradiation in live-cell imaging (*30, 31*). Although the excitation wavelength range for QDs is broad, QD emission peaks are narrow and symmetrical (Figure 3.3, bottom). QDs have uniquely tunable emissions moderated by adjusting the diameter of the CdSe core (*32*). Next generation QDs made with other semiconductor configurations allow for continuous tuning of the QD emission without changing the particle size. Examples include CdSeTe alloys that are tuned by varying the alloy concentration (*33*) and CdTe cores paired with various compressive shell materials that affect QD properties through lattice strain (*34*).

The combination of the broad excitation peak and narrow emission peak make QDs well suited to multiplexing applications because several QDs can be excited

simultaneously and their emission peaks can be easily distinguished (*24*, *35*-*37*). This is in contrast to organic fluorophores and fluorescent proteins, whose broad, asymmetrical emission peaks often overlap, reducing the number of discrete colors that can be discerned.

In addition to their unique spectral signatures, QDs have gained attention for fluorescence detection because they exhibit brightnesses up to 1,000-fold higher than most organic fluorophores. This arises from a combination of molar extinction coefficients 10-100 times higher than those measured for organic fluorophores (*38*, *39*) and quantum yields of up to 85% (*32*).

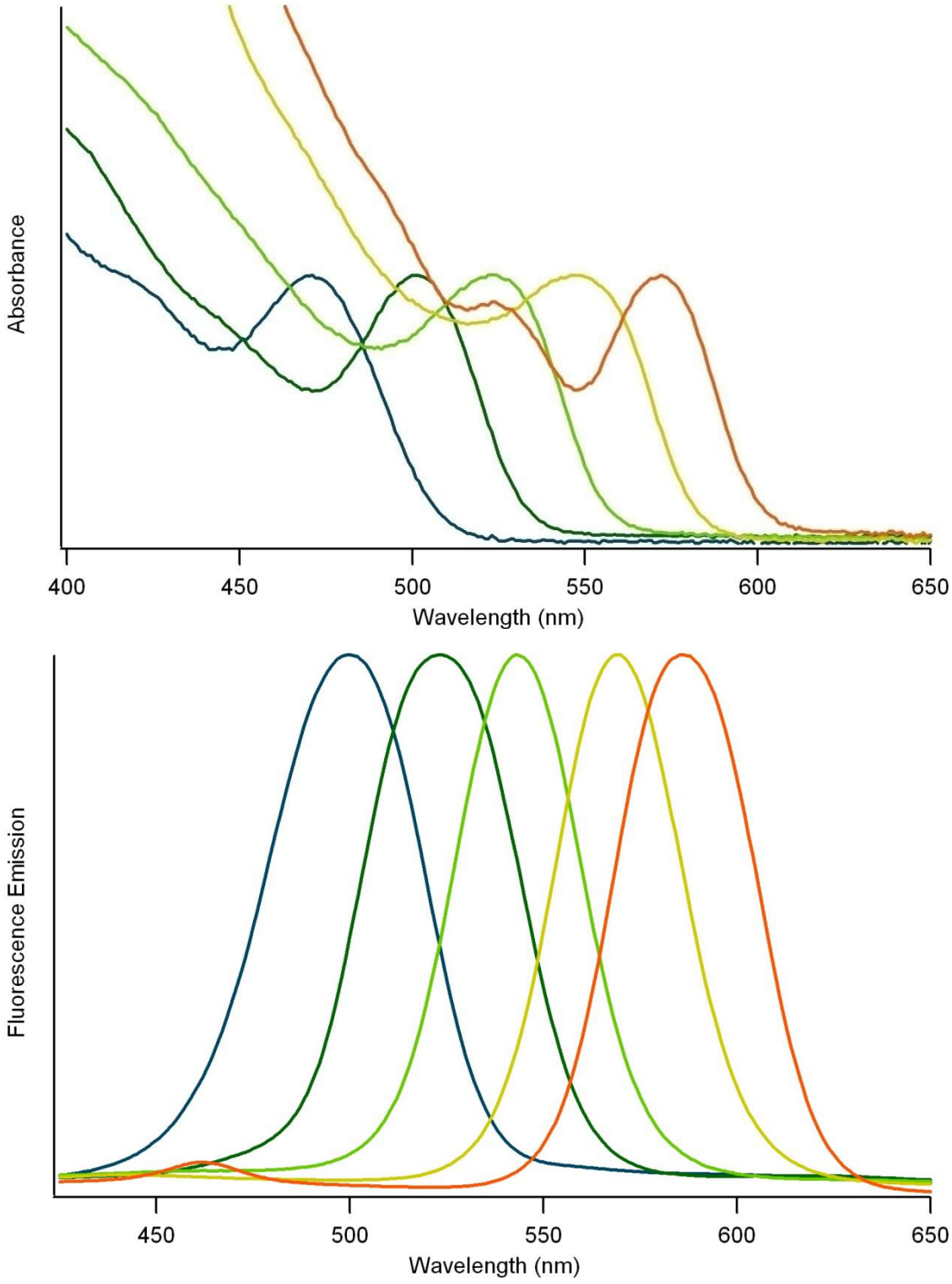

Figure 3.3: Characteristic QD absorption and emission spectra.
Absorption (top) and emission (bottom) spectra of water-soluble CdSe/ZnS core-shell QDs (from left to right) with peak emissions at 490, 520, 540, 560, and 585 nm. The absorbance spectra are normalized to the first exciton peak.

Quantum Dot Coatings

Because the inorganic synthesis of the core-shell QDs results in a water-insoluble colloid, a number of coating strategies have been devised to transfer the particles into aqueous solutions, a necessary step for biological applications (*40*). While all of the coatings result in a hydrophilic outer layer to interface with aqueous solutions, two basic approaches are most commonly used. In the first, amphiphilic materials are used such that their hydrophobic portions associate with the hydrophobic surfactants left on the crystalline surface following the inorganic synthesis and a hydrophilic region exposed to the surrounding media. In the second approach, the hydrophobic surfactant is removed and replaced with molecules that bind directly to the nanocrystal through ligand exchange. The colloids that result from these coating procedures are stabilized electrostatically, with steric hinderance, or both.

The first ligand exchange coatings utilized small molecules containing thiol groups that bind directly to the ZnS capping layer of the particle and contained a carboxyl group that is deprotonated at physiological pHs, stabilizing the colloid with electrostatic repulsion (*41*). While this approach results in small, uniform QDs that are water soluble, the thiol-QD bond is known to dissociate causing precipitation of the particles over time (*42*, *43*). This coating strategy has been improved by using molecules containing bidentate thiols such as dihydrolipoic acid (DHLA), which dissociate from the particle at a slower rate, improving the long-term stability of the coating (*44-46*). These coatings are very thin, resulting in quantum dots with hydrodynamic diameters around 10 nm, but they are prone to complications from the environment such as aggregation in acidic media (*45*). Ligand exchange coating of CdS nanocrystals that are capped with just a thin

shell of ZnS also seems to result in QDs with low quantum yields relative to the starting material with typical research articles citing QYs on the order of 10-30% QY (*45*).

More recently, PEGylated ligands have been used in ligand exchange protocols. These colloids are stabilized *via* steric hinderance, making them less susceptible to their environment and reducing non-specific interactions when used in applications such as intracellular imaging (*45, 47-49*). There are also a few recent reports of QD coating protocols that use ligand exchange with small molecules, but under gentle conditions that maintain better QYs (*50, 51*), and multidentate ligands that form thin but robust coatings (*52*). Small, bright QDs such as these hold great potential for both labeling and sensing applications. A number of amphiphilic moieties have been used to coat QDs without removing the hydrophobic surfactant layer, most notably alkylated polycarboxylates (*53, 54*), amphiphilic block copolymers (*37, 55*), and lipid-poly(ethylene glycol) (lipid-PEGs) that form a micelle-like layer around the QD (*56*). These coatings have the advantage of maintaining high QD QYs, but at the expense of an increased hydrodynamic diameter (*55*). While the amphiphilic polymer-coated QDs can be primarily stabilized electrostatically by using a polymer that contains a high density of carboxyl groups at the media interface, the inclusion of PEG chains at the surface reduces non-specific interactions with the environment (*57*). A schematic diagram of several QD coating approaches is included in Figure 3.4 and a comparison of various QD coatings is included in Chapter 5.

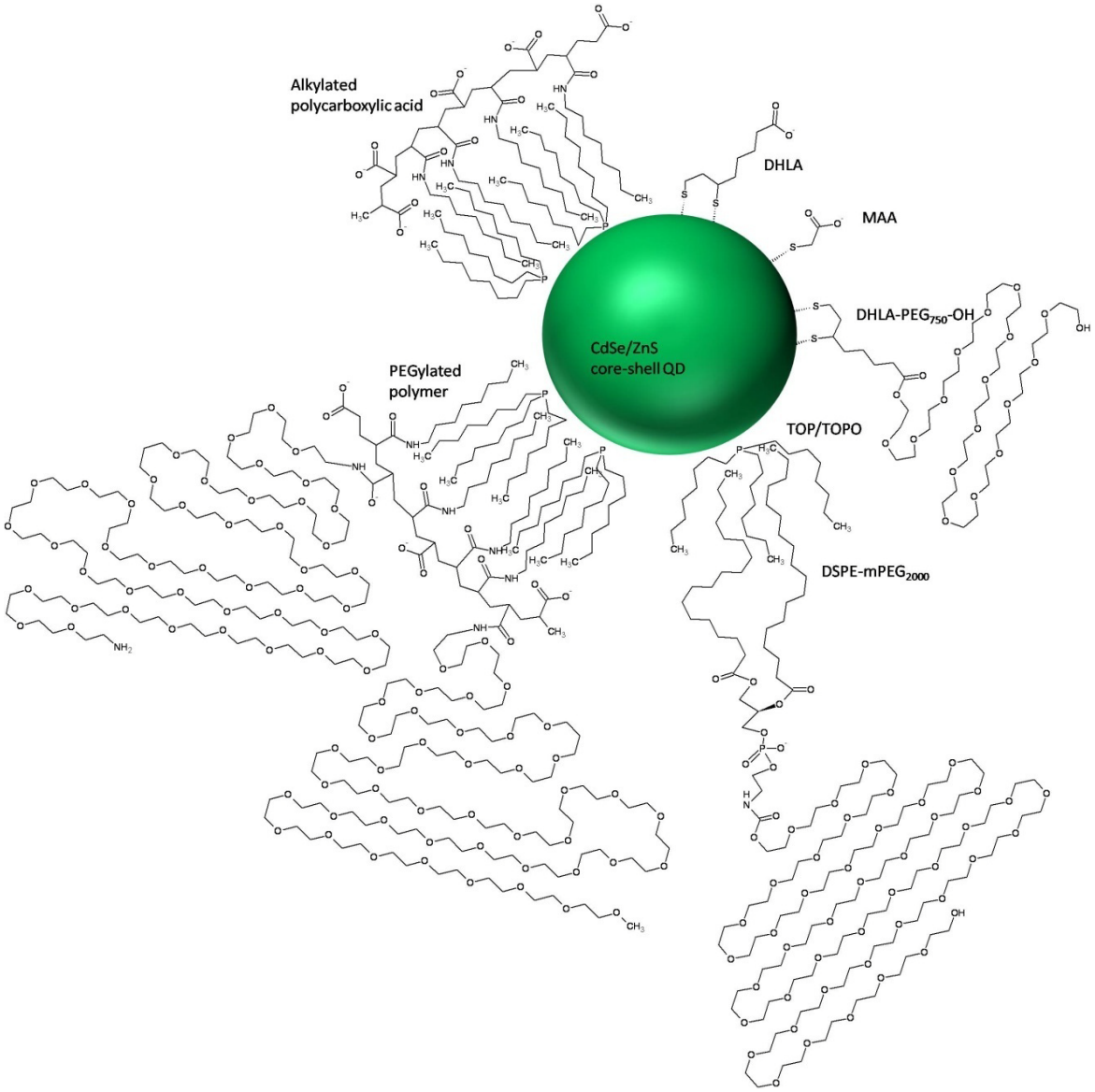

Figure 3.4: Schematic of some QD coating approaches.
Ligand exchange coatings like dihydrolipoic acid (DHLA), mercaptoacetic acid (MAA), and PEGylated DHLA derivatives (DHLA-PEG_{750}-OH shown here) remove the nonpolar surfactant residue remaining on the QD surface following inorganic synthesis (trioctyl phosphine (TOP) shown here). Other approaches include using lipid-PEG (such as DSPE-$mPEG_{2000}$) or amphiphilic polymers to interface with the hydrophobic surfactant rather than removing it.

Bioconjugation to QDs

The conjugation of biomolecules to QDs has been used to functionalize the nanoparticles for any number of applications, such as immunohistochemistry using QD-labeled antibodies (*54*), nucleic acid hybridization requiring DNA-tagged QDs (*58, 59*), and proteolytic activity using QDs bound to dye-labeled peptides (*14*, *60*). While there are enough possible bioconjugation strategies to fill a book (*61*), a few approaches that have become standards in the field are discussed here.

The assembly of biomolecules and QDs can be achieved with covalent chemistry, most frequently using a carbodiimide linker, as well as streptavidin-biotin binding or affinity based coordination based on either electrostatic interactions or metal coordination. Each of these approaches has advantages and limitations that need to be considered when designing a hybrid device.

Covalent coupling. Covalent coupling provides the most durable attachment of a protein to a QD. Many of the QD organic coatings used to water-solubolize QDs result in carboxyl groups exposed at the surface, so heterobifunctional cross-linkers that facilitate couplings between carboxyl groups and other functional groups, such as amines or thiols, are particularly useful for covalently attaching biomolecules to the QD surface. Cross-linking reagents, such as 1-ethyl-3-(3-dimethylaminopropyl) carbodiimide (EDC), used alone or in conjunction with N-hydroxysuccinimide (NHS) or its more water-soluble analogue sulfo-NHS (S-NHS), are readily commercially available and have been used extensively in the literature (*62-64*). EDC activates the carboxylic acid, priming it for reaction with a primary amine to form a stable amide bond (*65*). Both the EDC and the activated carboxyl group are highly water-labile, but the lifetime of the activated

carboxylic acid can be extended with the addition of NHS or S-NHS, which form a more stable intermediate (*61*). With or without NHS, reaction conditions must be tweaked to promote conjugation while minimizing aggregation. One-step reactions involve incubating the carboxylated nanoparticle with a large excess of a biomolecule, e.g. a 40-fold molar excess of protein, and a huge excess of EDC (up to a 1500-fold molar excess). In this protocol, the EDC is able to activate the carboxylates on the nanoparticle for reaction with the N-terminal amine as well as any lysines present in the protein. The EDC also, however, activates the carboxylic acids of the aspartic acid and glutamic acid residues in the protein. When protein amines react with activated carboxyl groups on other proteins, undesirable protein polymerization can result (*61*). These protein polymers may be bound to the nanoparticle surface, increasing its size and potentially negatively affecting other colloidal properties, or may be independent of the QD, but complicate purification of the conjugate. The size of the polymerized polymer may preclude them from being eliminated with oft-used centrifugal filtration devices.

In contrast, supplementation with NHS or S-NHS allows for use of a two-step reaction because of the increased stability the active intermediate. In the two step reaction, the nanoparticle is incubated with EDC and an NHS derivative to form activated carboxylic acids. The excess EDC is either removed with a centrifugal filtration device or quenched with the addition of β-mercaptoethanol prior to the addition of the biomolecule. The two-step process eliminates the possibility of protein polymerization, but aggregation of the particles is now a potential hazard as the extended lifetime of the activated carboxylate increases the chances that a protein will encounter two QDs and bind them

both. Careful testing of reaction conditions, particularly the concentration of the reactants, is important to minimize this undesirable aggregation.

Carbodiimide chemistry is particularly useful for the bioconjugation of proteins to QDs both because the QDs and biomolecules frequently exhibit the necessary carboxylic acids and primary amines, respectively, and because the zero-length crosslinking agents like EDC bind the two moieties directly to one another without the addition of any superfluous atoms (*61*). In instances where the addition of a short linker is acceptable, homo- and heterobifunctional cross-linkers expand the repertoire of applicable functional groups. Amine-functionalized QDs, for example, have been conjugated to protein amines and thiols using the homobifunctional cross-linker bis(sulfosuccinimidyl) suberate (BS^3) and the heterobifunctional succinimidyl 4-[N-maleimidomethyl] cyclohexane-1-carboxylate (SMCC), respectively (*66*, *67*).

While it is not in the scope of this thesis to provide a comprehensive examination of all of the possible means of covalent coupling that are applicable to QD bioconjugations, the discussion of the EDC coupling is intended to convey the accessibility of such bioconjugation methods, but also the potential for unintended products. The over-arching benefit of using convalent conjugation for QD-biomolecule probe assemblies is the stability of the final product. This is highly desirable in applications where further modification and down-stream processing of the probe is necessary, when probes are prepared in bulk for use at a later date, or if potential dissociation of some of the biomolecules could significantly and detrimentally impact assay results. Unfortunately, the covalent bioconjugations may cause nanoparticle aggregation, may result in a relatively low number of proteins per nanoparticle compared

to the reaction ratios, and often require purification steps that are also a source of loss, depressing the overall yield of the functional construct (*61*). In addition, the convalent reactions result in a lack control of component stochiometries and biomolecule orientation; heterogeneous conjugation, for example, may cause proteins to attach in an unproductive manner or to lose activity.

Streptavidin-biotin affinity. Streptavidin-biotin binding is another common and useful coupling mechanism that utilizes exceptionally simple protocols, provided the constituent components are already functionalized with the required streptavidin and biotin moieties. With femptomolar binding affinities, the streptavidin-biotin interaction is often considered to be effectively as stable as a covalent bond (*68, 69*). QDs have been derivatized with both streptavidin and biotin for labeling and imaging applications (*13, 49, 62, 70-72*).

With a molecular weight of *ca.* 53 kD, the addition of multiple streptavidin molecules to a single QD adds considerably to the overall size of the nanoparticle construct. This extra protein bulk could be detrimental in applications where the increase in size may impair function. FRET-based biosensors, for example, require short distances between their fluorescent donors and acceptors. As the efficiency of energy transfer is inversely related to the donor-acceptor distance to the sixth power (*4*), the additional separation by a few nanometers due to the size of streptavidin can dramatically reduce FRET efficiency.

Probe assemblies based on streptavidin-biotin binding are likely to remain popular for many applications because of the shear ease of their implementation, particularly as both streptavidin-labeled QDs and kits designed to biotinylate biomolecules are

commercially available. In some applications, however, the advantages of the streptavidin-biotin interaction may be overshadowed by the tetrameric nature of streptavidin, which can result in undesired multiple binding events and induce aggregation (*73*). The development of monovalent streptavidin QD conjugates that contain only one biotin binding site per QD have the potential to mitigate this concern (*74*).

Affinity-driven self-assembly. An alternative bioconjugation approach is derived from the affinities between biomolecular components and various substrates. These range in strength and specificity from electrostatic interactions to metal chelation to interactions culled from phage display (*44*, *46*, *75-78*). Although the binding affinities of these reactions cannot rival that of avidin-biotin, advantages arise because the minimal affinity tag can be genetically engineered into a protein of interest and bind to the QD without necessitating additional functionalization of the nanoparticle. Self-assembly based coupling requires only small tags, is facile, is typically not intrusive on the other components of the nanoparticle system, is orthogonal to most biological structures and activity, provides reasonable control over the relative component stoichiometries, and utilizes well-established protocols.

A specific example of one such small affinity tag is the polyhistidine sequence (His-tag), which has an affinity for divalent cations. It was discovered that His-tag chelation of metal ions, such as Ni^{2+}, Zn^{2+}, or Cu^{2+}, could be used to purify recombinant proteins using immobilized metal affinity chromatography (IMAC) (*79*). More recently, His-tags have been used to bind biomolecules, including proteins, peptides, and even His-modified DNA, to QDs displaying zinc ions on their surface in the form of the ZnS

capping layer of the CdSe/ZnS core-shell nanoparticles (*10, 15, 78, 80-82*). Although this coupling technique has been used with success in several QD-based sensing applications, the characteristics of the QD-polyhisitidine interaction appear to vary depending on the particular organic coating used to confer water solubility of the QDs (*83*). Chapter 5 of this thesis addresses this interaction, and its coating dependence at length.

Other small molecule polypeptides that have been used to bind directly to the QD surface typically have a high cysteine content for dative binding (*51, 70*), but electrostatic interactions have also been used to associate positively charged regions of a biomolecule with negatively charged QD coatings (*44, 46*). While this interaction would be transient and sensitive to environmental factors, such as high salt or low pH, there may be instances when this bioconjugation strategy is sufficient, or even preferred.

Quantum Dots and FRET

Quantum dots have been used in a variety of resonance energy transfer applications as FRET donors and, occasionally, as acceptors. Reports of QD FRET systems describe QD as donors paired with organic fluorophores, organic quenchers, or gold nanoparticles as the acceptor (*12-14*). The many advantages of QDs as a FRET donor include their high quantum yield, which improves FRET efficiency, and the particulate nature of the QDs, which enables the binding of multiple acceptor molecules per QD. As can be seen in Figure 3.5, the use of multiple acceptor molecules per donor

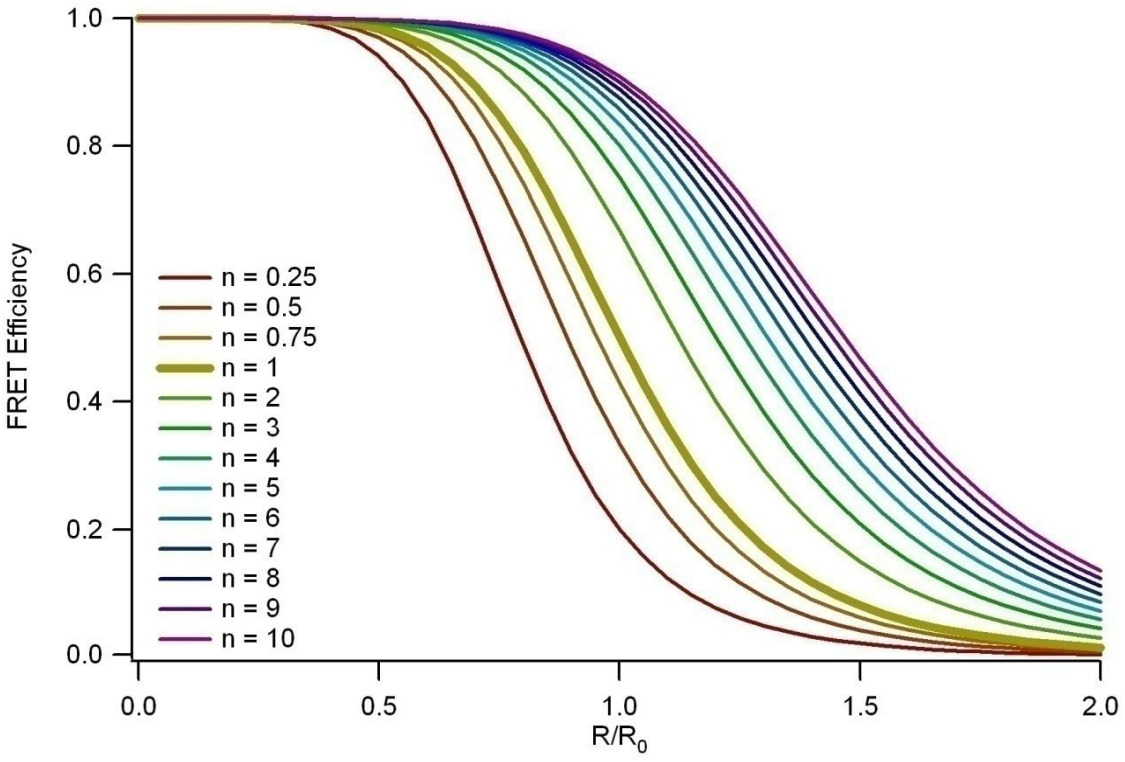

Figure 3.5: Distance dependance of FRET efficiency for multivalent systems.
The FRET efficiency at a given distance improves as the number of acceptors per donor increases.

shifts the distance *versus* FRET efficiency trace, increasing the FRET efficiency at a given distance with each additional acceptor. Likewise, having an average of less than one acceptor per donor molecule, say in the case of an incomplete conjugation that leaves some QDs unlabeled, greatly reduces the FRET efficiency at a given distance. It should also be noted that the multiple acceptor effect is non-linear such that the more acceptors present per donor, the less the impact of adding one more. That is to say that a more significant impact on the FRET efficiency is seen when the number of acceptors is increased from one to two than with an increase the number of acceptors per donor from eight to nine.

The broad excitation range of the QDs combined with a Stokes shift much larger than that seen for organic fluorophores or fluorescent proteins allows for excitation of QDs far from the excitation ranges of other fluorophores, reducing crosstalk when used in tandem with conventional dyes. This improves the signal-to-noise of QD-based FRET devices as more of the emission observed from the acceptor molecules is sensitized emission rather than a result of direct excitation.

The variety of FRET-based QD probes for protease activity demonstrate the versatility of QDs for FRET biosensing. In this sensor type, cleavable peptides are used to link the QD to another fluorophore or quencher. Gold nanoparticles (*12*), organic dyes (*14*, *60*), organic quencher molecules (*14*), and recently a fluorescent protein (*84*) have all been used as acceptor molecules in this scheme with varying levels of success. The QD-gold nanoparticle device suffered from unacceptably slow cleavage, presumably due to the difficulty the enzyme may have had in accessing a cleavage site between the two nanoparticles, highlighting a concern that arises when the size of the nanoparticles or

overall construct used grow ungainly (*12*), but reasonable results were seen with both the dye-labeled peptide and fluorescent protein biosensor designs (*14*, *84*). In a different approach, luciferase molecules containing a protease cleavage site were bound to QD to act as the energy donor in a bioluminescence resonance energy transfer (BRET) sensor (*85*, *86*).

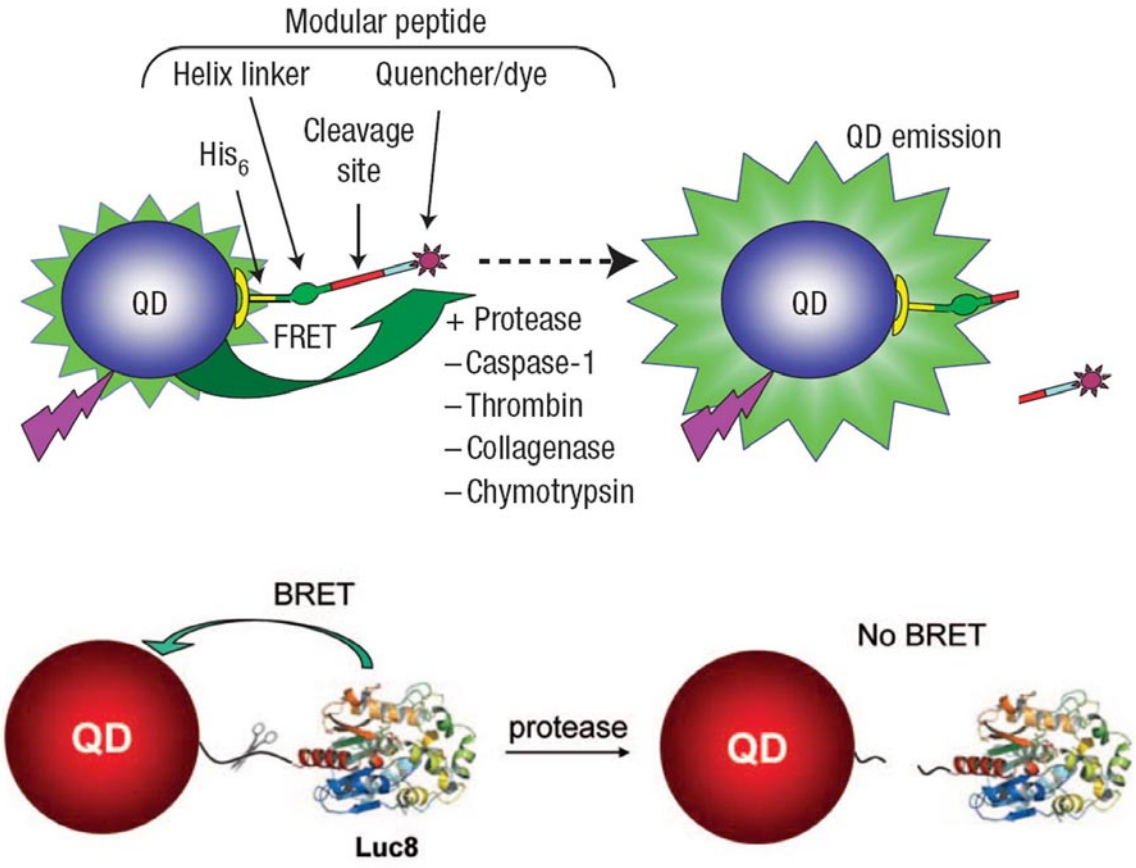

Figure 3.6: Schematics of QD biosensors for protease cleavage.
Top: A peptide containing an enzymatic cleavage site and an organic fluorophore or quencher is bound to a QD. The donor QD is quenched by FRET to the dye/quencher until protease cleavage releases the acceptor and QD photoluminescence is restored. Reprinted with permission (*14*).
Bottom: The bioluminescent protein luciferase acts as a BRET donor to a QD acceptor as long as the cleavable tether that links the two is intact. After protease cleavage, the protein is released and the QD fluorescence is no longer induced. Reprinted with permission (*86*).

GFP-LIKE FLUORESCENT PROTEINS

Source, History, and Development of GFP-like Fluorescent Proteins

Green fluorescent protein (GFP) is a naturally occurring fluorophore isolated from *Aequorea* jellyfish. While observations of the fluorescent properties protein isolations from the organism had been described in the literature as early as the 1960s (*87*), the existence of the genetically encodable fluorophore did not capture the imagination of the bioscience community until the gene was cloned (*88*) and it was shown that protein expression of GFP in other organisms induced fluorescence in 1994 (*7*). That the gene alone contains all of the information necessary for chromophore development—that no jellyfish-specific enzymes are necessary—was dramatically significant.

Since this groundbreaking discovery, which was later rewarded with the Nobel Prize in chemistry (*8*), the application of GFP and GFP-like fluorescent proteins to intracellular imaging and sensing applications has revolutionized cell biology. Proteins can be monitored in live cells with fluorescence microscopy by creating fusions with GFP, promoting the visualization of protein transport and localization. Cell processes can be observed using fluorescent protein-based biosensors, elucidating signaling pathways and protease activity (*87*).

Since the discovery of the utility of GFP for cell biology studies, a number of other structural homologues to GFP have been discovered either through their isolation from natural sources, such as the cloning of DsRed from *Discosoma* coral (*89, 90*), or by mutagenesis of other fluorescent proteins to modify protein characteristics (*91, 92*).

Protein and Chromophore Structure

Wild-type GFP consists of a single polypeptide chain 238 amino acids long and has a molecular weight around 27 kDa. Crystal structure analysis has revealed that the peptide chain folds into a compact cylinder composed of a rolled eleven-sheet β-barrel capped with short α-helices and loops. An α-helix containing the three amino acids that comprise the chromophore thread through the center of the so-called β-barrel (*93*). The posttranslational cyclization of the amino acids Ser^{65}-Tyr^{66}-Gly^{67} to form an imidazolone ring following protein folding is necessary for maturation of the chromophore, which has excitation peaks at 395 and 470 nm and emits at 504 nm (*94*). Proper folding and configuration of the residues adjacent to the chromophore is essential for fluorescence; the isolated chromophore is not fluorescent in aqueous solution (*95*).

Although the red fluorescent protein isolated from coral *Discosoma* sp. and commercialized by Clontech as DsRed has only ~22% sequence homology to GFP, it maintains the same β-barrel structure and similar chromophore structure, albeit with a substitution of a glutamine for the GFP serine (*96*). The maturation of the DsRed chromophore involves the same cyclization as GFP, but is followed by oxidation of the Gln^{66} peptide bond . Native DsRed is an obligate tetramer, making it less than ideal for use as a fusion protein (*90, 97*), but mutations to the wild type DsRed have produced subsequent generations of proteins with improved properties for cell biology studies (*91, 92*).

The studies in this thesis utilize derivatives of DsRed belonging to the so-called “Fruit Basket” family of proteins. The three proteins of interest here evolved as follows. Tetrameric DsRed was mutated to form a stable dimer, from which a further point

mutation created the dimer dTomato. The plasmid for dTomato was cloned so to contain two Tomato genes in succession, linked end-to-end, creating the so-called tandem dimer, tdTomato (*91*). By creating this protein that is twice as large as the individual barrel structures that typically make up the GFP-like proteins, the designers were able to circumvent issues of protein aggregation that arise when using proteins that are obligate oligomers, simultaneously producing a protein that is twice as bright as the lone Tomato subunit. An alternative evolution focused on the amino acids at the interfaces of the subunits of the tetrameric DsRed. The resulting mRFP1 is stably monomeric; subsequent mutations have produced a series of GFP-like proteins with a variety of spectral properties. mOrange and mCherry were a result of those modifications. While mOrange and mCherry have similar molar extinction coefficients (about half that of tdTomato, as they also have half the chromophore), mCherry exhibits a significantly lower quantum yield than either mOrange or tdTomato. On the other hand, mOrange photobleaches much more rapidly than the other two proteins and is pH sensitive as well (*91*). While these are just a few of the rainbow of fluorescent proteins available, mCherry, mOrange, and tdTomato provide sufficient variety for the studies described in this thesis. In addition to their differences in size, brightness, photosensitivity, and pH sensitivity, they also represent a range of excitation and emission wavelengths.

FRET Sensing with GFP-like Fluorescent Proteins

FP-based FRET biosensors have been developed using several common methodologies that have been summarized as focusing on intermolecular interactions, intramolecular interactions, or proteolytic cleavage (*3*). To study binding interactions between proteins, for example, donor and acceptor fluorescent proteins are separately

fused to the proteins of interest. When the two FPs are brought into close proximity by the interaction of their fusion partners, a FRET signal will be observed, giving spatial and temporal information about their interaction. A similar mechanism was used to design a FP-FRET-based biosensor for cAMP: YFP was fused to protein kinase A and CFP to its cAMD-dependent binding substrate. With this indicator, a FRET signal is only produced when the presence of cAMP induces the binding of the two fusion partners (*98, 99*).

In contrast to the binding-induced FRET seen with the intermolecular sensors, protease cleavage is detected when two FPs that are tethered to one another by a cleavable linker are separated by an enzymatic event. In this case either the loss of the FRET signal or the recovery of the donor signal can be monitored. The use of FRET sensors for caspase cleavage, for example, enabled the monitoring of caspase-8 activation during apoptosis, clarifying that caspase-8 is activated prior to caspase-3 (*100*).

FP-FRET biosensors reliant on intramolecular sensory events are depicted in (a) – (c) of Figure 3.7. In all three instances, the donor and acceptor FPs are both fused to the sensory domain in one contiguous polypeptide, but the events to which the sensor reacts can vary (*3, 101*). The changes in FRET signal in response to intramolecular biosensing are a product in changes in the donor-acceptor distance rather than in absolute association or dissociation of the donor and acceptor FPs as with the intermolecular or protease sensors.

FP FRET has revolutionized fluorescence sensing because the biosensors are genetically encodable: natural sensor domains are easily integrated into the design and biosensor-containing plasmids are readily introduced into most cell lines, making the sensors broadly applicable. Issues arise with interpreting FP-FRET data, however (*102*).

A major hurdle with FRET results is cross-talk, i.e. bleed-through, between two fluorophore colors. Cross-talk can occur when the acceptor is unintentionally excited with the excitation light intended for the donor, leading to acceptor emission due to direct excitation in addition to, and indistinguishable from, its sensitized emission. Alternatively, cross-talk occurs when the emission light form the donor bleeds through to the acceptor channel. Both of these instances are of particular concern with FP-FRET because of the broad absorption and emission peaks of the fluorescent proteins (*102*).

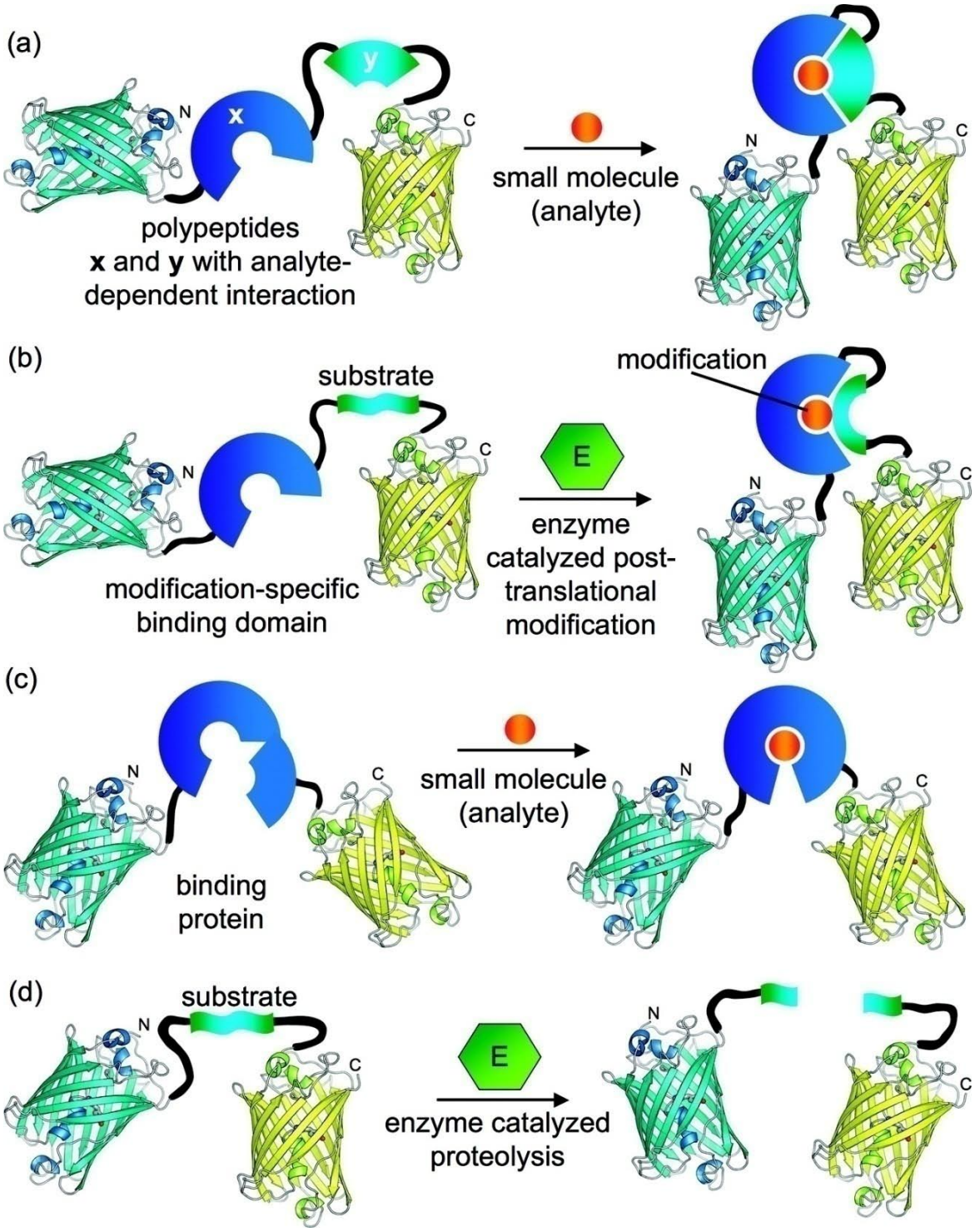

Figure 3.7: Schematic of various FP-based FRET biosensors.
Representative FRET-based biosensors for small molecule detection and enzyme activity assays. FRET signal is moderated in response to (a) analyte-induced peptide association, (b) post-translational modification, (c) binding-induced conformational changes, and (d) protease activity. Reproduced with permission (*101*).

SUMMARY

It is clear that both QDs and GFP-like FPs have many characteristics that have facilitated their successful application in biosensing. The unique optical properties of QDs facilitate highly sensitive detection of multiple analytes through multiplexing. The broadening range of available FPs is expanding the possibilities for efficient FRET and multiplexing potential even as the variety of the genetically encoded biosensors expands. There were, however, no examples in the literature of these two fluorescent indicators being used in conjunction for FRET-based biosensing. The studies performed in the pursuit of this thesis aim to demonstrate the potential of using these two components in tandem. QD-FP hybrid devices exploit the advantages of each fluorophore by utilizing the QD brightness to enhance sensitivity and FRET efficiency and by genetically engineering sensor-specific regions directly into the FP. Important issues include, but are not limited to, the synthesis of such hybrid probes, i.e. QD-protein conjugation, and evaluation of the optical properties of the devices.

CHAPTER 4

MATERIALS AND METHODS

MATERIALS

Quantum Dots

Quantum dots (QDs) were acquired from several sources for the studies included in this thesis. Several varieties of EviTags produced by Evident Technologies (Troy, NY) were used in the completion of Aims 1 and 2 (Chapter 5 and Chapter 6). T2-MP EviTags are Evident Technologies' CdSe/ZnS core-shell quantum dots, called EviDots, coated with 1,2-distearoyl-*sn*-glycero-3-phosphoethanolamine-N-[polyethylene glycol-2000] (ammonium salt), i.e. DSPE-PEG_{2000}, from Avanti Polar Lipids (Alabaster, Alabama). In Chapter 5, three different varieties of the EviTags emitting at 540 nm were tested, each with a slightly different lipid-PEG coating. Although all three varieties were made water soluble using DSPE-PEG_{2000}, the functional group on the PEG terminus is varied, making three distinct quantum dots. Specifically, the lipid-PEG was terminated with either a carboxyl group, an amine, or a methoxyl group, forming the so-called carboxyl-functionalized, amine-functionalized, and non-functionalized EviTags, respectively. In Chapter 6, all of the EviTags employed were carboxyl-functionalized, but three different wavelength emitters were utilized, specifically QDs emitting at 520 nm, 540 nm, and 560 nm. (Note: EviTags are now sold as eFluor Nanocrystals by eBioscience in San Diego, CA).

Qdot ITK quantum dots from Invitrogen's Molecular Probes division (Eugene, OR) were included in the studies presented in Chapter 5 and Chapter 7. Qdot ITK

carboxyl quantum dots are CdSe/ZnS nanocrystals water-solubolized with a polymer that contains a high density of carboxyl groups at the particle surface. 545 nm Qdot ITK carboxyl quantum dots were employed in Chapter 5 while 525 nm Qdot ITK carboxyl quantum dots were used for the work presented in Chapter 7. The Qdot ITK carboxyl quantum dots are derivatized with the addition of amine-terminated PEG2000 molecules to create Qdot ITK amino-PEG quantum dots. Data using the 545 nm Qdot ITK amino-PEG quantum dots are presented in Chapter 5.

Quantum dots coated using ligand exchange were kindly provided by collaboration partners at the Naval Research Laboratories (NRL) in Bethesda, Maryland. These QDs are again CdSe/ZnS nanocrystals. In this case, however, the trioctylphosphine/trioctylphosphine oxide (TOP/TOPO) surfactant that is present on the surface of the nanoparticles following their synthesis in organic solvents was physically removed and replaced with a thiol-containing molecule, specifically dihydrolipoic acid (DHLA) or one of its derivatives. Three variants of DHLA-coated QDs were used in the study presented in Chapter 5. All three originated from the same batch of 550 nm emitting QDs and were coated with DHLA or DHLA derivatized with hydroxyl- or methoxy-PEG, i.e. DHLA-PEG_{600}-OH and DHLA-PEG_{750}-OCH_3, respectively, also called DHLA-PEG and DHLA-mPEG.

PCR Primers

The dioxyribonucleic acid (DNA) primers used for modifications to plasmids in polymerase chain reaction (PCR) protocols were special ordered from Integrated DNA Technologies, Inc. (IDT; Coralville, IA). A list of the primers used is included in Table 4.1.

Table 4.1: List of PCR primers.

Primer	Primer Sequence	Purification[a]
50	5'-/5Phos/**CAT CAC CAT CAC CAT CAC GGA GGT GGA** GTG AGC AAG GGC GAG GAG-3'	HPLC
51	5'-/5Phos/**CAT CAC CAT CAC CAT CAC CAT CAC CAT CAC GGA GGT GGA** GTG AGC AAG GGC GAG GAG-3'	PAGE
63	5'-/5Phos/GTG AGC AAG GGC GAG GAG-3'	S.D.
91	5'-TAA TAC GAC TCA CTA TAG GG-3'	S.D.
98	5'-ACC CCG CAT ATG TAT ATC TCC TTC TTA AAG-3'	S.D.
114	5'-/5Phos/GAG GCC T**G**C TCC GAG CG-3'	S.D.
116	5'-/5Phos/CCA GCC CAT GGT CTT CTT CTG-3'	S.D.
118	5'-/5Phos/CTT CAG GGC GCC GTC CTC-3'	S.D.
122	5'-/5Phos/GGC GAG A**A**C AAG CAG AGG CTG-3'	S.D.
127	5'-TAG TTA TTG CTC AGC GGT GG-3'	S.D.
132	5'-/5Phos/GGC GAG AAC AAG ATG AGG CTG AAG-3'	S.D.
133	5'-/5Phos/CTT CAG GGC GCC GTC CTC-3'	S.D.
134	5'-/5Phos/CGA GAT CAA GAA AAG GCT GAA GCT G-3'	S.D.
135	5'-/5Phos/CCC TTC AGG GCG CCG TC-3'	S.D.
145	5'-/5Phos/GAA TTC GAA GCT TGA TCC GGC TG-3'	S.D
146	5'-/5Phos/TTA ACG ACG ACG ACG ACG ACG ACG ACG ACG CTT GTA CAG CTC GTC CAT GCC-3'	S.D.

[a]HPLC: high performance liquid chromatography; PAGE: polyacrylamide gel electrophoresis; S.D.: standard desalting

Chemicals

Luria Bertani (LB) agar, LB broth, ampicillin (Amp), chloramphenicol (Cam), lysozyme: chicken RZ3 (muramidase), isopropyl-β-D-thiogalactoside (IPTG), and imidazole were purchased from US Biological (Swampscott, MA). Phosphate buffered saline (PBS) envelopes, bovine serum albumin (BSA), sodium choloride, sodium phosphate, imidazole, Tris-EDTA (TE) buffer (50x solution), borax, and nickel (II) chloride were procured from Sigma Aldrich (St. Louis, MO). A HHHHHHHHHH peptide (His10) was custom synthesized by AnaSpec (San Jose, CA).

Purified His-tagged maltose binding protein (His5-MBP) was provided by our collaborators at NRL.

METHODS

Protein Engineering

pRSET-b plasmids containing inserts for the fluorescent proteins (FP) mOrange, tdTomato, and mCherry were kindly provided by Roger Tsien's laboratory at the University of California, San Diego. These plasmids were modified using a PCR insertion/deletion protocol to produce the control FPs, which lack a terminal polyhistidine sequence, and His6- and His10-FPs, which contain a polyhisititidine sequence linked to the fluorescent protein with three glycines. The forward primer #63 was used to produce the non-His-tagged control proteins (see Table 4.1), while the forward primers #50 and #51 were used to create the His6- and His10-tagged proteins, respectively. In all three cases, the reverse primer #98 was used, which binds to the template plasmid in a position so as to remove an unnecessary multiple cloning site, a His6-tag that was present in the original plasmid, an Xpress Epitope, and an enterokinase cleavage site from the N-terminus region of the original plasmid. In order to maintain a reasonable melting temperature for the PCR reaction, however, it was necessary to retain two non-critical amino acids at the N-terminus, specifically an arginine and a glycine.

Phusion High-Fidelity Master Mix (New England Biolabs (NEB), Ipswich, MA) was used for all PCR reactions with 10 pg template DNA and 25 pmol of each primer per 50 µl reaction. Thermocycler conditions were chosen as directed in the Phusion manual with an annealing temperature of 69.6˚C being used for each of the reactions described above.

Following the PCR insertion or mutagenesis, which involved amplifying the entire plasmid *in vitro* and resulted in a linear plasmid, the plasmid was recircularized by

ligating its blunt ends using the NEB Quick Ligation Kit. After ligation, the plasmid DNA was transformed into a 50 µl aliquot of Subcloning Efficiency™ DH5α™ Competent Cells (Invitrogen) following the manufacturer's protocol. In the final step of the transformation, cells were plated on LB agar plates containing Amp to select for plasmid incorporation and were grown overnight at 37˚C. Tubes containing 5 ml of LB Amp were inoculated with single colonies from the plates and grown overnight to produce cultures from which to isolate the plasmid. The Promega Wizard® Plus Miniprep Kit was then used as directed to purify the plasmid DNA. The plasmids were analyzed for concentration and purity using UV-Vis absorbance measurements at 230, 260, and 280 nm with either an Ultrospec 2100 *pro* UV/Visible Spectrophotometer (GE Healthcare Life Sciences, Pittsburgh, PA) or a NanoDrop ND-1000 Spectrophotometer (Thermo Fisher Scientific, Inc., Wilmington, DE) before being sent to the Nevada Genomics Center (Reno, NV) for sequencing using primers #91 and #127 (Table 4.1).

The non-fluorescent, non-chromogenic GFP-like protein His6-mCherry-NF was produced by making three single point mutations to the His6-mCherry plasmid produced as described above. The S144C, I161N, and Q163M mutations were introduced sequentially using PCR mutagenesis protocols. The pHis6-mCherry plasmid was first amplified using primers #114 and #116 (Table 4.1) to produce pHis6-mCherry-S144C. The resulting plasmid was ligated, transformed, amplified, purified, and sequenced as described above. The mutation process was repeated utilizing primers #118 and #122 to produce pHis6-mCherry-S144C-I161N and again with primers #132 and #133 to create pHis6-mCherry-S144C-I161N-Q163M. The mOrange M163K point mutation was introduced using primers #134 and #135.

FPs that contained a polyhistidine tag at the N-terminus and a polyarginine tail at the C-terminus were produced by modifying the pHis6-FP plasmids with the same PCR insertion protocol described above using primers #145 and #146 (Table 4.1).

Protein Production and Purification

Plasmids coding for the FPs were transformed into the Rosetta 2(DE3) strain of *E.coli* (Novagen, Madison, WI) per the manufacturer's protocol and plated on LB/Amp/Cam agar plates for selection. Single colonies were plucked from the plates for overnight cultures in 10 mL LB/Amp/Cam broth grown at 30˚C and 200 rpm. The overnight cultures were used to inoculate 500 mL cultures, which were incubated at 37˚C and 200 rpm. After 3-4 hours, the cultures were induced with 0.5 mL of 1 M IPTG. After culturing another 5-6 hours at 37˚C or overnight at 30˚C, the *E.coli* were pelleted at 5,000 rpm in 500 mL jars in a Beckman J2-21 centrifuge. The cell pellets were frozen at -20˚C until they were needed.

The cell pellets containing expressed fluorescent protein were thawed and resuspended in 25 mL TE buffer. To digest the cells, the suspension was incubated with 25 mg of lysozyme for one hour on ice. While on ice, the cells were further disrupted with five cycles of sonication (ten seconds on, ten seconds off) with the Branson Sonifier 150 sonicator probe at level four. The cell slurry was centrifuged for fifteen minutes at 15,000 rpm in 50 mL tubes in the Beckman JA-21 centrifuge to produce a cleared cell lysate. Ammonium sulfate precipitation was used to isolate the protein from the rest of the cell lysate.

Chromatographic methods were used to extract each protein of interest from the protein mixture using an ÄKTAprime plus system (GE Healthcare, Piscataway, NJ). His-

tagged protein precipitates were resuspended in HisTrap Binding Buffer (20 mM sodium phosphate, 0.5 M NaCl, 30 mM imidazole, pH 7.4) and centrifuged to remove any insoluble fractions. The His-tag facilitated binding of the protein to a 1 or 5 mL HisTrap HF column and the low concentration of imidazole in the binding buffer minimized non-specific binding of non-His-tagged proteins. After washing with the binding buffer, the protein was eluted using a linear gradient that gradually increased the imidazole concentration up to 500 mM. The elution fractions containing the fluorescent protein were concentrated and buffer-exchanged into PBS using centrifugal filtration devices (Centricon Plus-20; Millipore, Bedford, MA).

Purification of the untagged proteins required two discrete chromatographic methods used in sequence: proteins were separated first using a hydrophobic column (HiPrep 16/10 Butyl FF) followed by size-exclusion chromatography (HiPrep 16/60 Sephacryl S-300 HR). The protein precipitate was solubolized in TE buffer containing 30% ammonium sulfate and centrifuged to remove any insoluble proteins. Using this concentration of ammonium sulfate, the FPs were soluble in solution, but precipitated on the hydrophobic column. Following ample washing with that same buffer, a linear gradient that gradually eliminated the ammonium sulfate in the buffer was used to elute the protein. The elution fractions containing the fluorescent proteins were concentrated and buffer-exchanged into PBS using centrifugal filtration devices prior to size-exclusion chromatography (SEC). Following SEC the protein-containing fractions were again concentrated using the centrifugal filtration devices.

The proteins were aliquoted into PCR tubes and snap frozen in liquid nitrogen as previously described (*103*). The protein purity was checked with SDS-PAGE, and the

protein concentrations were determined using a BCA Assay (Pierce, Rockford, IL) or by measuring the absorbance spectra of the protein solution and applying the molar extinction coefficients published in the literature (*91*) to calculate the concentration of functioning fluorophores.

Circular Dichroism

Circular dichroism was used to confirm the presence of the characteristic β-barrel structure of the GFP-like fluorescent proteins. This was used to verify that point mutations incorporated to produce the non-fluorescent GFP-like protein mCherry-NF did not inhibit the formation of the chromophore by dramatically altering the protein structure and tested whether structural changes in response to pH could explain the pH-sensitivity of mOrange and mOrange M163K. Protein solutions at a concentration of either 20 or 30 μM were measured on a Jasco J-815 CD Spectrometer (Jasco, Inc., Easton, MD) with a 1 nm stepsize. The measurements of mOrange and mOrange M163K started in 20 mM phosphate buffered saline, pH 10.0, and were titrated with 1 N HCl.

The recorded spectra in millidegrees of ellipticity (θ) were converted to mean residue ellipticity ([θ]) using the equation:

$$[\theta] = \frac{\theta \times 100 \times M}{c \times l \times n_r}, \qquad (1)$$

where c is the concentration of the protein in mg/ml, l is the pathlength in cm, M is the protein molecular weight, and n_r is the number of amino acid residues. All presented spectra are the average of three accumulations.

Quantum Dot and Fluorescent Protein Spectral Measurements

The QD absorbance spectra of the stock solutions were taken using a NanoDrop ND-1000 with a stepsize of 3 nm. The QD emission spectra as well as the excitation and emission scans of the fluorescent proteins were all measured on a Tecan Safire multiplate reader (Durham, NC) using 1 nm stepsizes, excitation bandwidths of 12 nm, and emission bandwidths of 5 nm. Non-binding black flat-bottomed 384-well plates from Corning were used for all fluorescence measurements on the Tecan Safire. A 100 nM solution of the EviTags were used to take emission spectra with an excitation at 400 nm. The fluorescent proteins were diluted to 5 µM for the spectral measurements. The excitation spectrum of mOrange was taken from 450 – 590 nm with a fixed emission wavelength of 605 nm. The same protein was excited at 500 nm for the measurement of its emission. tdTomato was excited at 510 nm for the emission measurement, and the emission was fixed at 620 nm while the excitation spectrum was taken. The excitation spectrum of mCherry was taken with a fixed emission wavelength of 650 nm, while the excitation wavelength was static at 550 nm during the emission scan. Spectra were graphed in Igor (v5.05A, Wavemetrics Inc., Lake Oswego, OR).

Dynamic Light Scattering Measurements

In order to make a proper comparison of the eight different quantum dots studied in Aim 1, the hydrodynamic diameter and zeta potential of each variety were measured. Dynamic light scattering (DLS) was used to measure the hydrodynamic diameter and zeta potential using the Nicomp 280 from Particle Sizing Systems (PSS; Goleta, CA). Each QD stock solution was diluted with distilled water and filtered through a 0.2 µm syringe filter before the hydrodynamic diameter was measured. The same sample was then

further diluted with distilled water for measurement of the Zeta potential at pH 7. Subsequently, a KOH solution in water was added to the sample to raise the pH to 9.5 before the Zeta potential was measured again.

Quantum Yield Measurements

The absorbance and emission spectra of a series of dilutions of QDs were measured using an Ultrospec 2100 *pro* UV-Vis Spectrophotometer and a Tecan Safire^2 multiplate reader (Männedorf, Switzerland), respectively. The QD quantum yields were measured against rhodamine 6G in water.

The integrated emission was plotted against the peak absorbance for each of the dilutions of the QDs and rhodamine. The data points for each were fitted to a line and the slopes were used in the following equation to determine the QYs:

$$\Phi_{QD} = \Phi_R \left(\frac{Slope_{QD}}{Slope_R} \right) \left(\frac{\eta_{QD}^2}{\eta_R^2} \right), \qquad (2)$$

where the subscripts *QD* and *R* stand for the QDs and rhodamine, Φ is the fluorescence quantum yield, *Slope* is the slope of the linear fit of the integrated emission versus absorbance, and η is the refractive index of the solvent, which was assumed to be 1.33 for both the QDs and rhodamine.

Quantum Dot Stability Assay

Quantum dot stock solutions were diluted into either 10 mM tetraborate buffered saline, pH 9.5, or 10 mM tetraborate buffer with 1 M NaCl, pH 9.5, to a concentration between 100 and 200 nM in 384 well flat-bottomed, black well plates. The fluorescence emission spectra were measured in a Tecan Safire^2 with 400 nm excitation as soon as feasible and every ten minutes thereafter for a total of 50 measurements. The

photoluminescence intensity at its peak wavelength was normalized to the maximum intensity for that QD and buffer condition and plotted *versus* time to see how the fluorescence of that nanoparticle changed with time in the assay conditions used for the study described in Chapter 5.

Spectral Overlap and Förster Distance Calculations

Igor software was used as previously described (*4, 104*) to calculate the overlap integral and Förster distance for each of the possible FRET pairs. The spectral overlap integral:

$$J = \int F_D(\lambda)\varepsilon_A(\lambda)\lambda^4 d\lambda \qquad (3)$$

describes the degree of coincidence between the donor emission and the acceptor absorption, where F_D is the normalized emission spectrum of the donor, ε_A is the molar extinction coefficient of the acceptor, and λ is the wavelength in nanometers (*4*). Once the overlap integral was calculated, the Förster distance (R_0), the distance between the donor and acceptor at which the FRET efficiency is 50%, was determined using the equation:

$$R_0^6 = 8.785 \times 10^{-5} \kappa^2 Q_D \frac{J}{n_r^4}, \qquad (4)$$

where κ^2 is the dipole orientation factor, assumed to be ⅔, Q_D is the quantum yield of the donor, and n_r is the refractive index of the medium (*4*).

FRET Assay Protocol (Chapter 5)

Assays assessing the binding of His-tagged mCherry to diverse QDs were conducted by measuring the FRET efficiency of the various pairs in black, flat-bottomed, non-binding 384-well plates (Corning). QDs and FPs were mixed directly in the well plates with a final QD concentration of 50 nM and 1 to 12 molar equivalents of protein

per QD in either 10 mM tetraborate buffered saline, pH 9.5 or 10 mM tetraborate buffer, 1M NaCl, pH 9.5, as indicated. After allowing at least 15 minutes for self-assembly, the emission spectra of the FRET pairs were measured in a Tecan Safire^2 multiplate reader with an excitation wavelength of 400 nm, excitation bandwidth of 10 nm, emission bandwidth of 5 nm, integration time of 100 μs, and a stepsize of 2 nm. All of the assays were performed in triplicate, as were FP-only controls.

For QD-FP binding studies involving Ni^{2+}, the FRET pairs were measured first with just the QDs and FPs present, then 1 μL of 20 mM $NiCl_2$ was added to the 80 μL reaction volume, resulting in a final Ni^{2+} concentration around 250 μM. The solutions were incubated at room temperature for at least fifteen minutes to allow binding to reach a steady state and then the emission spectra were measured in the Tecan Safire^2 multiplate reader.

Modified FRET Assay (Chapter 5)

Both the DHLA QDs and carboxyl-functionalized EviTags were utilized in an alternative FRET assay, where the number of fluorescent protein acceptors was varied, but the same total number of His-tagged proteins was maintained in each reaction well. The DHLA QDs were incubated with a total of twelve proteins per QD, with either His5-MBP or His6-mCherry-NF making up the balance between the number of His6-mCherry molecules and the total number of proteins per QD. The carboxyl-functionalized EviTags were incubated with a total of six proteins, using combinations of His6-mCherry and His6-mCherry-NF.

FRET Assay Protocol (Chapter 6)

Alternating serial dilutions of the acceptor molecule were made in 384 well plates to produce a range of average QD:FP ratios ranging from 16 FPs per QD to fewer than 0.2 FPs per QD. EviTag QDs were then added to the wells at final concentration of 50 nM. All of the assays were prepared in PBS, pH 7.4, with 1% BSA added to minimize non-specific binding. After a 15 minute incubation to allow for self-assembly, the emission spectra were measured in a Tecan Safire multiplate reader with an excitation wavelength of 400 nm, excitation bandwidth of 12 nm, emission bandwidth of 5 nm, and a stepsize of 3 nm. Assays were performed using His-tagged fluorescent proteins, non-His-tagged fluorescent proteins, and a His10 polypeptide. All of the assays were performed in triplicate, as were FP-only controls.

FRET Assay Analysis

Prior to analysis, the FRET spectra were corrected for any background emission due to the direct excitation of the acceptor, autofluorescence of the buffer (particularly when the buffer contained BSA), and detector noise. To this end, the emission spectra from the FP-only control wells were subtracted from each of the FRET spectra at the same FP concentration. Each background-subtracted spectrum was then deconvolved using PeakFit (v.4.12, Systat, San Jose, CA); the symmetrical EviTag emission was fitted to a Voigt Area peak, while an exponentially modified Gaussian (EMG) curve was used to account for the tailing seen in the asymmetrical FP emission. The areas under the QD peaks with FRET were normalized by the area under the QD spectrum in the absence of FP. The resulting normalized QD emission intensities were plotted versus the acceptor concentrations.

The FRET efficiencies at each specific QD:FP ratio were calculated using the equation:

$$E = 1 - \frac{F_{DA}}{F_D}, \quad (5)$$

where F_{DA} is the fluorescence of the donor in the presence of the acceptor and F_D is the fluorescence of the donor in the absence of the acceptor (*4*).

Curve-fitting

The non-His-tagged FP results were fitted to the Stern-Volmer equation:

$$\frac{F_D}{F_{DA}} = 1 + K_{SV}[Q], \quad (6)$$

where [*Q*] is the quencher concentration, and K_{SV} is the Stern-Volmer quenching coefficient.

In order to estimate the strength of binding between the EviTags and the His-tagged proteins under steady-state conditions, the His6- and His10-FP data were fitted to a modified Hill equation. The traditional Hill equation (*105*):

$$\theta = \frac{1}{1 + \left(\frac{K_D}{c}\right)^h}, \quad (7)$$

relates the fraction of ligand binding sites filled (θ) to the ligand concentration I, the dissociation constant or ligand concentration at which 50% of the binding sites are filled (K_D), and the Hill coefficient (*h*). Several assumptions were made to adapt this equation for the current application. First, the number of ligand binding sites filled is not being measured, but rather the fluorescence emission of the QD in the presence of the ligand, i.e. the fluorescent protein. Because the fluorescence does not change uniformly

regardless of the ligand used, but rather depends on the effectiveness of the donor-acceptor pair being studied, the FRET efficiency (E_{max}) of the pair is included in the expression. Also, because the fluorescence decreases with increased binding, the expression is subtracted from the maximum possible value, which for the normalized fluorescence is unity. These changes result in the expression:

$$\frac{F_{DA}}{F_D} = 1 - E_{\max}\left[\frac{1}{1+\left(\frac{K_D}{c}\right)^h}\right], \tag{8}$$

where F_{DA} is the fluorescence of the donor in the presence of the acceptor, F_D is the fluorescence of the donor in the absence of the acceptor, and E_{max} is the maximum FRET efficiency (*106*). In this case, the nominal K_D is not the concentration at which there is 50% binding, but rather the concentration at which there is 50% quenching of the QD. The two are distinct because the fluorescent quenching is not linearly related to the number of acceptors bound (*4*, *10*).

Calculation of Donor-Acceptor Distance

Using the FRET efficiencies determined for each QD:FP ratio and the Förster distance (R_0) calculated for each FRET pair, the distance between the donor and the acceptor, R, was estimated using an equation that takes into account the binding of multiple acceptor FPs to each donor QD. The equation used for the FRET efficiency as a function of n, the average number of acceptors attached to the donor, is given by (*4*, *10*):

$$E(n) = \frac{nR_0^6}{nR_0^6 + R^6}. \tag{9}$$

For any given ratio of donors to acceptors (or average number of acceptors per donor), the specific number of acceptors, *k*, attached to the donors is described by a Poisson distribution (*107*):

$$p(k,n) = \frac{n^k e^{-n}}{k!} \quad (10)$$

The efficiency of the FRET interaction can be more accurately calculated for each donor-acceptor ratio using a weighted distribution of efficiencies, taking into account the effect of the Poisson distribution (*14*, *82*):

$$E(n) = \sum_n p(k,n)E(k) = \sum_{k=1}^{\infty} \frac{n^k e^{-n}}{k!} \frac{kR_0^6}{\left(kR_0^6 + R^6\right)} \quad (11)$$

We used Mathematica (v.6.0.1, Wolfram Research, Inc., Champaign, IL) to solve this equation for *R* for each value of *n* for each FRET pair.

pH Sensor Bioconjugation

Various fluorescent protein variants were covalently coupled to Invitrogen 525 nm ITK Carboxyl Qdots using standard carbodiimide chemistry (*61*). The 8 µM Qdot stock solutions were diluted 1:10 in 10 mM borate buffer, pH 7.4, with a 40-fold molar excess of protein and 1,500-fold molar excess of EDC. The reaction mixture was protected from light and incubated overnight at 4˚C. Excess EDC and unbound protein was removed using a centrifugal filtration device with 100 kDa molecular weight cutoff (Microcon Ultracel YM-100, Millipore) at 1000 rcf. This procedure was applied to make probes with His6-mOrange, His6-mOrange M163K, and His6-mCherry-NF.

The Beer-Lambert Law:

$$A = \varepsilon \cdot c \cdot l \ , \qquad (12)$$

where A is the absorbance, ε is the molar extinction coefficienct (M^{-1} cm^{-1}) and l is the pathlength of the cuvette (cm), was used to determine the probe concentration using the Qdot $\varepsilon_{405\ nm}$ of 360,000 M^{-1} cm^{-1} (Invitrogen product data sheet). For probes containing fluorescent proteins (excludes probes made with mCherry-NF variants), the degree of conjugation was determined by comparing the absorbance spectra of the probe to the absorbance profile of unconjugated Qdots. By subtracting the Qdot spectra from the probe spectra, the spectra of the conjugated protein could be isolated. The Beer-Lambert Law was used to determine the number of proteins per Qdot using the measured molar extinction coefficients (see below).

pH Titrations of mOrange, QDs, and FRET Probe

mOrange and mOrange M163K were analyzed for their spectral properties in response to changes in the solution pH, as were their QD-conjugated probes. For absorption, fluorescence excitation, and fluorescence emission spectroscopy, the proteins were diluted in 20 mM phosphate buffered saline with 1% (w/v) BSA, pH 10.0. The BSA served to block protein adsorption to the cuvette surfaces. This precaution was found to be important because adsorption profiles could vary with pH, introducing error into the measurements.

Titrations were performed by adding small, regular volumes of 1 N HCl to the buffer and mixing thoroughly. This procedure was first performed on the buffer and the pH measured with a pH meter (Orion perpHect LogR meter model 310) and the appropriate volumes of acid to be added were determined to ensure regular spacing of the measurements. Absorbance spectra were measured on the Ultrospec 2100 *pro* UV/Visible

Spectrophotometer with 1 nm step sizes. Excitation spectra with 5 nm stepsize were measured on a Horiba Jobin Yvon Fluorolog-3 Spectrofluorometer with 1 nm excitation bandwidth and 5 nm emission bandwidth at 585nm. Emission spectra were measured with 1 nm excitation bandwidth at 525 nm and 3 nm emission bandwidth and a 5 nm step size.

Molar extinction coefficients for mOrange and mOrange M163K were extracted using the absorption spectra and the Beer-Lambert law. For the sake of obtaining the most accurate concentration measurement of the proteins possible for use in the molar extinction coefficient determination, protein samples were sent to the W. M. Keck Foundation Biotechnology Resource Laboratory at Yale University for amino acid analysis. There the protein samples were hydrolyzed and analyzed on a Hitachi amino acid analyzer. The protein concentrations were back-calculated from the nanomoles of individual amino acids measured from the resulting spectra using the known protein sequence.

CHAPTER 5

SURFACE-LIGAND EFFECTS ON METAL-AFFINITY COORDINATION TO QUANTUM DOTS: IMPLICATIONS FOR NANOPROBE SELF-ASSEMBLY*

INTRODUCTION

The integration of biomolecules and inorganic nanocrystals into functional devices is a core requirement for future advances in nanobiotechnology. By developing protocols that yield better understanding and, ultimately, control of the construction of these hybrid devices, we will be able to design nanoparticle-based imaging probes and delivery systems in a much more concerted and deliberate manner.

Assembly of biomolecule-QD constructs has proven to be a challenge even as orthogonal bioconjugation techniques become available (*61*). An optimal bioconjugation strategy would be quick and facile with high affinity, would not require subsequent purification, and would enable control of the molar ratios of the component parts, all while not disrupting the biological function of the biomolecule. Standard protocols include chemical coupling with covalent bonds (*61*), non-covalent interactions exploiting ligand-receptor affinities such as biotin-avidin binding (*71*), and more general affinity-driven self-assemblies using electrostatic interactions (*46, 108*) or metal chelation (*10, 15, 78, 80-82*). Each of these techniques has advantages and disadvantages, which must be assessed when choosing the bioconjugation method for a particular design of the biomolecule-QD construct.

* Modified from Dennis AM, Sotto D, Mei BC, Medintz IL, Mattoussi H and G Bao. Surface Ligand Effects on Metal-Affinity Coordination to Quantum Dots: Implications for Nanoprobe Self-Assembly, in preparation.

Covalent coupling provides the most durable attachment of a biomolecule to a QD with carbodiimide (EDC) chemistry being the most commonly utilized. However, this often causes nanoparticle aggregation, may result in a relatively low number of biomolecules per nanoparticle compared to the reaction ratios, and often requires purification steps that are also a source of loss, depressing the overall yield of the functional construct (*61*). In addition, the heterogeneous conjugation may cause proteins to attach in an unproductive manner or to lose activity.

Streptavidin-biotin binding is another common and useful coupling mechanism that utilizes exceptionally simple protocols, provided the constituent components are already functionalized with the required streptavidin and biotin moieties. With femptomolar binding affinities, the streptavidin-biotin interaction is often considered to be effectively as stable as a covalent bond (*68*). In some applications, however, the advantages of the streptavidin-biotin interaction may be overshadowed by the tetrameric nature of streptavidin, which can result in undesired multiple binding events and induce aggregation (*73*). With a molecular weight of *ca.* 53 kD, the addition of multiple streptavidin molecules to a single QD adds considerably to the overall size of the nanoparticle construct. This extra protein bulk could be detrimental in applications where the increase in size may impair function. Optical biosensors based on fluorescence resonance energy transfer (FRET), for example, require short distances between their fluorescent donors and acceptors. As the efficiency of energy transfer is inversely related to the donor-acceptor distance to the sixth power (*4*), the additional separation by a few nanometers due to the size of streptavidin can dramatically reduce FRET efficiency.

An alternative assembly option derives from the affinities between biomolecular components and various substrates. These range in strength and specificity from electrostatic interactions to metal chelation to interactions culled from phage display. Although the binding affinities of these reactions cannot rival that of avidin-biotin, advantages arise because the minimal affinity tag can often be naturally incorporated into the biomolecule of interest and bind to the QD without necessitating additional functionalization of the nanoparticle. Self-assembly based coupling requires only small tags, is facile, is typically not intrusive on the other components of the nanoparticle system, is orthogonal to most biological structures and activity, provides reasonable control over the relative component stoichiometries, and utilizes well-established protocols. As this fulfills many of the characteristics of ideal nanoparticle bioconjugation chemistry, it is thus highly desirable.

A specific example of one such small affinity tag is the polyhistidine sequence (His-tag), which has an affinity for divalent cations. It was discovered that His-tag chelation of metal ions, such as Ni^{2+}, Zn^{2+}, or Cu^{2+}, could be used to purify recombinant proteins using immobilized metal affinity chromatography (IMAC) (*79*). More recently, His-tags have been used to bind biomolecules, including proteins, peptides, and even His-modified DNA, to QDs displaying zinc ions on their surface in the form of the ZnS capping layer of the CdSe/ZnS core-shell nanoparticles (*10, 15, 78, 80-82*). Although this coupling technique has been used with success in several QD-based sensing applications, the characteristics of the QD-polyhisitidine interaction appear to vary depending on the particular organic coating used to confer water solubility of the QDs (*83*).

In this chapter, a fluorescence resonance energy transfer (FRET) assay was developed and implemented to study the self-assembly of polyhistidine-tagged fluorescent proteins (FPs) and semiconductor quantum dots (QDs). QDs with eight different organic coatings from three distinct sources were evaluated using the FRET assay to determine their capacity for self-assembly. The three major categories of QDs consist of (1) QDs coated using ligand exchange with DHLA, DHLA-PEG_{600}-OH (DHLA-PEG), or DHLA-PEG_{750}-OCH_3 (DHLA-mPEG); (2) Invitrogen Qdots, which are coated with an amphiphilic block co-polymer, including carboxyl Qdots and amino-PEG Qdots; and (3) lipid-PEG coated QDs, specifically carboxyl-functionalized, amine-

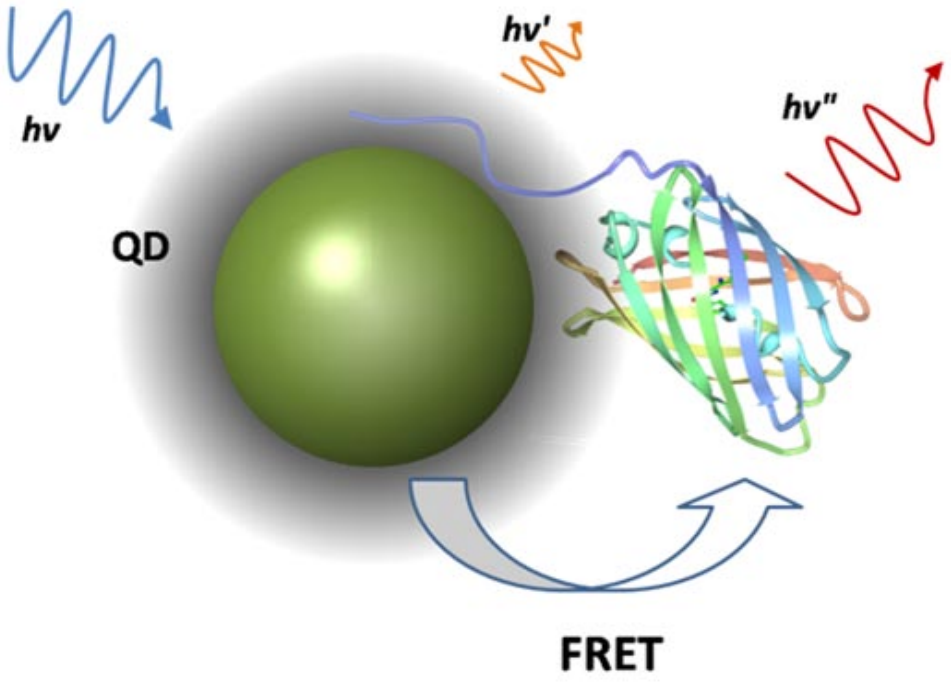

Figure 5.1: FRET-based assessment of QD-FP self-assembly.
Schematic of the FRET assay used to investigate the **H**is-tag self-assembly on quantum dots. An N-terminal polyhistidine sequence is used to assemble mCherry (PDB 2H5Q) on the surface of the quantum dot. If assembly is successful, the proximity of the QD and FP will facilitate energy transfer and a measurable FRET signal will be detected.

functionalized, and non-functionalized EviTags (Evident Technologies). In order to relate the results of the FRET assay to the fundamentals of the interaction between the His-tagged fluorescent protein and the QD, basic QD properties, such as core-shell size, hydrodynamic diameter, zeta potential, quantum yield (QY), and photoluminescence (PL) stability, were first characterized and compared. The advantages and disadvantages of using each QD coating scheme in nanoprobe self-assembly are discussed. The outcomes of this study provide guide for which QD coating is most appropriate for any given biosensor application.

RESULTS

Protein Properties

A non-fluorescent, non-chromogenic GFP-like protein was developed as a control for the effect of His-tag binding on QDs by introducing three point mutations (S144C I161N Q163M) into mCherry to produce His6-mCherry-NF. Circular dichroism (CD) was used to verify the structural similarities with respect to protein folding and secondary structure formation between the proteins His6-mCherry and His6-mCherry-NF. The two CD spectra overlap nicely (Figure 5.2) with minima below 220 nm, which is characteristic of the beta sheets that make up the barrel structure of all GFP-like proteins (Figure 5.2, inset) (*97, 109*).

Absorbance and emission measurements (with excitation at 560 nm) of 10 µM

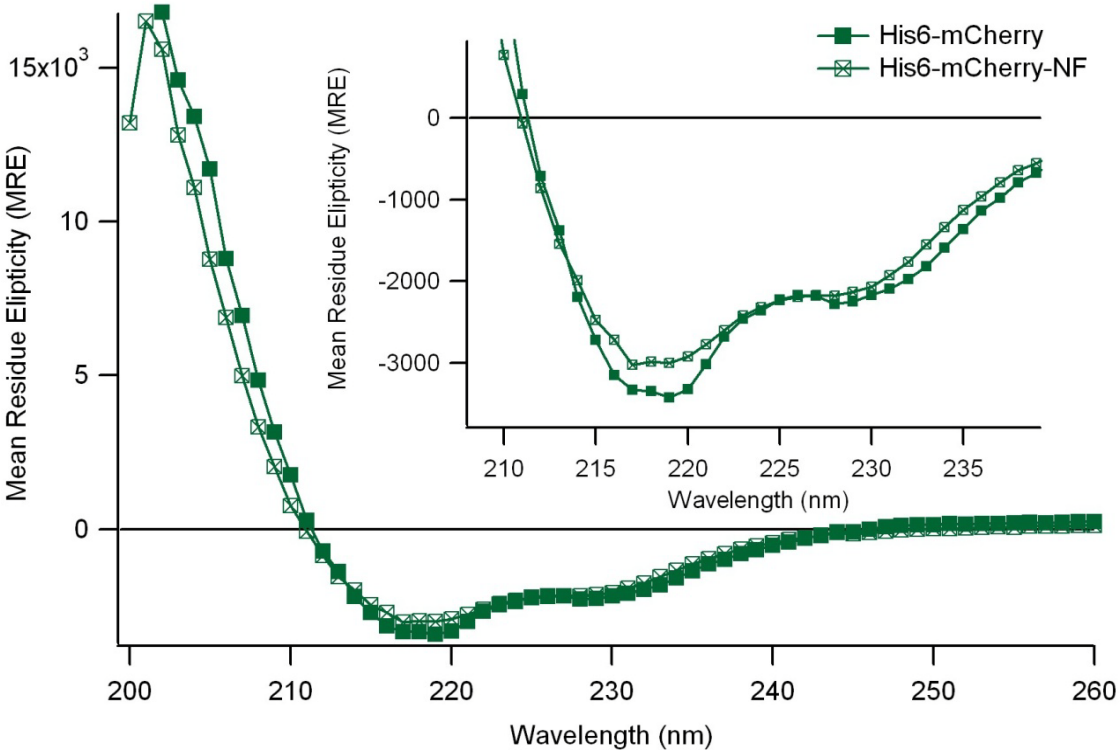

Figure 5.2: CD spectra of His6-mCherry and His6-mCherry-NF.

(28 µg/mL) solutions of the two proteins were made on a Tecan Safire^2 multiplate reader. His6-mCherry-NF showed no capacity for either absorbance or emission in the visible wavelength range (Figure 5.3). The emission of His6-mCherry-NF remained flat even with greatly increased detector sensitivity (data not shown).

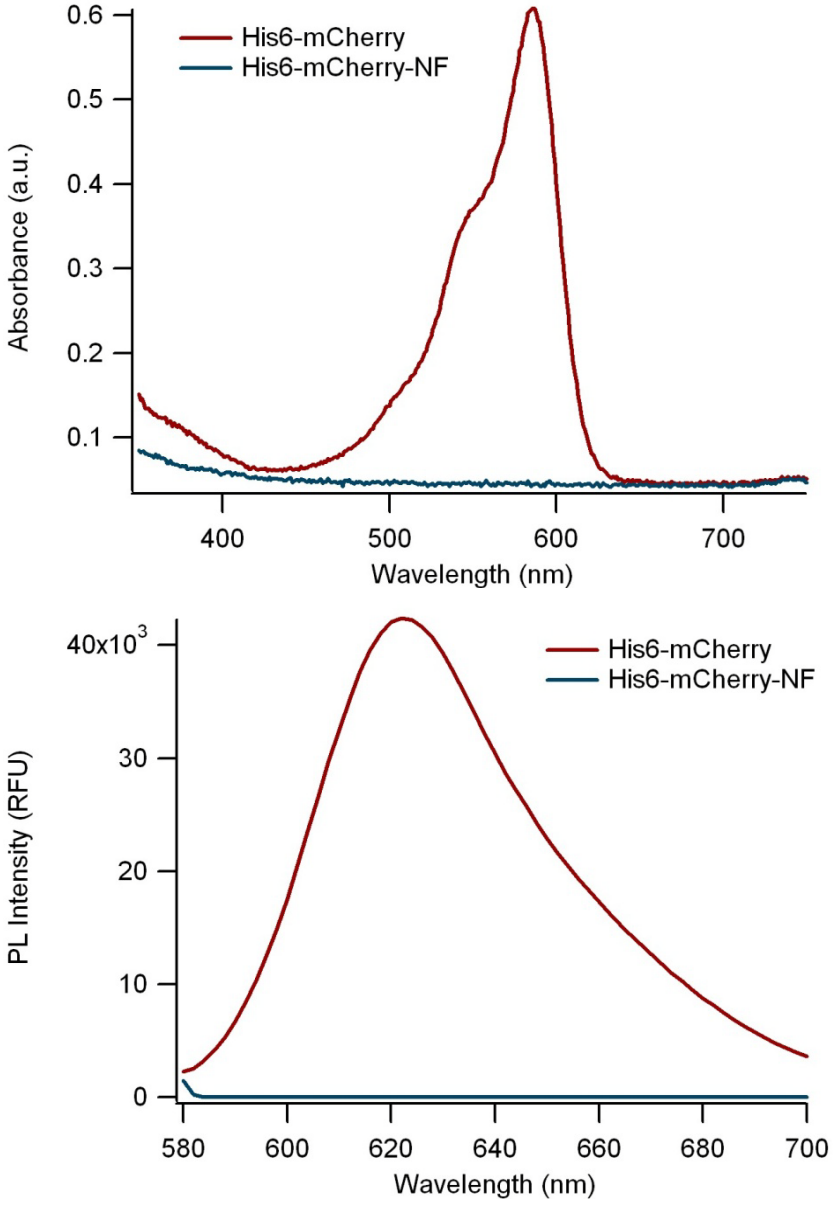

Figure 5.3: Spectral properties of His6-mCherry and His6-mCherry-NF.
Absorbance (top) and emission (bottom) spectra of His6-mCherry and His6-mCherry-NF.

Quantum Dot Properties

Transmission electron microscopy (TEM) images verified that the core-shell sizes of the CdSe/ZnS QDs studied were all approximately 5 nm in diameter regardless of the material source (data not shown). Significant differences in the hydrodynamic diameter were, however, apparent in dynamic light scattering (DLS) measurements (Table 5.1), which reflect the effect of the hydrated organic coating on the particle dimensions in solution.

The hydrodynamic diameter of the three ligand exchange-coated QDs varied as expected with the presence and length of the PEG moiety, ranging from 9.8 to 12.9 nm. All three varieties originated from the same batch of core-shell QDs and had quantum yields between 0.10 and 0.12 (Table 5.1).

The amphiphilic block co-polymer coated carboxyl Qdots from Invitrogen exhibited the smallest hydrodynamic diameter (13 nm) of the commercially available QDs (Table 5.1). The amine-terminated PEG_{2000} chains are conjugated to the carboxyl Qdots to produce amino-PEG Qdots, adding almost 3 nm to the hydrodynamic diameter of the carboxyl Qdots (Table 5.1). Both of these QD varieties have QYs above 0.7.

Table 5.1: Summary of quantum dot properties.

Name	Water-soluble coating	QY[a]	Hydrodynamic Diameter(nm)[b]	Zeta Potential at pH 7 (mV)[c]	Zeta Potential at pH 9.5 (mV)[c]
Evident Technologies: T2-MP EviTags	Lipid-PEG-COOH	0.29	14.9 ± 1.7	-0.6 ± 0.2	-26.5 ± 0.8
	Lipid-PEG-NH_2	0.77	20.8 ± 0.5	-4.0 ± 0.6	-31.8 ± 0.5
	Lipid-PEG-OCH_3	0.39	23.2 ± 0.7	-10.0 ± 0.5	-15.5 ± 1.3
Invitrogen: Qdot 545 ITK	Polymer (-COOH)	0.75	13.0 ± 0.3	-3.4 ± 0.8	-31.0 ± 1.3
	Polymer (-PEG_{2000}-NH_2)	0.74	15.9 ± 0.8	-2.3 ± 0.7	-4.8 ± 1.2
Dihydrolipoic acid (DHLA)-coated QDs	DHLA	0.11	9.8 ± 0.3	-29.8 ± 1.8	-23.3 ± 2.6
	DHLA-PEG_{600}-OH	0.10	12.2 ± 0.9	-12.9 ± 1.3	-34.6 ± 2.0
	DHLA-PEG_{750}-OCH_3	0.12	12.9 ± 0.5	-2.8 ± 0.5	-182 ± 0.6

[a] QY measured relative to Rhodamine 6G in water.
[b] Hydrodynamic diameter values are the mean ± standard deviation of the volume-weighted size distribution.
[c] Zeta potential values are means ± standard deviations of n = 3 or n = 4 measurements.

With an average hydrodynamic diameter of 23.2 nm, the non-functionalized T2-MP EviTags were the bulkiest among the eight types of QDs studied (Table 5.1). Although the amine-functionalized EviTags merely substituted an $–NH_2$ for the $–OCH_3$ terminal group on the non-functionalized EviTags, their hydrodynamic diameter was reduced to 20.8 nm. Changing the terminal functional group to –COOH further reduced the hydrodynamic diameter of the carboxyl-functionalized EviTag to 14.9 nm (Table 5.1). The lipid-PEG coated QDs showed significant batch-to-batch variations in their QYs, with measured values ranging from 0.29 to 0.77.

Quantum Dot Stability

All of the DHLA-coated QDs exhibited an approximately 20% decrease in photoluminescence (PL) in the first several readings after being dispersed in 10 mM tetraborate buffered saline, pH 9.5 (Figure 5.4). While the PEGylated QDs recovered their initial PL intensity, the QDs coated with only DHLA did not recover, but did reach a stasis where the PL was much better maintained from one measurement to the next. All three of the QD types showed slow, but steady, declines in the PL intensity with time. Under high salt conditions (10 mM tetraborate buffer, 1 M NaCl, pH 9.5), the PEGylated QDs did not show the same PL recovery seen in saline, but were stable enough to exhibit only a very gradual decrease in PL intensity with time once equilibrium was reached. The QDs coated with only DHLA, in contrast, were not stable in the high salt conditions and demonstrated a dramatic decrease in PL over time.

The PL of Qdots from Invitrogen also showed instability immediately following dilution into the buffers (Figure 5.5). Although the carboxyl Qdot showed a much larger decrease in PL in the first few measurements than the amino-PEG Qdots, there were not

dramatic differences between the saline and high salt conditions for either Qdot, although the high salt reduced the rate of PL decline in both cases.

All of the EviTags dropped 30 – 40% of their PL in the first few measurements before achieving a certain level of PL stability (Figure 5.6). No significant differences were seen based on coating functionality or buffer conditions.

The PLs were erratic for the first 10% of the stability measurements by time, but thereafter the data points could be fit to a line. The value of that slope was graphed in Figure 5.7 to summarize the differences in the rate of PL change for all of the QDs and buffer conditions. Six of the eight QDs (excepting the DHLA QDs and carboxyl-functionalized EviTags) displayed a less steep slope in the high salt conditions than in buffered saline. This may indicate that the high salt content reduces electrostatic interactions with the vessel surfaces, thereby preventing adsorption of particles to the well plate walls.

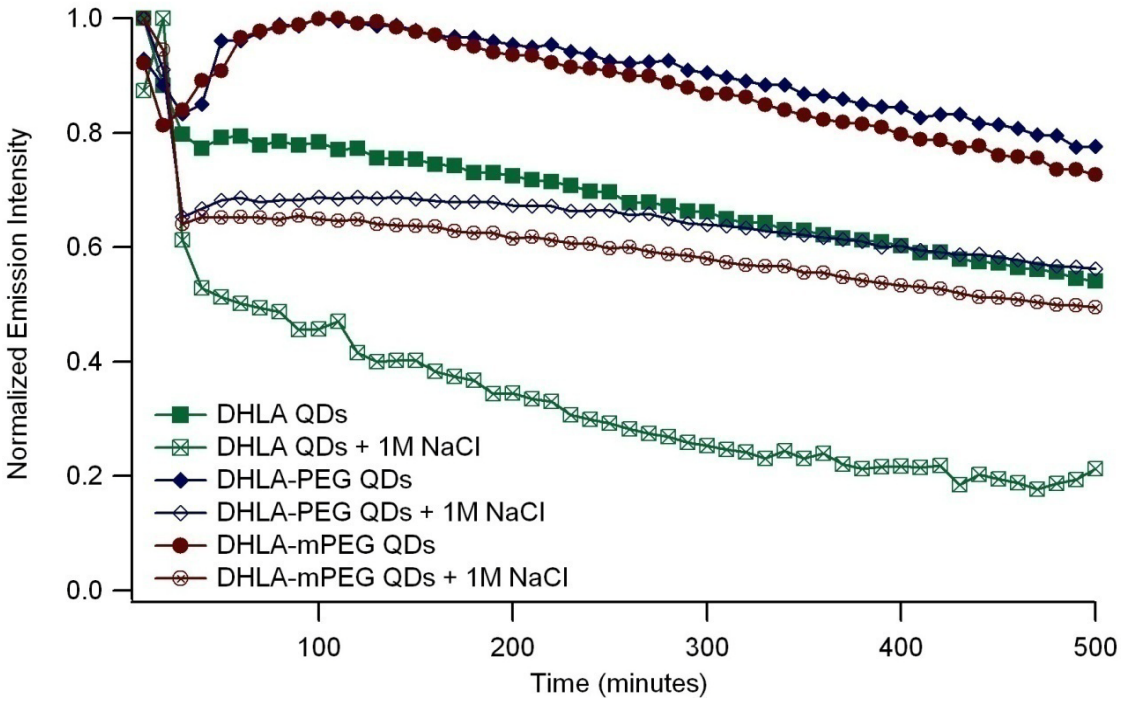

Figure 5.4: Stability plot of DHLA-coated QDs.

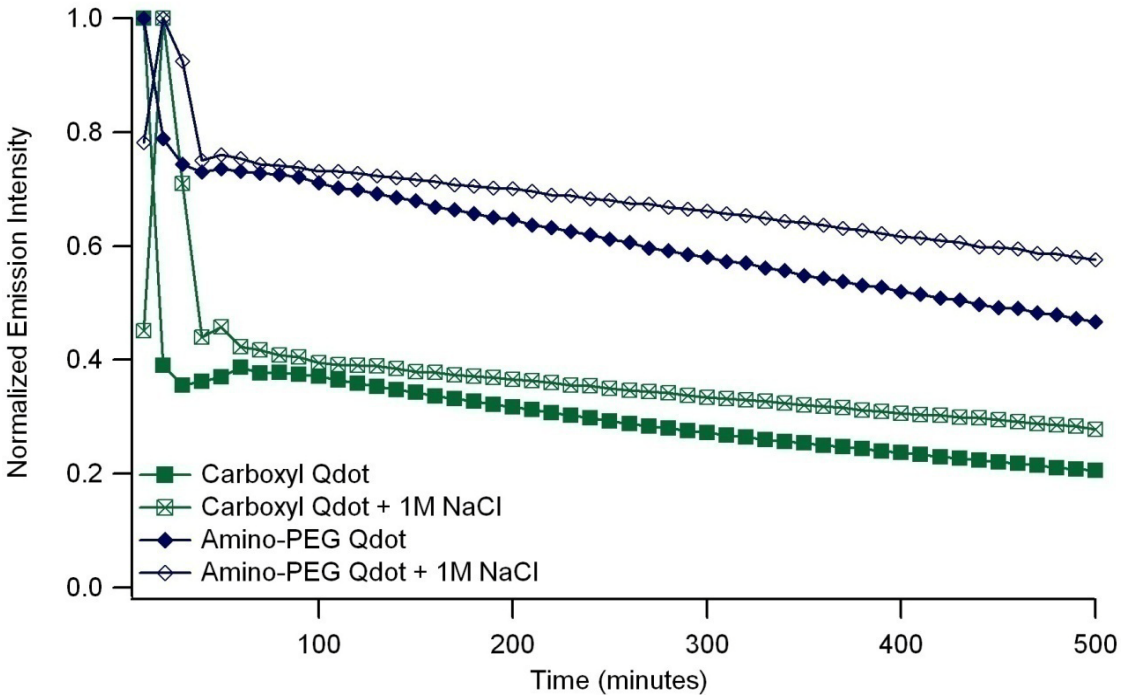

Figure 5.5: Stability plot of Qdots from Invitrogen.

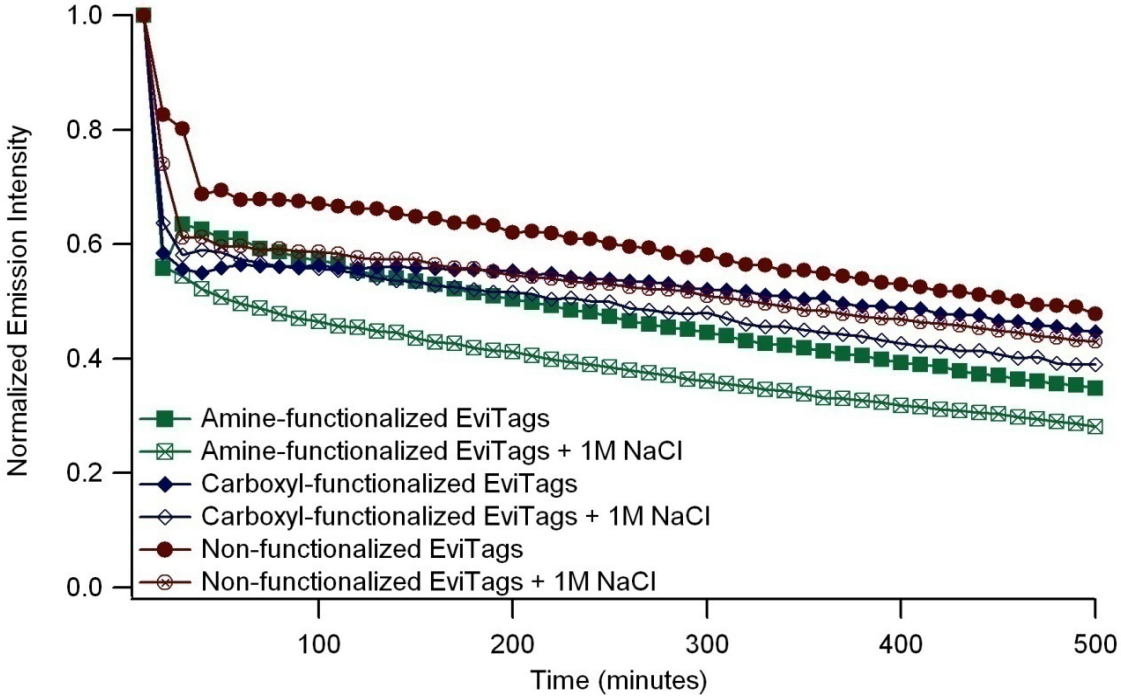

Figure 5.6: Stability plot of T2-MP EviTags.

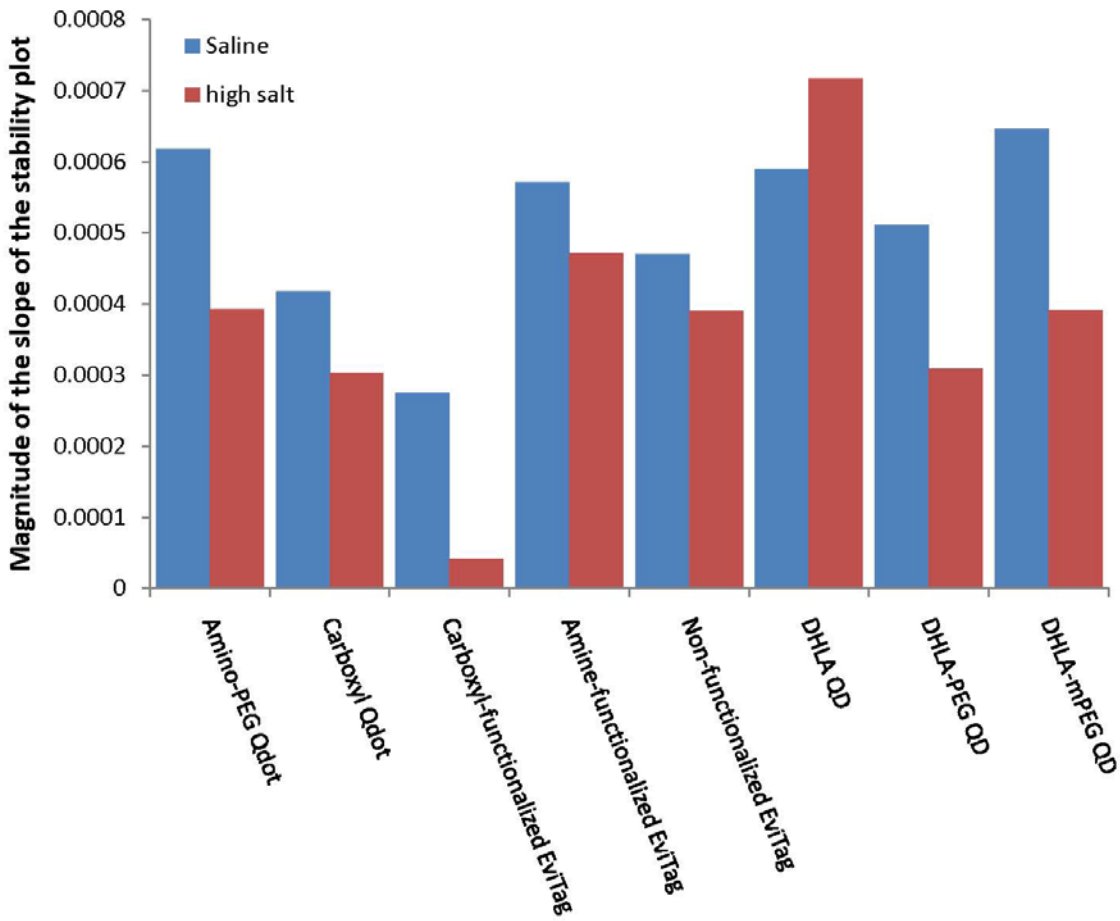

Figure 5.7: Magnitude of the slopes of the stability plots.

FRET Assays

Calculations of the overlap integral and Förster distance for each of the FRET pairs, as well as the FRET efficiency observed at a 1:1 ratio of donors to acceptors and the maximum FRET efficiency observed for each donor-acceptor pair is summarized in Table 5.2.

Our FRET assays revealed that, of the three DHLA-based organic coatings, only QDs coated with DHLA itself demonstrated a significant capacity for self-assembly *via* polyhistidine coordination (Figure 5.8). The spectra plots of the DHLA incubated with

His6-mCherry show a decrease in the QD emission with a concomitant dose-dependent increase in the sensitized emission of the fluorescent protein with a clear isosbestic point around 580 nm (Figure 5.8, top). It was not possible to test the DHLA QDs under high salt conditions because the electrostatically stabilized QDs were not stable in that buffer (Figure 5.4), but the addition of the divalent cation (Ni^{2+}) did not seem to further enhance the interaction between the FPs and the quantum dot (Figure 5.8, bottom). Both PEG-conjugated DHLA moieties exhibited minimal quenching of the QD emission and negligible sensitized emission from His6-mCherry (Figure 5.9 and Figure 5.10).

The carboxyl Qdots from Invitrogen showed only a limited capacity as a FRET donor to the His6-tagged mCherry in borate buffered saline, and this subtle interaction was disrupted in the presence of 1 M NaCl (Figure 5.11). However, a stronger FRET signal was observed following supplementation with $NiCl_2$. The Ni^{2+}-dependent FRET signal was also reduced in the presence of 1 M NaCl, but not eliminated as in the non-Ni^{2+}-dependent case (Figure 5.12). The amino-PEG ITK Qdots showed no difference in QD emission regardless of whether His-tagged or control mCherry was used (Figure

Table 5.2: FRET pair results summary.

FRET Donor (Acceptor: His6-mCherry)	J (10^{-15} M^{-1} cm^3)	R_0 (Å)	E at 1:1 QD:FP	max E
Carboxyl-functionalized 540 nm T2-MP EviTag	4.77	52.6	0.51	0.76
Amine-functionalized 540 nm T2-MP EviTag	3.82	59.6	0.37	0.64
Non-functionalized 540 nm T2-MP EviTag	4.20	53.9	N/A	N/A
Qdot® 545 ITK™ carboxyl quantum dots	4.56	61.1	<0.01 (0.09)[a]	0.21 (0.47)[a]
Qdot® 545 ITK™ amino (PEG) quantum dots	5.10	62.1	N/A	N/A
DHLA 550 nm QDs	4.73	44.9	0.15	0.48
DHLA-PEG 550 nm QDs	4.57	43.8	0.02	0.18
DHLA-mPEG 550 nm QDs	4.76	45.2	0.01	0.17

[a] Ni^{2+} added to enhance QD-FP interaction.

5.13). The addition of $NiCl_2$ to the reaction buffer did not increase the level of interaction between the amino-PEG Qdot and His6-mCherry (Figure 5.14).

The carboxyl-functionalized EviTags were shown to be excellent FRET donors with 70% quenching of the QD emission at a donor to acceptor ratio of 1:3 (Figure 5.15). This interaction was relatively unchanged in the presence of 1M NaCl. Amine-functionalized EviTags also demonstrated a capacity for the polyhistidine-mediated self-assembly (Figure 5.16), but this interaction was more susceptible to disruption from high salt concentrations. Using the FRET assay, we found that the non-functionalized EviTags showed no capacity for polyhistidine-mediated self-assembly (Figure 5.17).

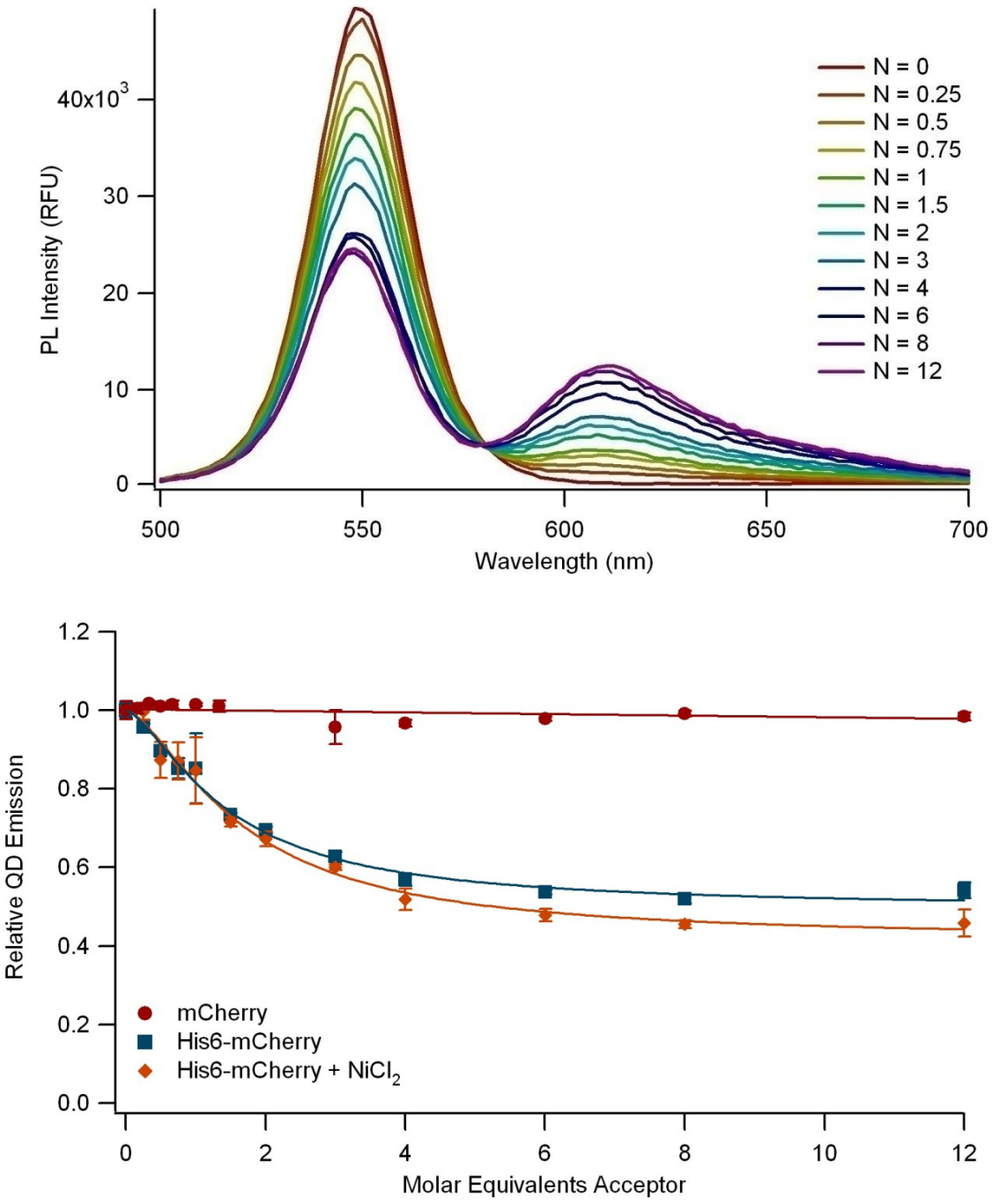

Figure 5.8: Self-assembly to DHLA QDs.
Top: Spectra of DHLA QDs incubated with varying ratios (N) of His6-mCherry monomers per QD. Bottom: Graph of the normalized QD emission relative to the number of acceptor molecules per QD. All points are mean ± standard deviation with n = 3.

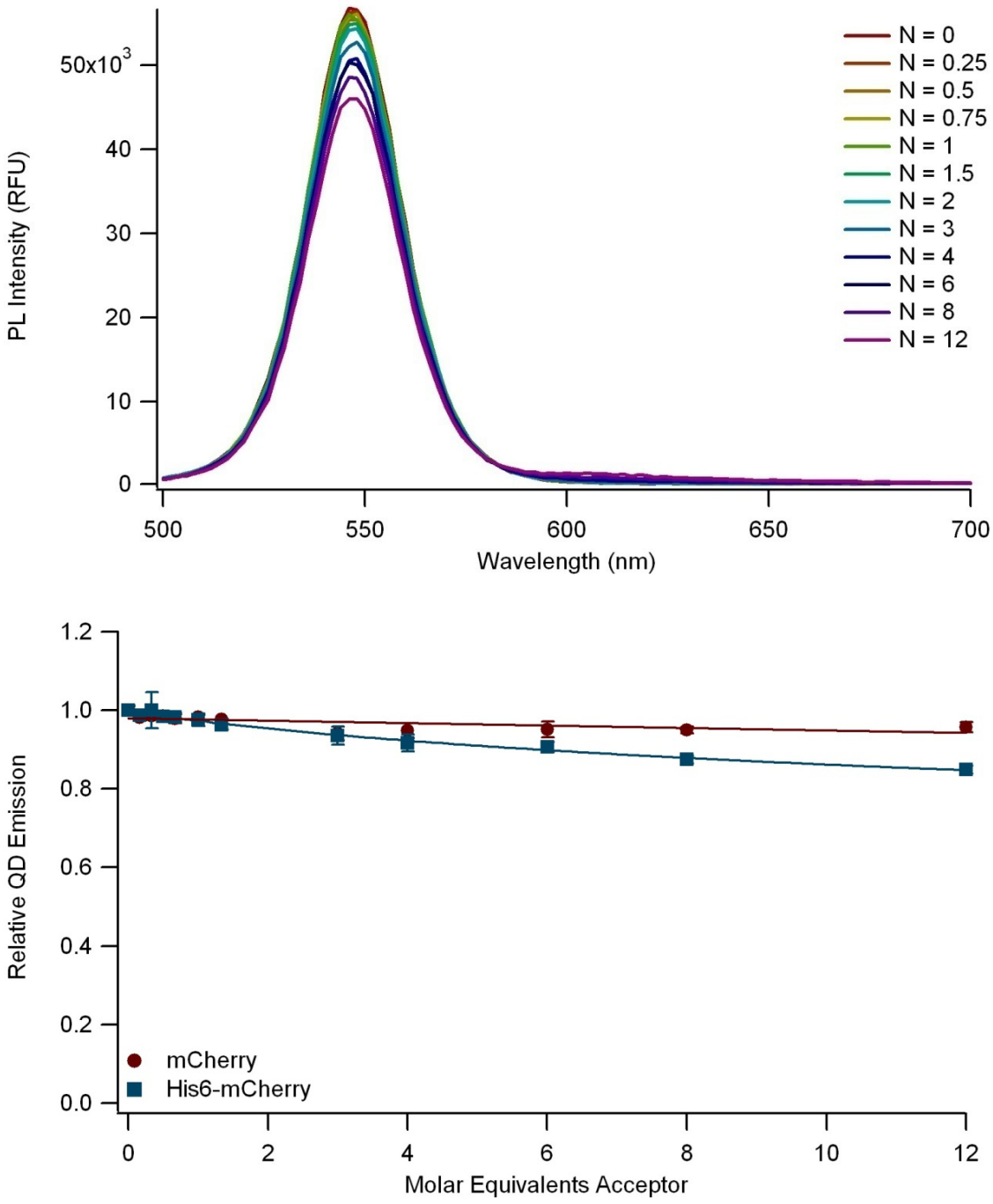

Figure 5.9: Self-assembly to DHLA-PEG QDs.
Top: Spectra of DHLA-PEG QDs incubated with varying ratios (N) of His6-mCherry monomers per QD. Bottom: Graph of the normalized QD emission relative to the number of acceptor molecules per QD. All points are mean ± standard deviation with n = 3.

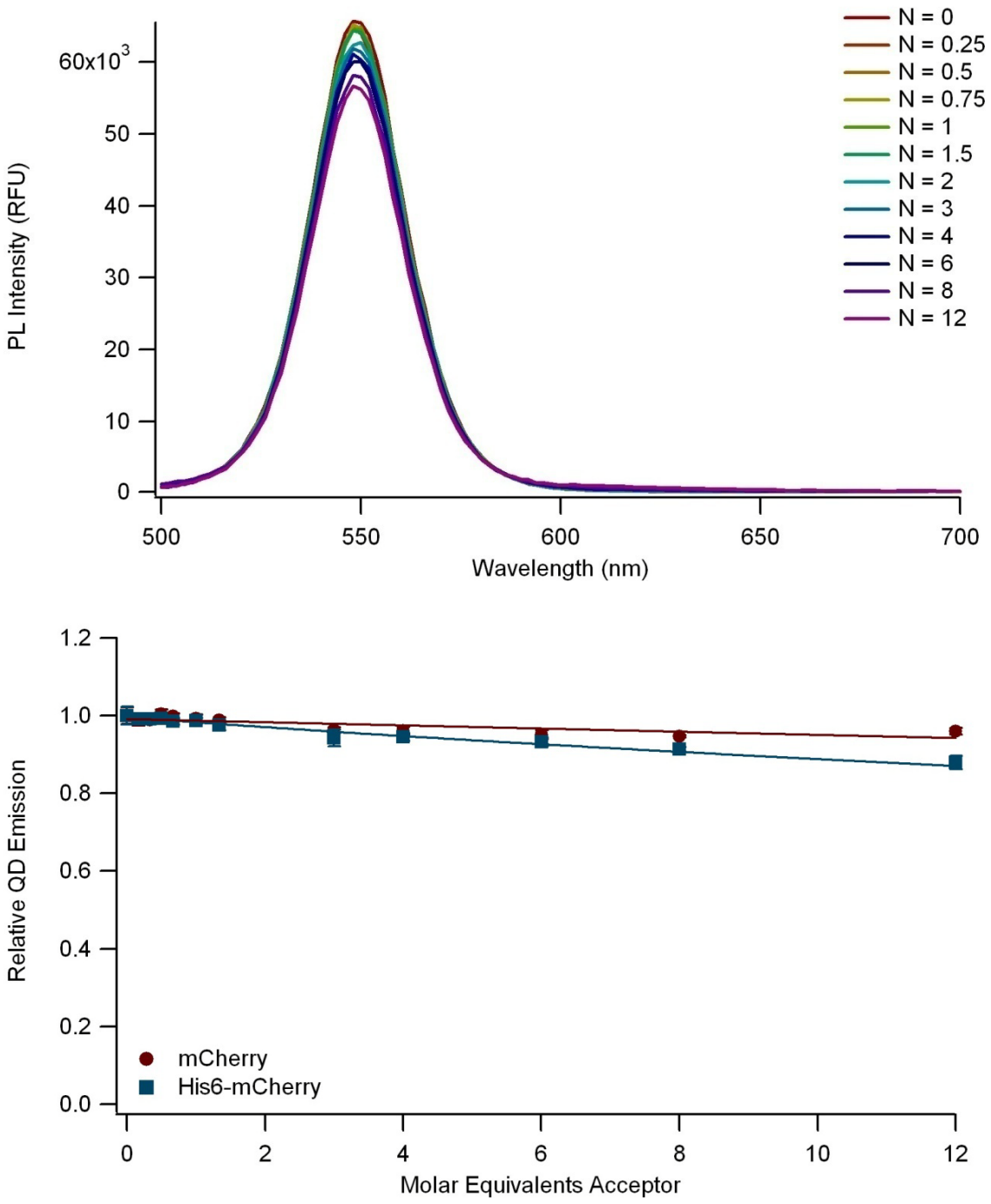

Figure 5.10: Self-assembly to DHLA-mPEG QDs.
Top: Spectra of DHLA-mPEG QDs incubated with varying ratios (N) of His6-mCherry monomers per QD. Bottom: Graph of the normalized QD emission relative to the number of acceptor molecules per QD. All points are mean ± standard deviation with n = 3.

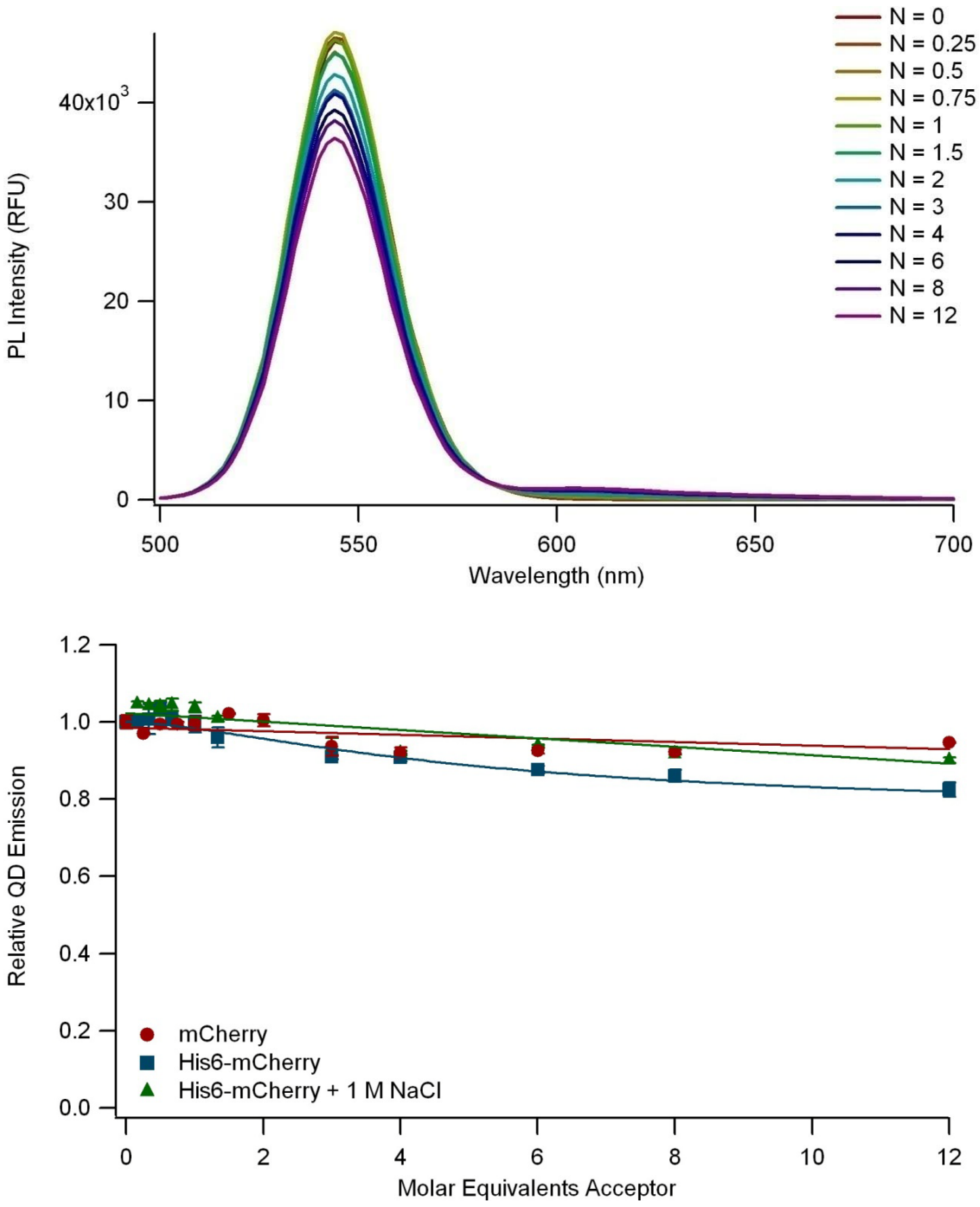

Figure 5.11: Self-assembly to carboxyl Qdots.
Top: Spectra of carboxyl Qdots incubated with varying ratios (N) of His6-mCherry monomers per QD. Bottom: Graph of the normalized QD emission relative to the number of acceptor molecules per QD. All points are mean ± standard deviation with n = 3.

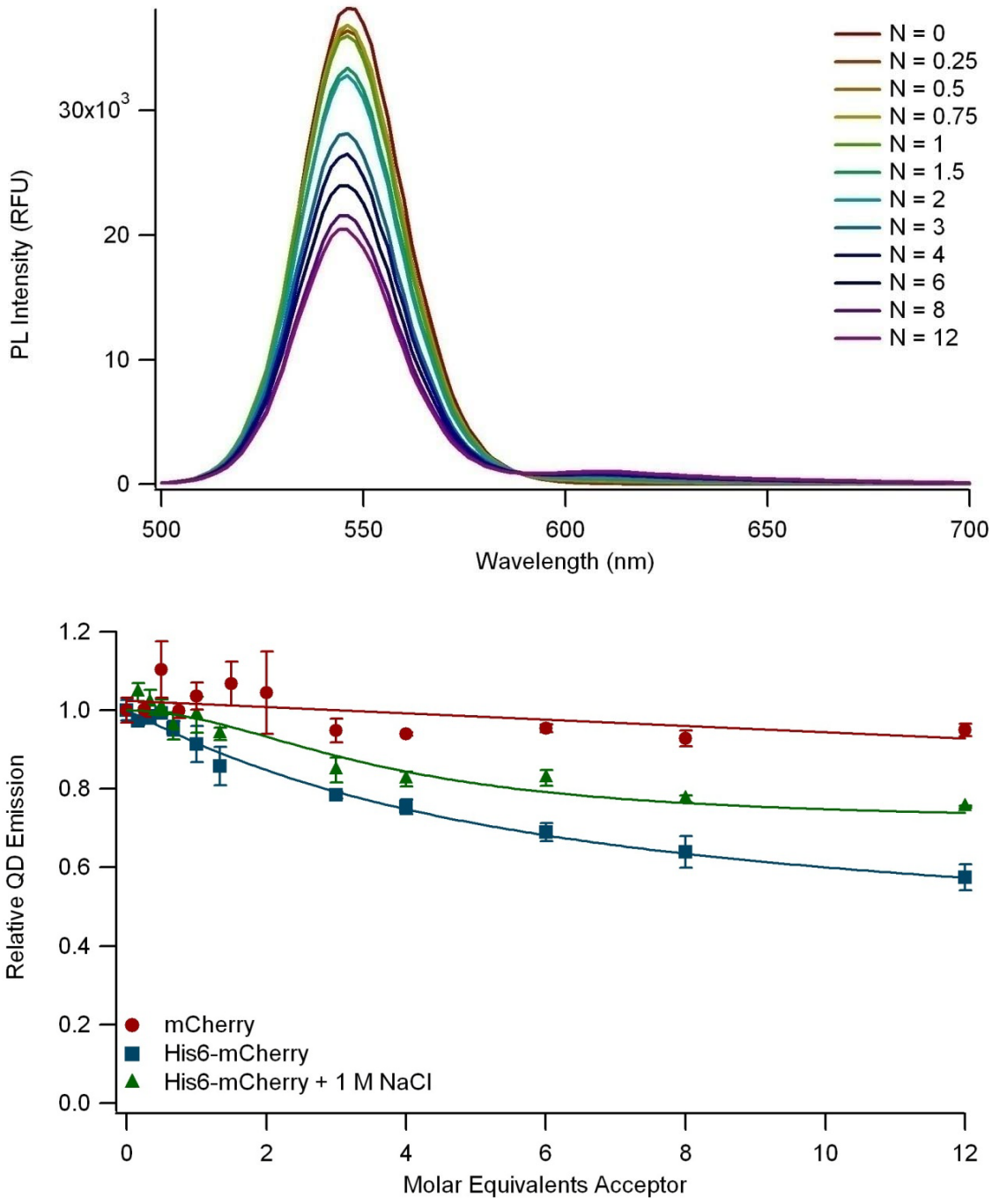

Figure 5.12: Self-assembly to carboxyl Qdots with Ni^{2+} supplementation.
Top: Spectra of carboxyl Qdots incubated with varying ratios (N) of His6-mCherry monomers per QD after addition of $NiCl_2$. Bottom: Graph of the normalized QD emission relative to the number of acceptor molecules per QD. All points are mean ± standard deviation with n = 3.

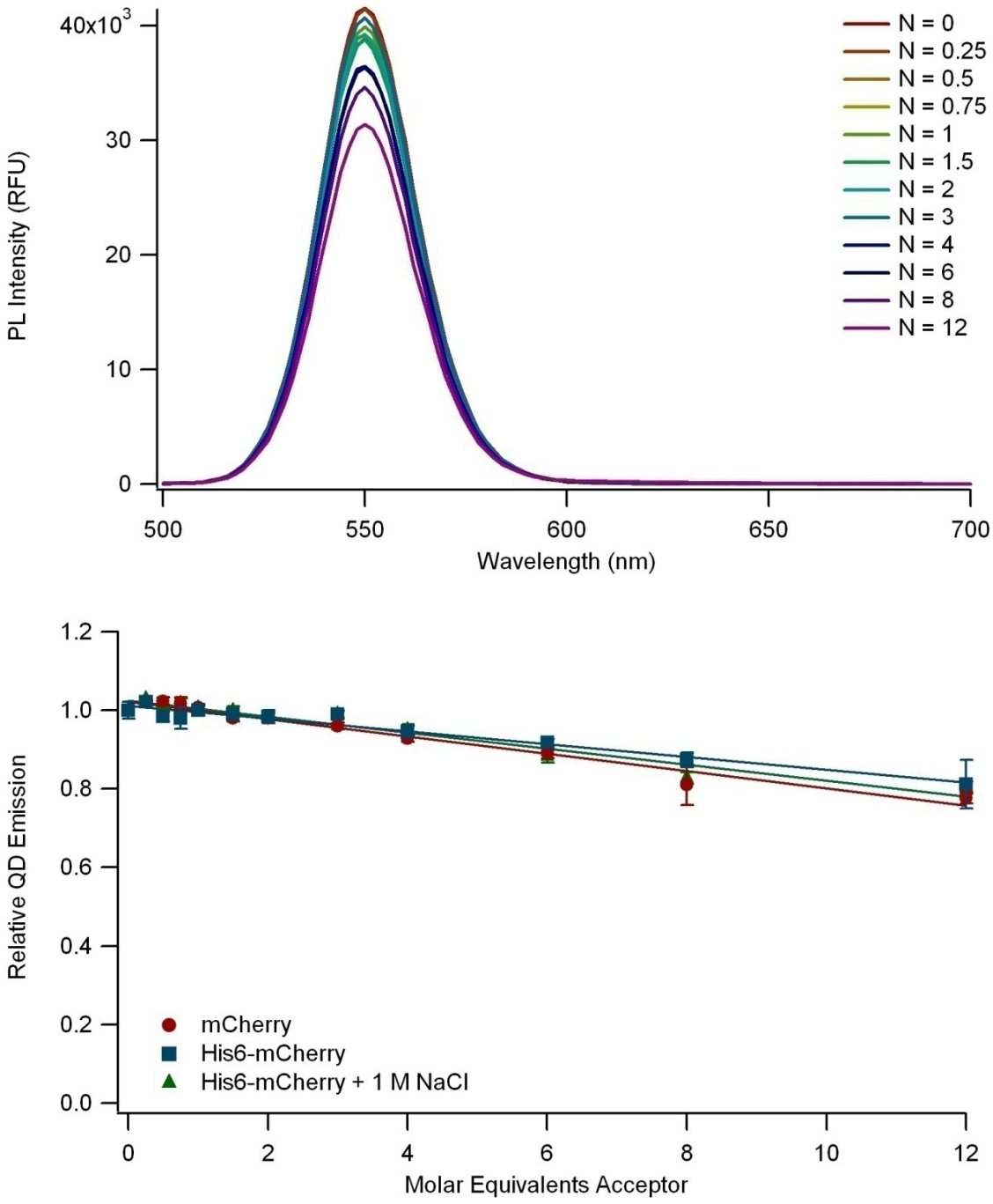

Figure 5.13: Self-assembly to amino-PEG Qdot.
Top: Spectra of amino-PEG Qdots incubated with varying ratios (N) of His6-mCherry monomers per QD. Bottom: Graph of the normalized QD emission relative to the number of acceptor molecules per QD. All points are mean ± standard deviation with n = 3.

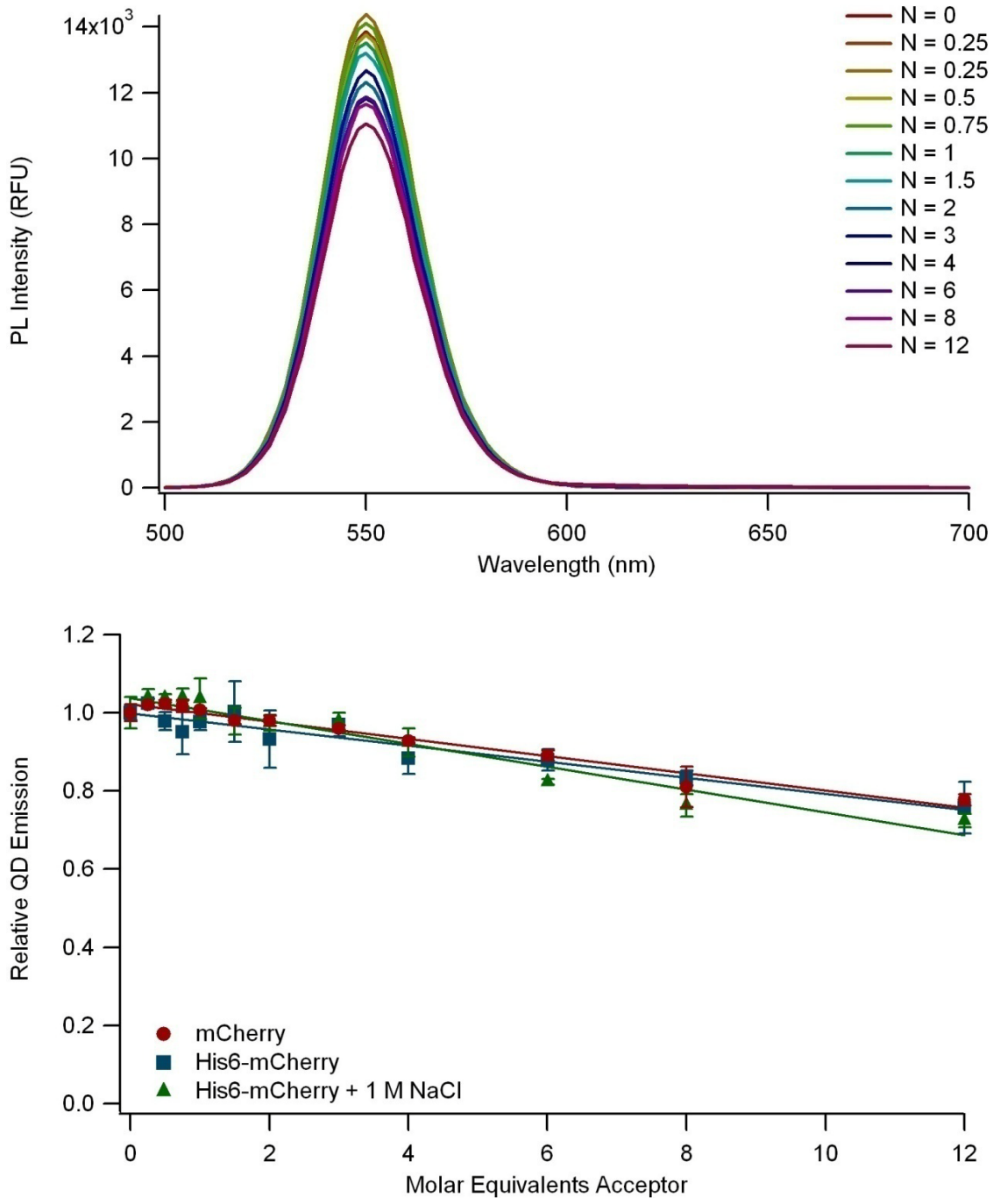

Figure 5.14: Self-assembly to amino-PEG Qdots with Ni^{2+} supplementation.
Top: Spectra of amino-PEG Qdots incubated with varying ratios (N) of His6-mCherry monomers per QD after addition of $NiCl_2$. Bottom: Graph of the normalized QD emission relative to the number of acceptor molecules per QD. All points are mean ± standard deviation with n = 3.

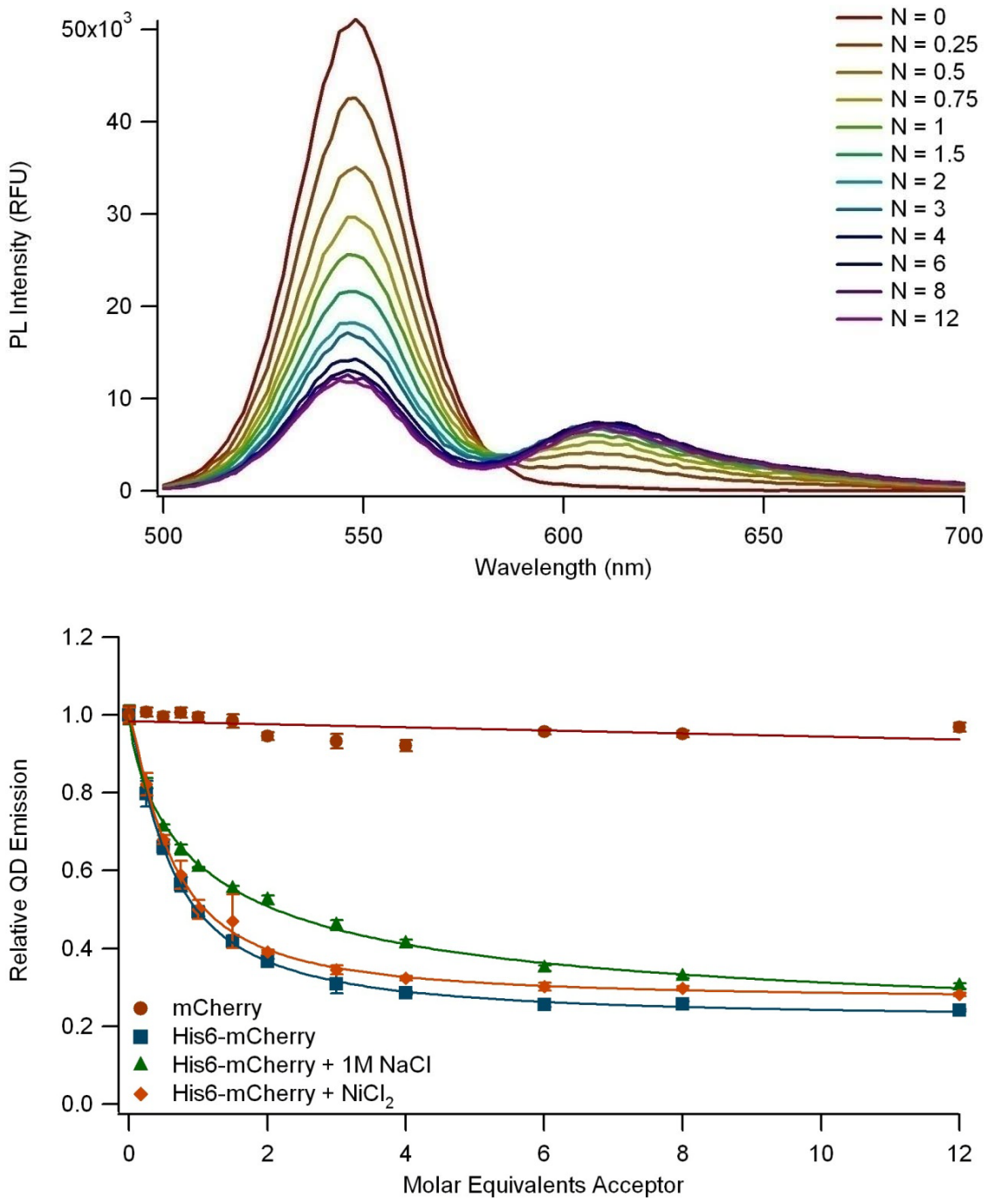

Figure 5.15: Self-assembly to carboxyl-functionalized EviTags.
Top: Spectra of carboxyl-functionalized EviTags incubated with varying ratios (N) of His6-mCherry monomers per QD. Bottom: Graph of the normalized QD emission relative to the number of acceptor molecules per QD. All points are mean ± standard deviation with n = 3.

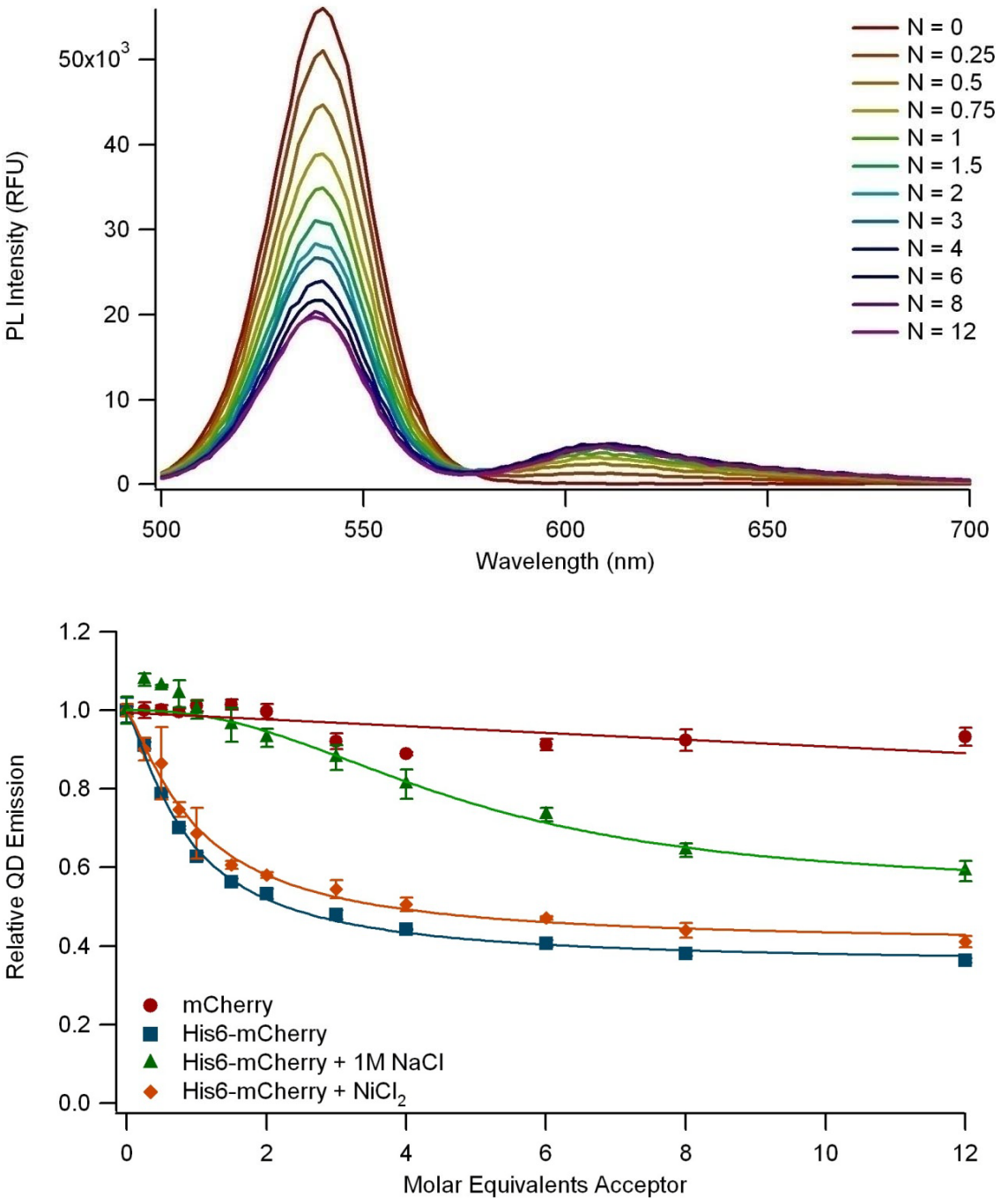

Figure 5.16: Self-assembly to amine-functionalized EviTags.
Top: Spectra of amine-functionalized EviTags incubated with varying ratios (N) of His6-mCherry monomers per QD. Bottom: Graph of the normalized QD emission relative to the number of acceptor molecules per QD. All points are mean ± standard deviation with n = 3.

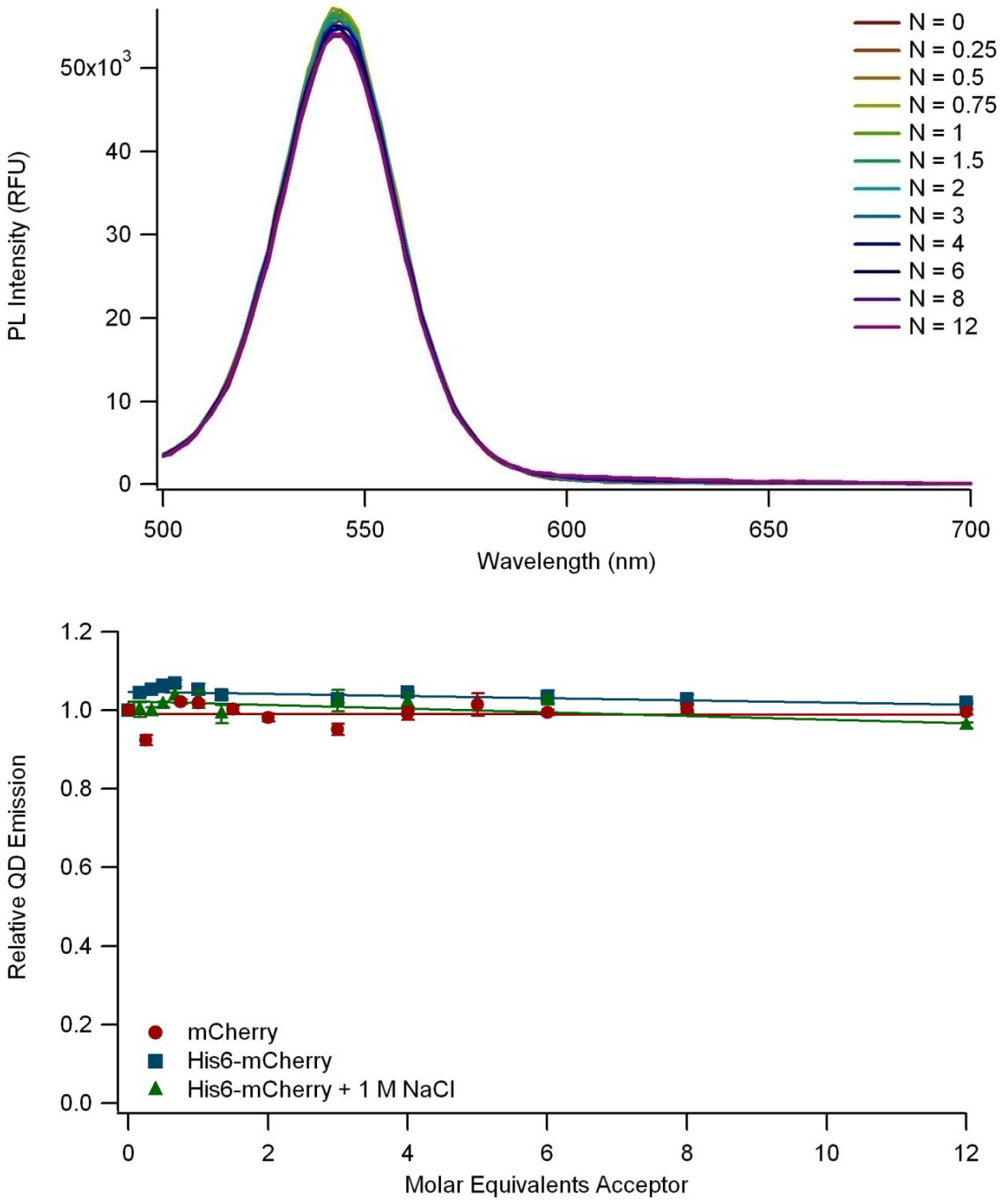

Figure 5.17: Self-assembly to non-functional EviTags.
Top: Spectra of non-functionalized EviTags incubated with varying ratios (N) of His6-mCherry monomers per QD. Bottom: Graph of the normalized QD emission relative to the number of acceptor molecules per QD. All points are mean ± standard deviation with n = 3.

Modified FRET Assay

As changes in the QD environment may affect the brightness of the QD, any change in the QD photoluminescence as a result of His-tag binding is of general importance when using this self-assembly method, particularly in FRET assays. As has been previously documented (*11*), the polyhistidine-mediated coordination of a non-fluorescent protein such as maltose-binding protein (MBP) to the DHLA-coated QDs results in a photoluminescence increase of up to 20%. This was attributed to the filling of surface defects in the DHLA coating by His-tags, thereby reducing the emission loss. This effect could be problematic for the analysis of the FRET assays described above, since His-tag binding increases the QD emission concomitantly as the QD emission is being reduced by energy transfer to the His6-mCherry proteins. This concern was mitigated, however, by using a modified FRET assay, consisting of incubating the QDs with a fixed number of His-tagged proteins while varying the ratio of fluorescently-labeled proteins to non-fluorescent His5-MBP proteins (*11*). This alternative assay resulted in an increased FRET efficiency compared to the standard protocol where the non-fluorescent His-tagged protein is not present in the reaction.

Both the His5-MBP that has previously been used (*11*) and a non-fluorescent, non-chromogenic GFP-like protein were tested for their effect on the QDs. The His5-MBP was used for comparison to the results seen previously, while the new GFP-like protein was engineered using a series of three point mutations to mCherry (S144C I161N Q163M) to create a protein that is structurally analogous to mCherry, but would not by itself affect the photoluminescence of the QDs as it neither absorbs nor emits light at visible wavelengths. The use of a protein that is structurally identical to mCherry, while

not exhibiting the optical properties that affect the QD, provides a control for the ways in which environmental changes, such as His-tag binding or the presence of a protein corona, could affect the QD PL.

Most of the QDs were relatively unaffected by the presence of the non-fluorescent His-tagged proteins (Figure 5.18). Both the DHLA-coated QDs and carboxyl-functionalized EviTags, however, demonstrated a small increase in photoluminescence in the presence of His-tagged proteins, although it was not reliably dose-dependent. This increase in QD PL may indicate that both the DHLA QDs and carboxyl-functionalized EviTags have defects in their organic coatings that reduce their quantum yields in the aqueous environment.

In order to account for the small increase seen in the PL of these two QDs upon binding of a non-fluorescent His-tagged protein, a modified FRET assay was performed in which the total number of proteins in the solution was maintained, but the ratio of fluorescent to non-fluorescent proteins was varied. DHLA-coated QDs were incubated with a total of 12 proteins per QD: the total number of His6-mCherry molecules was increased with corresponding decreases in either His6-mCherry-NF or His5-MBP. There was not a dramatic difference between the experiments using His6-mCherry-NF or His5-MBP, but the shape of those two quenching curves was distinct from that of the DHLA-coated QDs incubated with His6-mCherry in the absence of any filler proteins (Figure 5.19, top). The carboxyl-functionalized EviTags were likewise incubated with a mix of His6-mCherry-NF and His6-mCherry, but in this case the total number of proteins in solution was limited to six per QD. The carboxyl-functionalized EviTags exhibited the same quenching profile with or without the His6-mCherry-NF filler proteins present

(Figure 5.19, bottom), but at each FP:QD ratio there was slightly less quenching in the presence of the non-fluorescent protein.

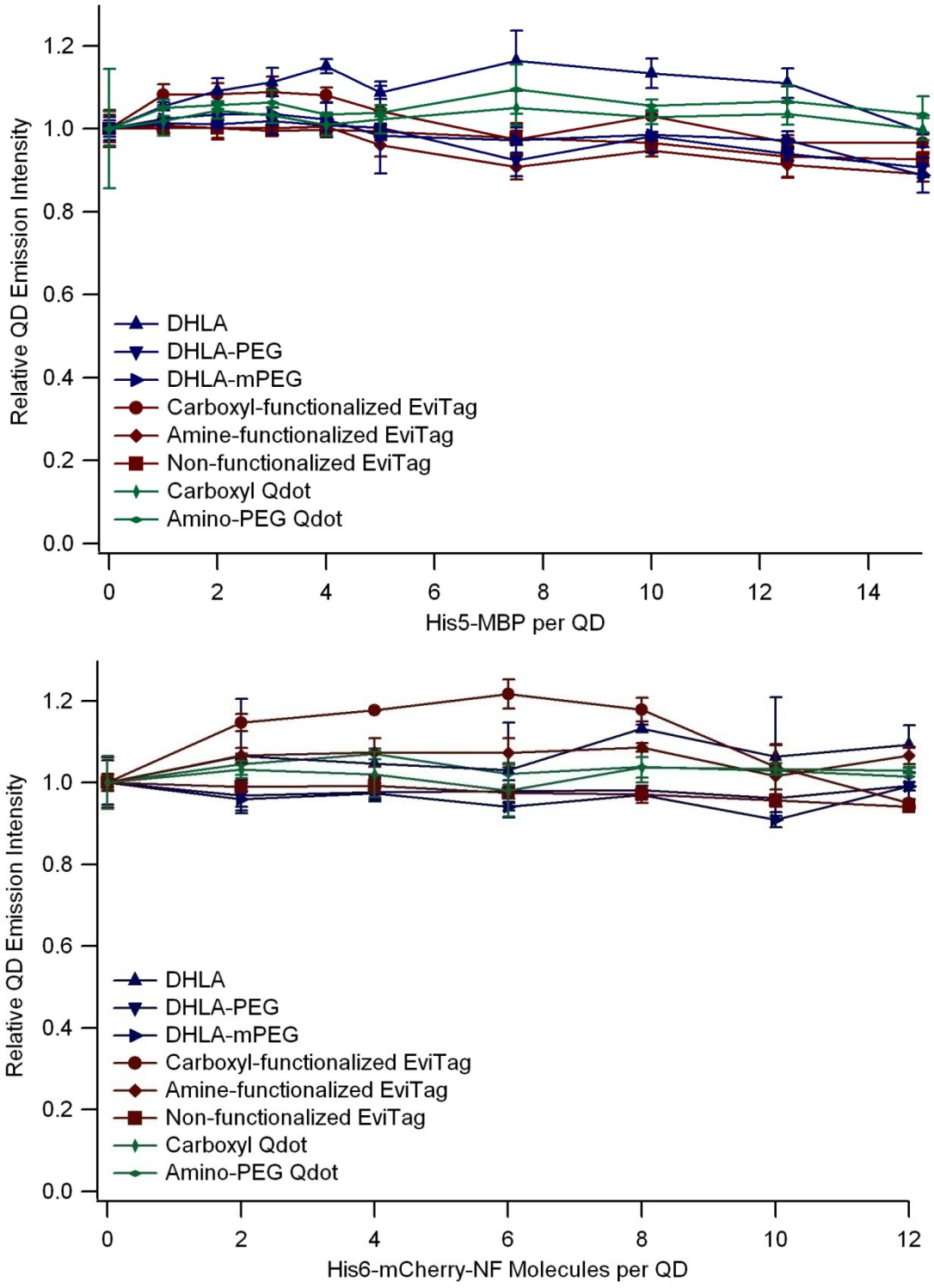

Figure 5.18: Effect of His-tag binding on quantum dot photoluminescence.
Relative emission of QDs incubated with varying concentrations of either His5-MBP (top) or His6-mCherry-NF (bottom).

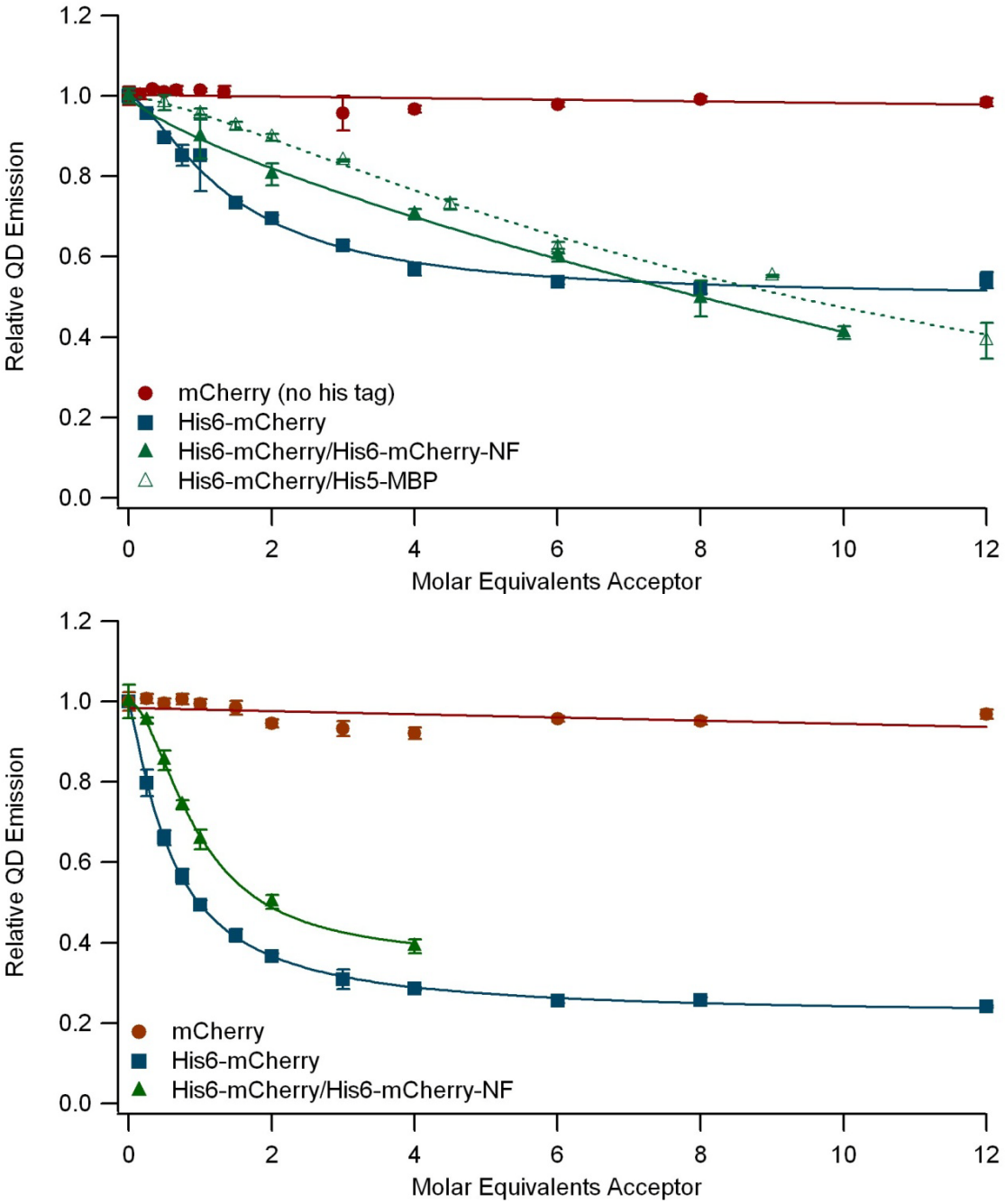

Figure 5.19: Results of modified FRET assay.
Effect of using a mixture of fluorescence and non-fuorescent proteins in FRET assay on DHLA-coated (top) and carboxyl-functionalaliezed EviTags (bottom). All points are mean ± standard deviation with n = 3.

The differences between the results from the standard FRET assay and the modified FRET assay did not appear to improve energy transfer sufficiently to warrant the change in protocol. It is possible that the non-fluorescent proteins proved to be competition for binding on the QD surface, thereby mitigating the positive effect that could have been seen by enhancing the QD PL.

Donor-Acceptor Distance Calculations

As described in the Methods (page 49), the donor-acceptor distance was calculated taking into account the fact that multiple acceptors may be bound to each donor molecule. The donor-acceptor distances were calculated both using the standard equation for multivalent systems (Equation (9), page 49), which uses the average number of donors per acceptor, and using an equation where the Poisson distribution of acceptors per donor was taken into account (Equation (11), page 50).

The calculated donor-acceptor distances for the four conditions in which calculating a donor-acceptor distance was the most relevant are listed in Table 5.3. While the trends are the same whether the Poisson distribution was used or not, significant differences in the resulting donor-acceptor distances were apparent in cases where significant FRET efficiencies were observed at low acceptor to donor ratios. This discrepancy, which is the most dramatic for the carboxyl-functionalized EviTags, is due to the underestimation of the donor-acceptor distance that occurs at low acceptor to donor ratios when the Poisson distribution is not taken into account. Errors of up to 40% have been described as theoretically possible at 1:1 acceptor to donor ratios (*107*).

Table 5.3: Calculated donor-acceptor distances.

	Amine-functionalized EviTags[a]		Carboxyl-functionalized EviTags		DHLA			Carboxyl Qdots with Ni2+	
FP:QD[b]	+[c]	-[d]	+	-	+	-	FP:QD	+	-
0.25	69.6	64.5	52.4	35.5	59.8	57.9	0.167	82.4	80.0
0.5	66.0	59.6	52.3	39.6	57.2	55.0	0.334	99.7	98.8
0.75	65.5	59.4	52.3	42.1	57.3	55.2	0.5	126.7	126.4
1	65.0	59.3	52.4	43.9	60.1	58.4	0.668	95.0	93.9
1.5	66.5	62.2	53.2	47.3	56.8	54.9	1	90.5	89.2
2	68.4	65.0	53.8	49.3	57.8	56.1	1.336	86.6	84.9
3	70.6	68.1	55.2	52.2	58.8	57.4	3	91.1	90.0
4	72.2	70.3	56.9	54.7	59.2	58.0	4	92.9	91.9
6	75.5	74.1	59.3	57.8	62.0	61.2	6	94.2	93.3
8	77.7	76.6	62.3	61.2	64.3	63.6	8	95.1	94.4
12	82.1	80.8	65.7	64.3	69.8	69.0	12	97.3	96.2
Min	65.0	59.3	52.3	35.5	56.8	54.9		82.4	80.0
Max	82.1	80.8	65.7	64.3	69.8	69.0		126.7	126.4
Mean	70.8	67.35	56.0	49.8	60.3	58.8		95.6	94.5
Median	69.6	65.0	53.8	49.3	59.2	57.9		94.2	93.3

[a] All distance values reported are in angstroms (Å).

[b] The mixing ratio of acceptor to donor molecules.

[c] Calculation of the donor-acceptor distance *with* application of the Poisson's distribution.

[d] Calculation of the donor-acceptor distance *without* application of the Poisson's distribution.

DISCUSSION

FRET assays were performed to determine under what conditions and to what extent the His-tag mediates self-assembly of fluorescent proteins to QDs in order to discern the effect that various QDs organic coatings have on self-assembly. The FRET-based assay is particularly useful here because it both confirms the proximity of the nanoparticle and biomolecule and allows the derivation of a separation distance due to its distance dependence. This provides insight into both self-assembly and the overall conjugate structure. In all cases, a non-His-tagged fluorescent protein, mCherry, was used as a negative control in order to ascertain that the His-tag was necessary to induce the interaction between the donor and acceptor. When possible, assays were repeated under high salt conditions (1 M NaCl) in order to disrupt electrostatic interactions to demonstrate whether the interaction is metal chelation-based or mediated electrostatically. His-based metal chelation to immobilized metal (i.e. Ni-NTA) can tolerate extreme conditions including the presence of denaturing agents like 5% SDS, 6 M guanidine, 8 M urea, and greater than 1 M NaCl (*61*, *78, 79*). In addition, supplementation with Ni^{2+} was included to determine if the addition of a chelating ion could enhance the donor-acceptor interaction.

Ligand Exchange-coated QDs

Quantum Dot Properties. All three of the ligand exchange-coated QDs originated from the same batch of CdSe/ZnS QDs produced at high temperatures with organometallic precursors by our collaborators at the Naval Research Laboratories (NRL) in Washington, D.C. The coating procedure was the same for DHLA and the two DHLA-PEG derivatives and produced QDs with very similar QYs.

All of the QDs tested have similar core-shell sizes, which is expected as emission wavelength is directly correlated to the core size (*32*), but the DHLA QD was the only one of the eight tested that exhibited a sub-10 nm hydrodynamic diameter. This small diameter is possible because the ligand-exchange method used to coat the QDs with DHLA-based moieties removes the TOP/TOPO surfactant that is present on the surface of the CdSe/ZnS core-shell following the QD synthesis (*45*, *46*). DHLA binds to the ZnS capping layer *via* bidentate thiols and its deprotonated carboxylic acids hold the QD in suspension as a colloid. With a molecular weight of only 208 g/mole, DHLA is one of the smallest organic molecules capable of conferring water-solubility to the inorganic quantum dots (*40*). Although this ultra-thin organic coating is ideal for minimizing the donor-acceptor distance which is critical for achieving high FRET efficiencies, it comes with some caveats. First, the coating method decreases the QY of the QDs significantly relative to the starting QDs in organic solvents. In addition, the DHLA-coated QDs are further stabilized in aqueous solutions by their electrostatic repulsion of one another; thus, they are susceptible to changes in their colloidal stability depending on their environment and protonation state, i.e. pH, and are known to be more stable in alkaline solutions than at acidic pHs (*45*). Compared to the other seven QDs used in this study, the DHLA-coated QDs showed an accelerated decrease in photoluminescence over time when suspended in buffer containing 1 M NaCl. In contrast, the 25% and 32% increase in hydrodynamic diameter over the DHLA coating for the DHLA-PEG and DHLA-mPEG coated QDs, respectively, was accompanied by an increase in colloidal stability since solubility is mediated by the ethylene glycol repeats. These QDs also exhibited a more constant photoluminescent output over time, including under high salt conditions.

FRET Assay Results. The dose-dependent changes in the spectral profile of the DHLA-coated QDs mixed with His6-mCherry indicates that self-assembly proceeded under these conditions, confirming previous reports of His-tag-mediated self-assembly to DHLA-coated QDs (*10, 11*). The approximately 6 nm donor-acceptor distance calculated for the DHLA-coated QD and His6-mCherry does not give a clear indication of where the protein is positioned with respect to the organic coating, although it is clear that the FP barrel structure is very close to the QD core-shell surface. This is consistent with previously reported kinetic data on the binding of His-tagged biomolecules to DHLA-coated QDs, which indicated that the His-tag binds directly to the ZnS capping layer of the QD (*78*).

Both PEG-conjugated DHLA moieties exhibited minimal quenching of the QD emission and negligible sensitized emission from His6-mCherry, demonstrating an inability of the His-tag to stably interact with the nanoparticle with the steric hinderance from the PEG coating, despite the negative surface charges indicated by their zeta potentials. The steric hinderance provided by the PEG coatings on the DHLA-PEG and DHLA-mPEG QDs precluded those QDs from participating in self-assembly with His-tagged proteins, despite the negative surface charges indicated by their zeta potentials. While this eliminates QDs coated with DHLA-PEG derivatives as an option for His-tag mediated self-assembly, the improvements in stability and environmental sensitivity recommend this coating for other applications, such as intracellular imaging (*110*).

Polymer-coated QDs

Quantum Dot Properties. The hydrophobic region of the amphiphilic poly(acrylic) acid polymer used to coat the Qdots interdigitates with the surfactant

residues on the surface of the QDs following the inorganic synthesis. The hydrophilic portion of the polymer presents a high density of carboxyl groups at the QD-solvent interface. Although the water solubility of the Qdots is also conferred by the presence of hydrophilic carboxylic acids, the larger, more neutral polymer (compared to the small molecule DHLA) does appear to improve the QD passivation as well, providing the Qdot with relatively constant photoluminescence over time, even in high salt conditions. This coating type also preserves the high QY of the QDs even in aqueous solution. These high quantum yields make the Qdots excellent FRET donors, as evidenced by the high Förster radii calculated for both the carboxyl and amino-PEG Qdots, but the larger hydrodynamic diameter of the Qdots could extend the donor-acceptor distance, lowering FRET efficiency.

The amino-PEG Qdots add another layer to the same coating scheme used for the carboxyl Qdots. The amine-terminated PEG_{2000} that are conjugated to the carboxyl groups on the surface of the carboxyl Qdots provide an extreme hydration layer that results in a QD surface that significantly reduces non-specific interactions (*57*).

It is interesting to note that in the stability assays, six of the eight QDs tested, including both of the Qdots, actually showed a slower rate of PL decrease in the high salt buffer. Perhaps the high ion concentration mitigated any electrostatic interactions that the nanoparticles would have had with the surface of the well plate, thereby reducing somewhat the non-specific adsorption of the QDs to the plate.

FRET Assay Results. In the absence of supplemented Ni^{2+}, we found that the interaction between the fluorescent protein and the carboxyl Qdot is a non-specific, electrostatically-mediated interaction that can be disrupted with high salt concentrations.

The supplemented Ni^{2+}, however, appears to affiliate with the high density of carboxyl groups on the Qdot surface, enabling the interaction of the His-tag with the Qdot *via* Ni^{2+} chelation. The same interaction was observed in another study when His-tagged luciferase molecules were incubated with carboxyl Qdots in the presence of Ni^{2+} (*85*). Other divalent ions including Ca^{2+}, Mg^{2+}, and Mn^{2+} were tested in that study as well, but Ni^{2+} was the most effective one in inducing the interaction between the His-tagged protein and the Qdot, while maintaining protein functionality (*85*). Calculation of the corrected donor-acceptor distance yielded a median separation of 94 Å between the QD core and the FP fluorophore. This distance is significantly larger than the hydrodynamic radius of 65 Å measured for the QDs, and consistent with the model in which the FPs bind to the outer surface of a solid polymer coating that surrounds the QD core-shell. The presence of the amino-PEG moieties on the Qdot surface apparently shielded the nanoparticles from the non-specific electrostatic interactions seen with the carboxyl Qdots and, without the high-density of solvent-exposed carboxyl groups, the amino-PEG Qdot was unable to chelate Ni^{2+} ions from the solution to facilitate an interaction with His-tagged proteins. The zeta potential measurements showed that the carboxyl Qdots are highly negatively charged while the amino-PEG Qdots have a near neutral zeta potential, supporting the finding that the carboxyl Qdots are primed for both electrostatic interacqations and metal chelation whereas the amino-PEG Qdots are not.

Lipid-PEG-coated QDs

Quantum Dot Properties. The three EviTags exhibited rather different hydrodynamic diameters although they used the same core-shell structure and lipid-PEG coating scheme. These differences in the hydrodynamic diameter of the three EviTags

may indicate variations in the density and orientation of the lipid-PEG coating. A previous report on the thickness of DSPE-PEG_{2000} monolayers measured by neutron reflectivity of Langmuir-Blodgett films indicated that a densely packed monolayer of DSPE-PEG_{2000} could reach a thickness of 10.7 nm, but less densely packed monolayers demonstrated proportionally decreasing monolayer thicknesses. In that case, the decrease in the monolayer thickness was found to be related to the brush height of the PEG polymer; the lipid demonstrated no density-dependent variation in its geometry (*111*). This effect may be even more pronounced when the lipid-PEG is used to coat a nanoparticle, since the curvature of the particle inherently increases the surface volume available for the free movement of the PEG molecule even in densely packed coatings. Thus, it is possible that the lipid-PEG molecules of the non-functionalized EviTags are more densely packed, resulting in a brush-like configuration of the PEG chains, while amine-functionalized EviTags exhibit a more mushroom-like configuration, and the PEG strands in carboxyl-functionalized EviTags may relax into a pancake-like configuration due to a low packing density. Although it is unintuitive that just a couple of atoms at the extremity of the large lipid-PEG coating molecules could wield such influence on the packing density and structure of the entire coating layer, it is possible that charge repulsions of the amine and carboxyl functional groups could affect molecular interactions during the coating procedure. While the variation in coating thickness does not appear to affect PL stability of QDs, it does seem to influence polyhistidine self-assembly, as discussed below.

FRET Assay Results. When the EviTags were evaluated for their capacity for His-tag-mediated self-assembly, the interaction between the His6-mCherry and the

EviTags was found to be dependent on the functional group employed in the lipid-PEG coating. His-tag binding to carboxyl-functionalized EviTags proceeded in both saline and high salt and was not enhanced by the addition of Ni^{2+}. This indicates that the interaction was neither electrostatically driven nor dependent on the chelation of free divalent cations by the carboxyl groups, as is the case with the carboxyl Qdots.

The amine-functionalized EviTags also demonstrated a capacity for His-tag mediated binding, but the mechanism of the interaction is less clearly defined by the FRET results. Binding appeared to proceed similarly to that observed for the carboxyl-functionalized EviTags in buffer containing saline, but the extent of QD quenching was lessened in the high salt buffer. In addition, the shape of the dose-dependent quenching curve was altered under high salt conditions as well, indicating that the mechanism of the interaction between the amine-functionalized EviTags and His6-mCherry likely contains an electrostatic component, where transient non-specific interactions between the amines in the coating and the fluorescent protein may provide the opportunity for close proximity between the His-tag and the QD surface. Although these non-specific associations do appear to contribute to the probe assembly in this case, steady-state binding is not solely reliant on the electrostatic attraction.

There was no evidence of His-tag-mediated binding of the fluorescent protein to the non-functionalized EviTags in the FRET assay, indicating that this system is distinct from both the carboxyl- and amine-functionalized EviTags.

The significant differences in the quenching effect of the three EviTag QDs is surprising given that the only difference between the three QD types is the functional group at the terminal end of the lipid-PEG coating moiety. However it may be explained,

in part, by the hydrodynamic diameter measurements. If the large diameter of the non-functionalized EviTags is indeed indicative of a coating with closely packed lipid-PEG molecules that are extended brush-like, then this coating may be impenetrable to the His-tagged FP. If the 35% decrease in the hydrodynamic diameter of the carboxyl-functionalized EviTags, in contrast, indicates a less dense, or even patchy, lipid-PEG coating, then some regions of the QD surface may be exposed, thus amenable to the binding of the polyhistidine tag. It is unclear, however, what role the TOP/TOPO layer that passivated the surface following the inorganic synthesis plays in this scenario. The amine-functionalized EviTags exhibited a behavior between the two discussed above, both in hydrodynamic diameter and the extent of FRET. In fact, given the much higher quantum yield of the amine-functionalized EviTag, one would expect a greater quenching than that with the carboxyl-functionalized EviTag, if the same number of fluorescent proteins were bound to the QDs and were positioned at the same distance from the QD core. Instead, we found that quenching was reduced with the amine-functionalized EviTags. Calculations of the donor-acceptor distances using the Poisson distribution yielded median R values of 56 Å and 71 Å for the carboxyl- and amine-functionalized EviTags, respectively. Both of these donor-acceptor distances are shorter than half of the hydrodynamic diameter of the QDs, as measured with DLS, suggesting that in both cases the fluorescent proteins may be embedded in the coating layer rather than outside of the PEG corona. The flexibility of the hydrated PEG chains, particularly when not close-packed into a dense brush-like conformation, could permit this physical arrangement. Furthermore, the difference in the donor-acceptor distance for carboxyl-functionalized or amine-functionalized EviTags could arise if the amino acid linker region between the

His-tag and the FP barrel structure is fully extended when the protein is bound to the amine-functionalized EviTag due to the differences in their PEG conformations.

To ensure that the results of the EviTag FRET assays are not dependent on these particular batches of QDs, self-assembly experiments were repeated many times with different coating batches and QD emission wavelengths (paired with alternative GFP-like FPs to ensure appropriate spectral overlap where necessary) utilizing QDs purchased over several years, making it likely that multiple batches of Avanti's lipid-PEG were involved for each coating type as well. Our general observation of strong quenching of the carboxyl-functionalized EviTags, moderate quenching of the amine-functionalized EviTags, and no quenching of the non-functionalized EviTags was consistent for all experiments conducted (data not shown). Our previous results indicated that carboxyl-functionalized EviTags with three different coating batches all showed considerable quenching when bound to FPs *via* polyhistidine-mediated coordination (*15*). Thus, we believe that these results clearly demonstrate the merit of using polyhistidine coordination for the bioconjugation of biomolecules to QDs coated with carboxyl-functionalized lipid-PEG molecules.

The schematic in Figure 5.20 diagrams the specific QD-FP interactions that seem to be suggested by the data as well as the chemical structures of the various coatings, giving an indication of the resulting differences in hydrodynamic diameter.

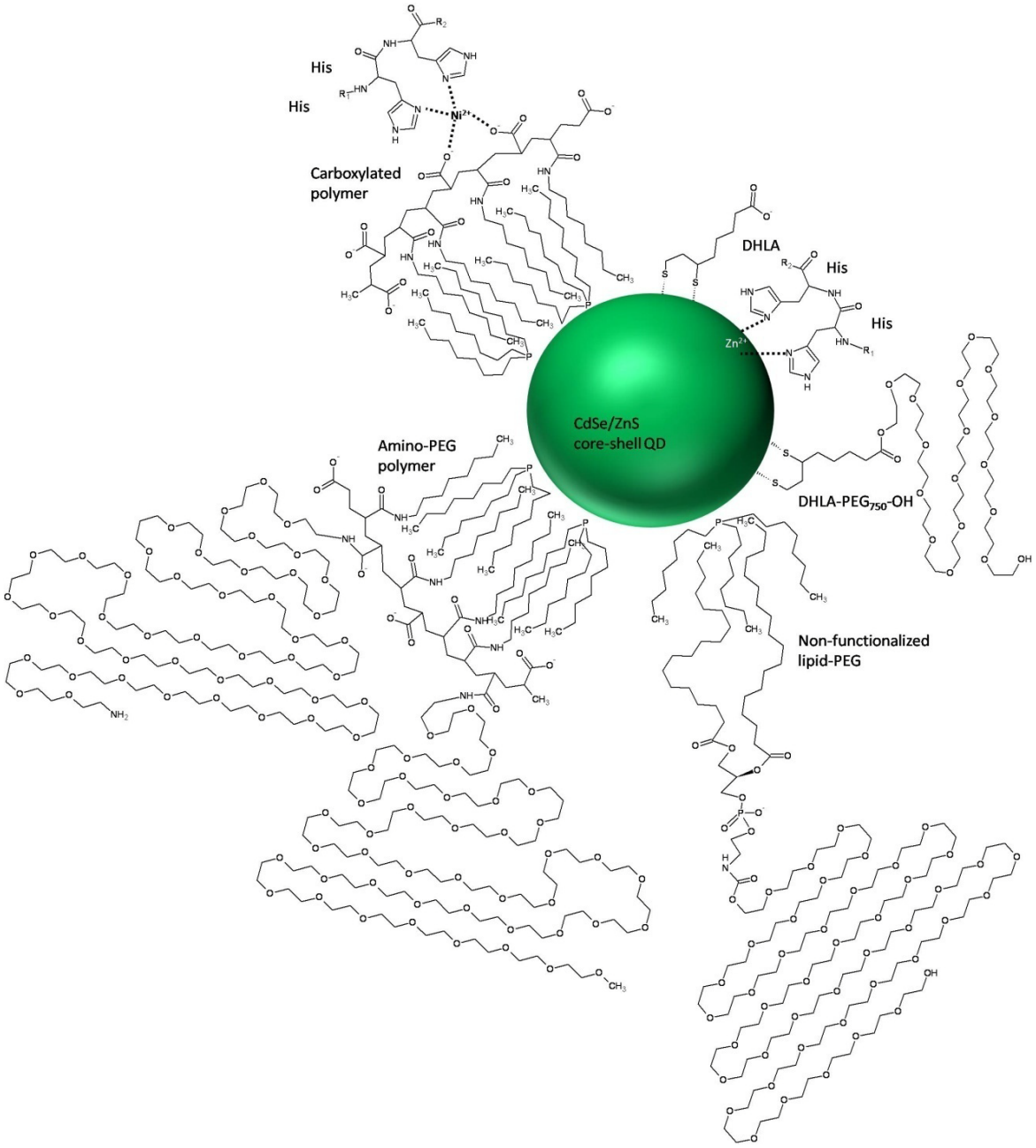

Figure 5.20: Schematic of various QD coatings and His-tag interactions.
Various coating moieties and their interaction with the polyhisitidine sequence are depicted. Where the His-tag can access the QD surface, coordination of the Zn^{2+} ions in the ZnS capping layer facilitate self-assembly. In the case of the carboxylated polymer, a divalent cation is chelated by both the carboxyl groups on the polymer surface and the histidine.

CONCLUSION

In this study, we compared QDs with eight different coatings using three different coating schemes and determined their capacity for polyhistidine coordination as a means to conjugate biomolecules to nanoparticles by self-assembly. This is highly desirable for the assembly of nanoparticle based imaging probes and delivery systems because of its technical simplicity. DHLA-coated QDs exhibited effective His-tag-mediated binding and short donor-acceptor distances, but are not universally applicable because of their low quantum yield, the environmental sensitivity of photoluminescence, and pH-dependent colloidal instability. Using QDs coated with PEGylated DHLA improved the stability and environmental sensitivity, making them advantageous for certain applications including intracellular imaging, but the PEGylated coating also precluded His-tagged proteins from penetrating to the QD surface, making them unsuitable for His-tag-mediated conjugation strategies. The ZnS surface of the carboxyl and amino-PEG Qdots was similarly inaccessible for His-tag binding, but chelation of supplemented Ni^{2+} to the high density of carboxyl groups on the carboxyl Qdot polymer coating did allow for Ni^{2+}-mediated association of the protein with the Qdot, similar to the way in which a His-tagged protein binds to a Ni^{2+}-containing metal affinity chromatography column. While the added distance between the donor and acceptor resulting from this binding scheme may make the strategy suboptimal for FRET-based assays, it may be useful for labeling Qdots with proteins for applications where the protein should be completely exposed at the QD surface to maintain functionality. Finally, the lipid-PEG coated EviTags demonstrated a range of His-tag binding permissiveness, depending on the specific functional group at the PEG terminus. Lipid-PEGs terminated with a methyl

group generated a thick, impenetrable coating, while coatings with terminal carboxyl-groups were much thinner and susceptible to His-tag binding. Amine-functionalized EviTags performed in between the two.

As the variety of protocols used to confer water-solubility to QDs diversifies, including to small molecule coatings that preserve the high QD QY (*50*) and QDs solubilized directly with biomolecules (*51*), the potential for discovering other QD varieties that are effective FRET donors and accessible for His-tag-mediated self-assembly increases. Expanding on these techniques to include PEG passivation would make them more broadly applicable both in *in vitro* assays and intracellular imaging.

The combination of reasonably bright, stable QDs amenable to His-tag mediated self-assembly with a PEG coating that could reduce non-specific interactions makes a very attractive nanoscaffold for bioconjugation. The fact that differences from minor modifications to the coating cannot be fully reconciled suggest far more remains to be learned about this particular nanoparticle-biological interface and will help improve the design of the next generation of materials.

CHAPTER 6

ASSESSING QUANTUM DOT-FLUORESCENT PROTEIN PAIRS AS FLUORESCENCE RESONANCE ENERGY TRANSFER PROBES[*]

INTRODUCTION

Chapter 5 discussed the effect of various quantum dot (QD) coatings and the resultant nanoparticle properties on the self-assembly of QDs and His-tagged fluorescent proteins (FPs). Here the changes in fluorescence resonance energy transfer (FRET) pair properties that result from changes to the QD spectral properties or to the FP acceptor are investigated.

The use of FPs as FRET acceptors has several benefits. Standard molecular biology techniques can easily be used to modify the FPs to include the polyhistidine tag, a variety of linkers between the protein bulk and the tag, and amino acid sequences that could contribute to the functionality of the QD-FRET probe, such as a cleavage sequence for a protease to produce a FRET-based probe to measure enzyme activity. Once a plasmid for the recombinant protein is designed, FPs can be expressed in *E.coli* in large quantities, and the presence of the polyhistidine on His-tagged proteins facilitates protein purification using immobilized metal affinity chromatography (IMAC). The large variety of GFP-like fluorescent proteins now available with emission wavelengths spanning the entire visible range also provides an array of possible fluorescent protein acceptors for QDs with different colors (*91, 112*).

The schematic in Figure 6.1 demonstrates how the interaction between a His-

[*] Modified from Dennis AM and G Bao. Quantum dot-fluorescent protein pairs as novel fluorescence resonance energy transfer probes. *Nano Letters* 2008. 8(5):1439-1435.

tagged fluorescent protein and a T2-MP carboxyl-functionalized EviTag results in FRET. The fluorescent protein self-assembles to the EviTag *via* polyhisitidine coordination as discussed in Chapter 5. When the QD is excited with UV irradiation, it emits at its characteristic wavelength. With the FP bound, some of the energy from the QD is transferred to the FP and emission is seen from both the QD and the FP in ratios that vary depending on the number of FPs attached to the QD, their spectral overlap, and the distance between the two. The differences found by varying the QD-FP combinations are explored in this chapter.

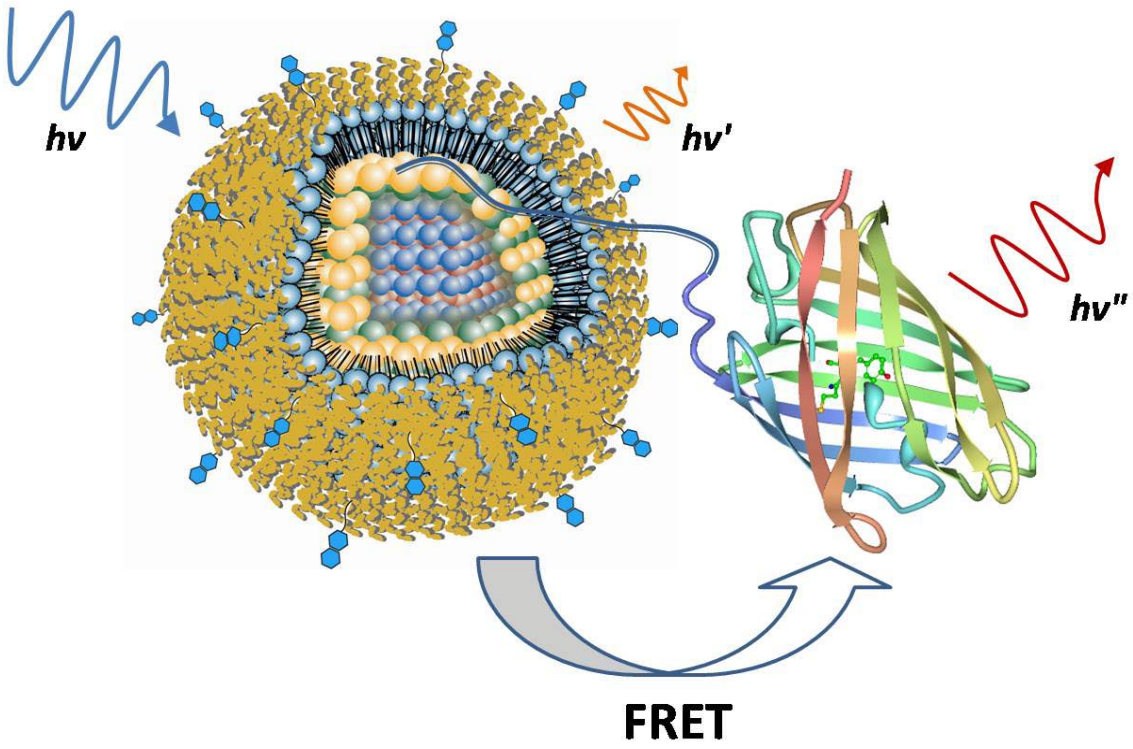

Figure 6.1: Schematic diagram of the QD-FP FRET interaction.
A polyhistidine sequence inserted at the N-terminus of the mCherry showen here coordinates to the ZnS capping layer of the T2-MP carboxyl-functionalized EviTag, bringing the two into close proximity. Under excitation of the QD, energy is non-radiatively transferred to the fluorescent protein and sensitized emission is observed. EviTag image courtesy of Evident Technologies. mCherry produced with PDB Protein Workshop 1.50 (*113*) using the PDB 2H5Q.

RESULTS

Quantum Dot and Fluorescent Protein Properties

The absorbance or excitation and emission spectra of the three QDs and three fluorescent proteins used in this study are displayed in Figure 6.2. Summaries of the other properties of the donor and acceptor component parts are listed in Table 6.1.

The absorption and emission spectra of the three different wavelength emitters of QDs are very similar, with just a slight red-shifting from one to the next. As expected, the wavelength of the emission increases with the size of the QD core-shell structure (*32*). This subtle difference in the semiconductor metal crystal mass is masked by the lipid-PEG coating, as the hydrodynamic diameters of the three different QDs are reported to be about the same (dynamic light scattering measurement, personal communication with Kayla Leach from Evident Technologies and product data sheet).

Table 6.1: Donor and acceptor properties.

FRET acceptor: Fluorescent Protein[a]						
Acceptor	**Peak Excitation (nm)**	**Peak Emission (nm)**	**Extinction Coefficient (M^{-1} cm^{-1})**	**Quantum Yield**	**Time to Photobleach ($t_{0.5}$; seconds)**	**Molecular Weight (kDa)**
mOrange	548	562	71,000	0.69	6.4	27
tdTomato	554	581	138,000	0.69	70	54
mCherry	587	610	72,000	0.22	68	27

FRET donor: T2-MP Carboxyl EviTags[b]						
Donor	**Water-soluble Coating**	**Preferred Excitation (nm)**	**Emission Peak (nm)**	**Quantum Yield**	**Core-shell Diameter (nm)**	**Hydrodynamic Diameter (nm)**
QD520	lipid PEG with carboxyl terminal groups	≤ 400	520 ± 10	0.28	7.5	~25
QD540			540 ± 10	0.35	7.7	
QD560			560 ± 10	0.31	8.0	

[a] Fluorescent Protein specifications previously published (Shaner, Campbell et al. 2004).
[b] EviTag specifications published at www.evidenttech.com or provided by Evident Technologies technical support.

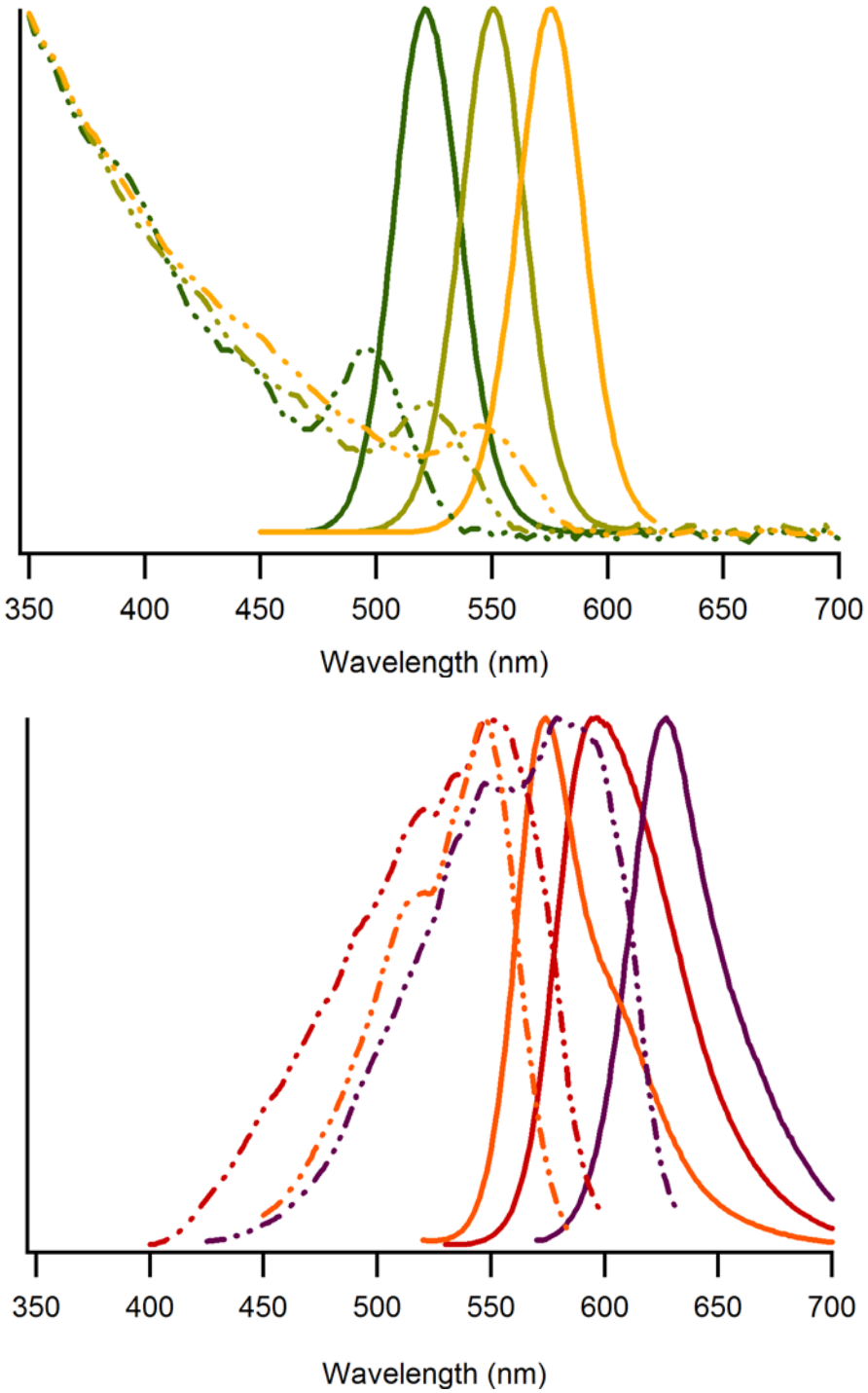

Figure 6.2: Spectral characteristics of the FRET donors and acceptors.
Top: Absorbance (dashed lines) and emission spectra (solid lines, with emission peaks from left to right) of 520 nm, 540 nm, and 560 nm T2-MP carboxyl-functionalized EviTags. Bottom: Excitation (dashed lines) and emission spectra (solid lines, with emission peaks from left to right) of fluorescent proteins mOrange, tdTomato, and mCherry.

The three fluorescent proteins used in this study have many similarities because they are all derived from a common ancestry, but the modifications that were made to create the diversity of macromolecules found in the so-called “Fruit Basket” of proteins do result in several significant differences. Because of the tandem dimer structure of tdTomato, its molecular weight is twice that of monomeric mOrange or mCherry, and its molar extinction coefficient is correspondingly doubled as well. Although mOrange and tdTomato have the same high quantum yields (QYs), tdTomato is twice as bright as mOrange because of this difference in the molar extinction coefficient. Similarly, although mCherry and mOrange have the same molar extinction coefficient, mOrange is much brighter than mCherry because its QY is three times higher. In addition to these differences in FP brightness, mOrange is also much more sensitive to photobleaching and changes in pH than the other two FPs (*91*).

Overlap Integrals and Förster Distances

The overlap integral and Förster distances were calculated for each of the nine possible FRET pairs using Equations (3) and (4) (page 45). The spectral overlaps of each of the possible quantum dot-fluorescent protein pairs are shown graphically in Figure 6.3, Figure 6.4, and Figure 6.5, and the calculated values for the overlap integrals and Förster distances are presented in Table 6.2. The overlap between mCherry and the QDs improved with the increasing emission wavelength of the EviTags. The overlap increased for tdTomato and mOrange as they moved from 520 to 540 nm emission wavelength, but then decreased with the 560 nm emitting QDs as the QD emitted at a lower energy than the FP was absorbing. At this point significant overlap of the QD and FP emission peaks also made the deconvolution of the FRET spectra less reliable, so three of the nine

possible pairs (QD540-mOrange, QD560-mOrange, and QD560-tdTomato) were not included in the FRET study. The Förster distances ranged from 4-6 nm, with the largest distances logically correlating with the most complete spectral overlaps, as observed visually and through the calculated overlap integral.

Table 6.2: Overlap integral and Förster distance for all possible donor-acceptor pairs.

Donor-Acceptor Pair	Overlap Integral J (10^{-15} M^{-1} cm^3)	Förster Distance R_0 (Å)
QD520-mOrange	3.74408	47.81
QD540-mOrange	4.67399	50.52
QD560-mOrange	1.87209	41.89
QD520-tdTomato	8.52283	54.84
QD540-tdTomato	11.2586	58.49
QD560-tdTomato	8.1611	53.54
QD520-mCherry	3.33902	46.91
QD540-mCherry	5.59474	52.06
QD560-mCherry	7.3026	52.56

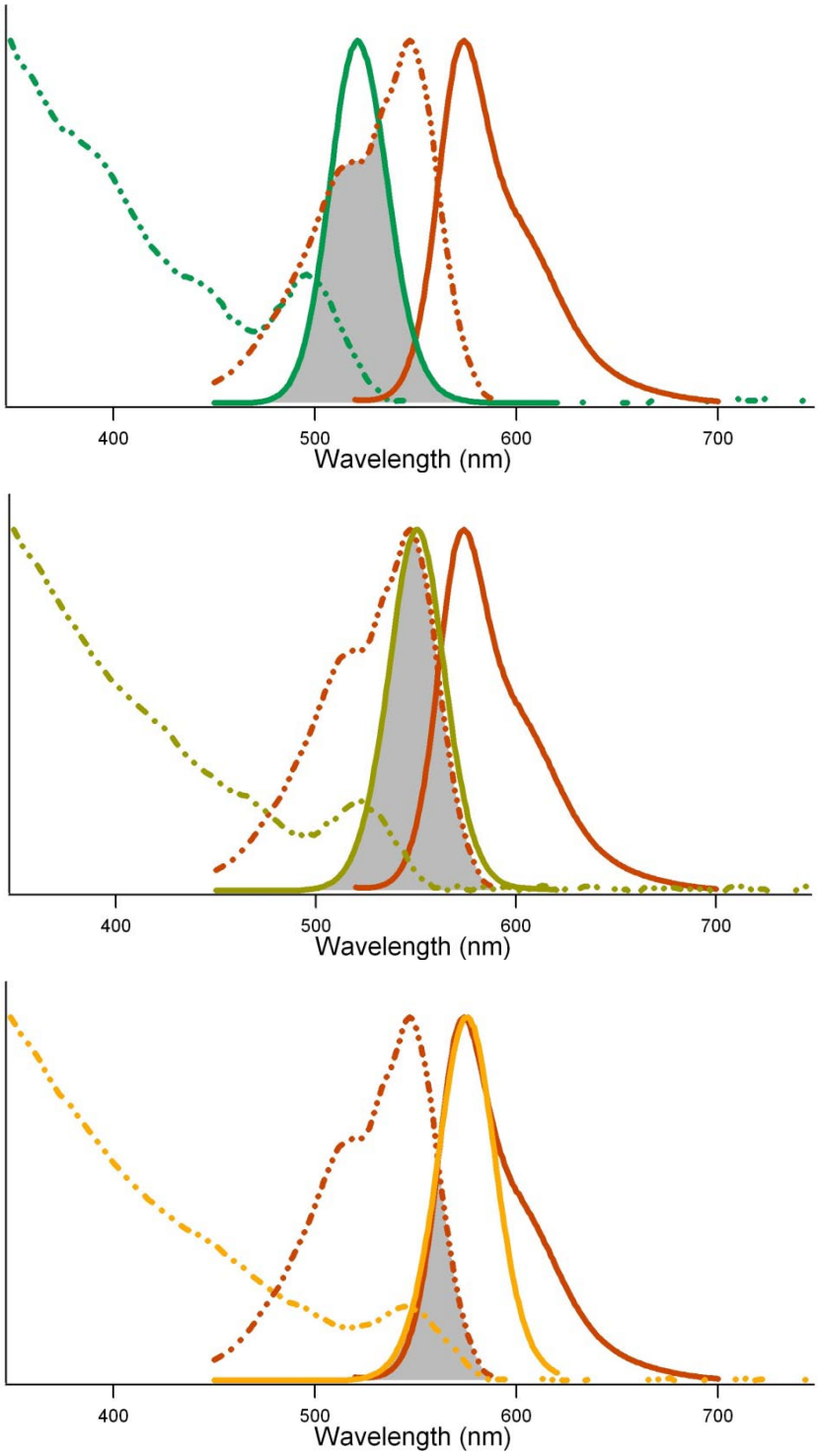

Figure 6.3: Spectral overlap of quantum dot donors and mOrange.
From top to bottom 520 nm, 540 nm, and 560 nm T2-MP carboxyl-functionalized EviTags.

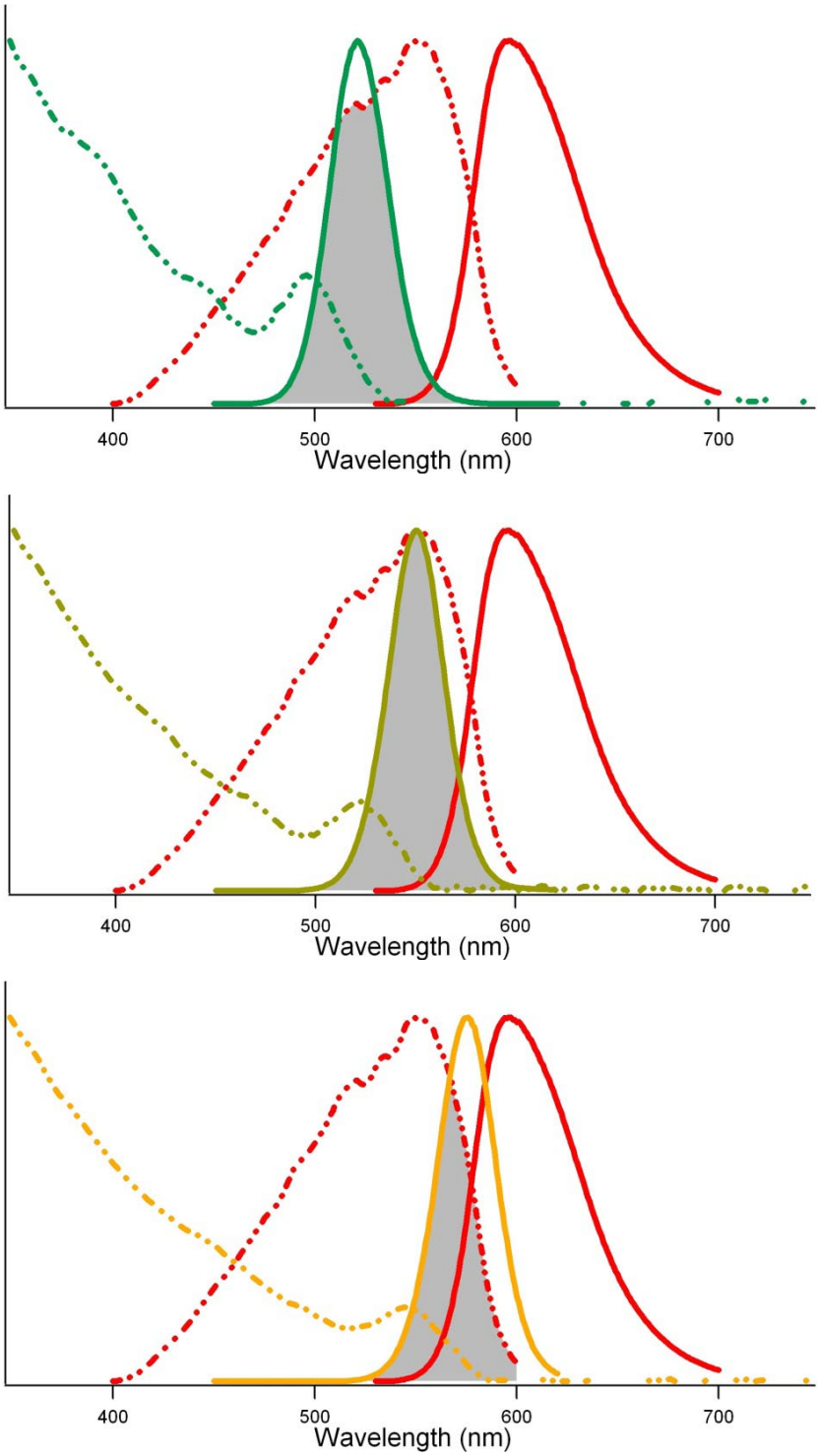

Figure 6.4: Spectral overlap of quantum dot donors and tdTomato.
From top to bottom 520 nm, 540 nm, and 560 nm T2-MP carboxyl-functionalized EviTags.

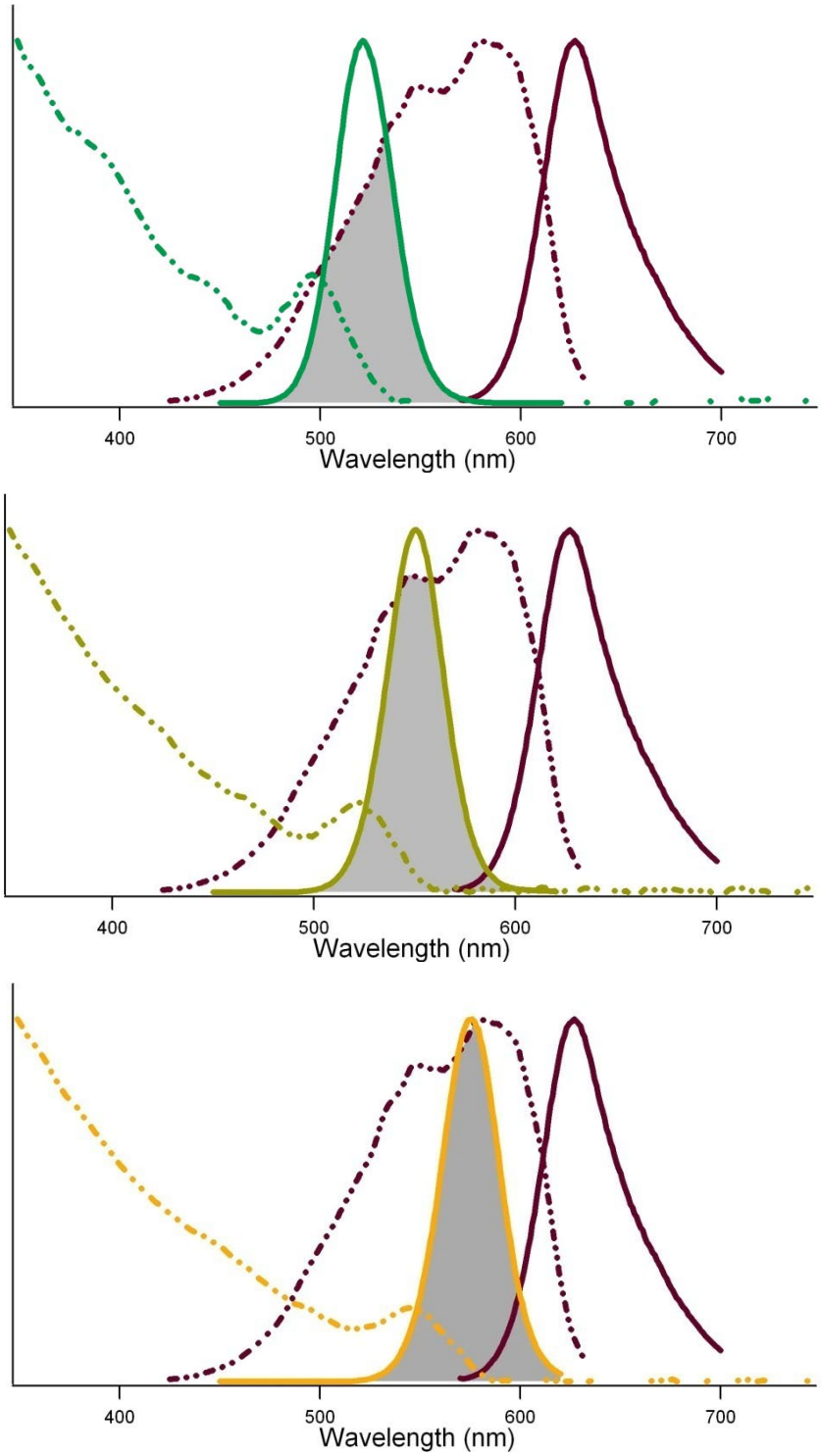

Figure 6.5: Spectral overlap of quantum dot donors and mCherry.
From top to bottom 520 nm, 540 nm, and 560 nm T2-MP carboxyl-functionalized EviTags.

FRET Assays

Assay Protocol. Assays examining the FRET efficiency of the various pairs were carried out in black, flat-bottomed, nobinding 384-well plates. Alternating serial dilutions of fluorescent proteins were made to produce a range of average QD:FP ratios ranging from 16 FPs per QD to fewer than 0.2 FPs per QD. T2-MP carboxyl-functionalized EviTags were then added to the wells at a final concentration of 50 nM. All of the assays were prepared in PBS, pH 7.4, with 1% bovine serum albumin (BSA) added to minimize any nonspecific binding. After allowing 15 minutes for self-assembly, the emission spectra were measured in a Tecan Safire multiplate reader with an excitation wavelength of 400 nm, excitation bandwidth of 12 nm, emission bandwidth of 5 nm, and a step size of 3 nm. All of the assays were performed in triplicate, as were FP-only controls.

Direct Excitation of FPs. Some direct excitation of the FRET acceptor is inevitable in FRET assays, although in this case the direct excitation was minimal due to the brightness of the QDs, which allows for low concentrations of the donor and thereby relatively low acceptor concentrations, and the minimal excitation of the FPs at 400 nm. By looking at the spectra in Figure 6.6, one can see that the majority of the FP emission in the FRET assays was indeed sensitized emission. The small peak at 500 nm seen in all of the samples was not due to the direct excitation of any of the FPs, but rather was consistent from well to well and was due to the autofluorescence of the BSA in the reaction buffer. Although the direct excitation of the FPs was low, the FP-only background control spectra were subtracted from the FRET spectra prior to peak deconvolution to improve the accuracy of the peak integrations.

Energy Transfer. As seen in Figure 6.7 through Figure 6.12, all three of the His-tagged fluorescent proteins exhibited an ability to substantially quench the QD emission due to FRET, as demonstrated by the across-the-board decrease in the QD emission peak, the correlation between the spectral overlap of the donor-acceptor pair and the change in the spectra, and the quenching efficiency (Table 6.3). Sensitized emission was observed from each of the protein acceptors, although tdTomato and mOrange emitted more strongly than mCherry.

The assays were each repeated using fluorescent proteins lacking the His-tag as negative controls to ensure that the QD-FP binding was indeed mediated by the polyhistidine, and a second control utilized a short His10 peptide without a fluorophore to demonstrate that the binding of the polyhistidine to the core-shell surface was not causing contact-quenching of the QD or otherwise affecting the QD emission.

Table 6.3: Donor-acceptor pair results summary.

Donor-Acceptor Pair	Donor-acceptor distance R (Å)	FRET efficiency (E) at 1:1 QD:FP[a]	Maximum measured FRET efficiency (E)
QD520-mOrange	57.4 ± 6.6	0.261	0.761
QD520-tdTomato	53.8 ± 3.4	0.428	0.867
QD540-tdTomato	52.7 ± 3.9	0.504	0.902
QD520-mCherry	52.0 ± 4.3	0.302	0.713
QD540-mCherry	56.2 ± 4.5	0.343	0.798
QD560-mCherry	53.6 ± 5.1	0.401	0.838

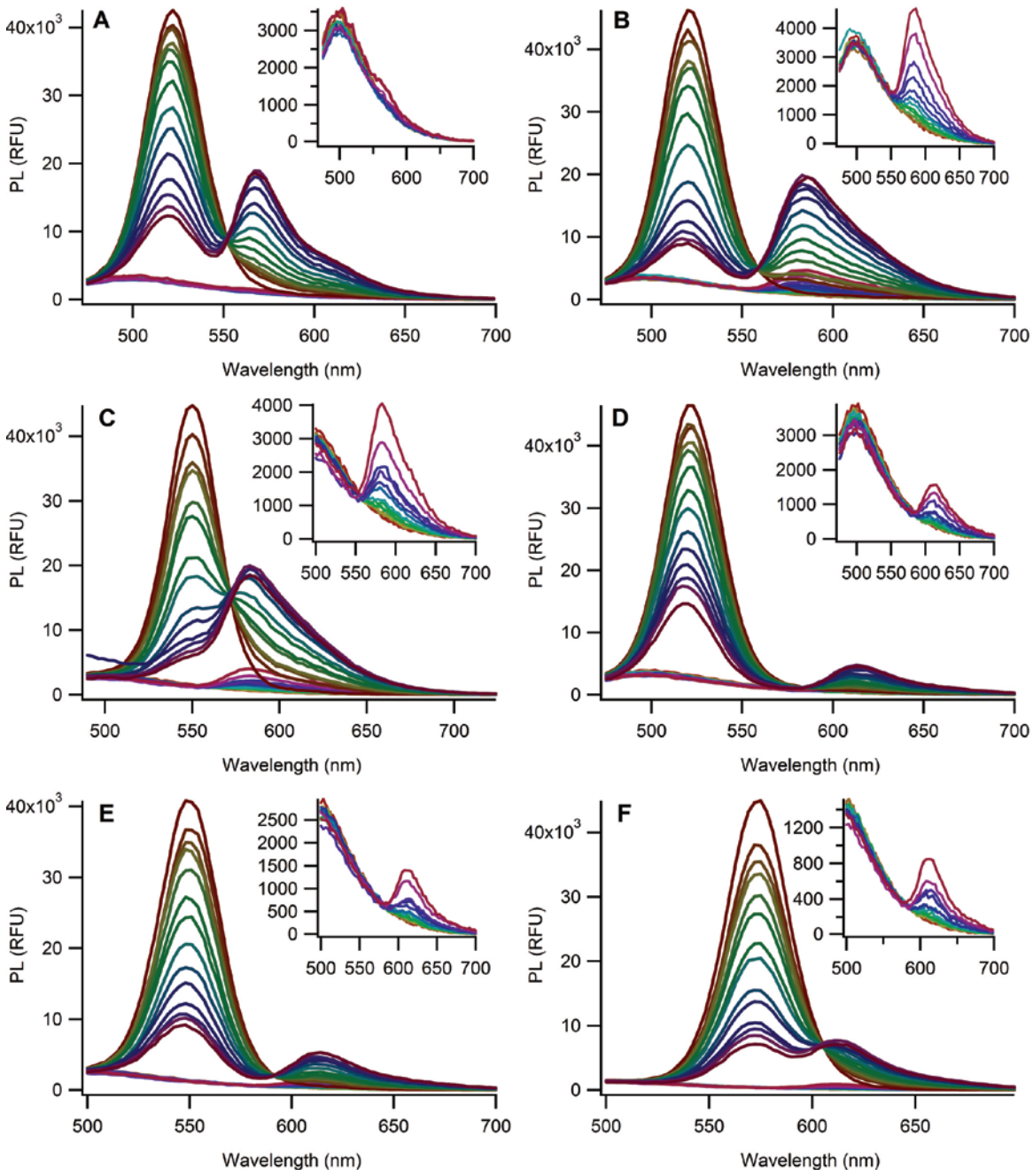

Figure 6.6: Direct excitation of the fluorescent proteins in the FRET assay.
A) QD520 + His6-mOrange; B) QD520 + His6-tdTomato; C) QD540 + His6-tdTomato; D) QD520 + His6-mCherry; E) QD540 + His6-mCherry; and F) QD560 + His6-mCherry. Insets: The background emission from the His6-FPs scaled for clarity. The QD concentration was fixed at 50 nM, while the FP concentration varied from 0-800 nM.

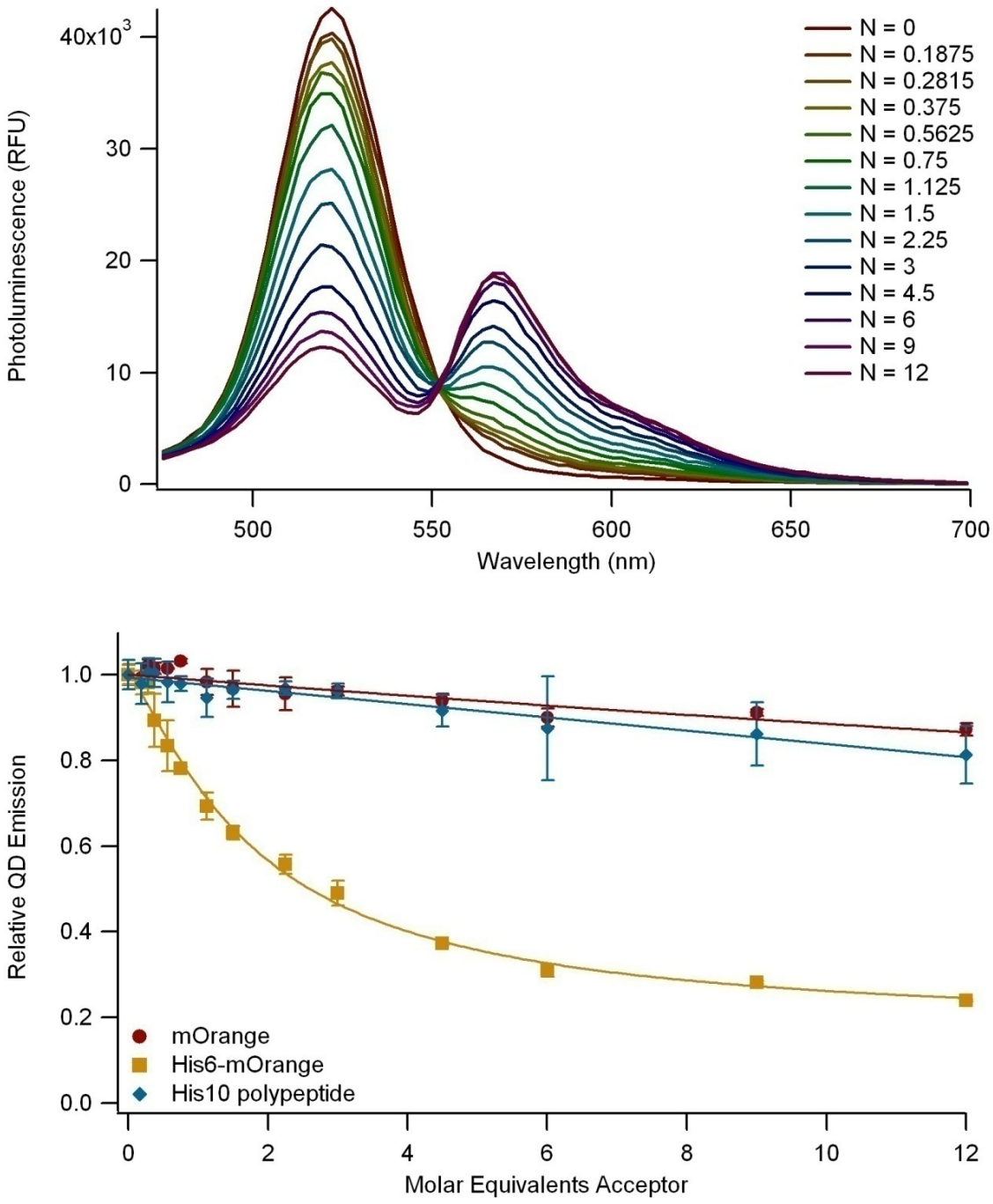

Figure 6.7: FRET between 520 nm EviTags and mOrange.
Top: Emission spectra of 520 nm T2-MP carboxyl-functionalized EviTags incubated with His6-mOrange, showing a dose-dependent decrease in QD emission and concomitant increase in the sensitized emission of mOrange.
Bottom: Plot of the relative QD emission *versus* the number of acceptor molecules per QD. Points represent mean ± standard deviation of $n = 3$

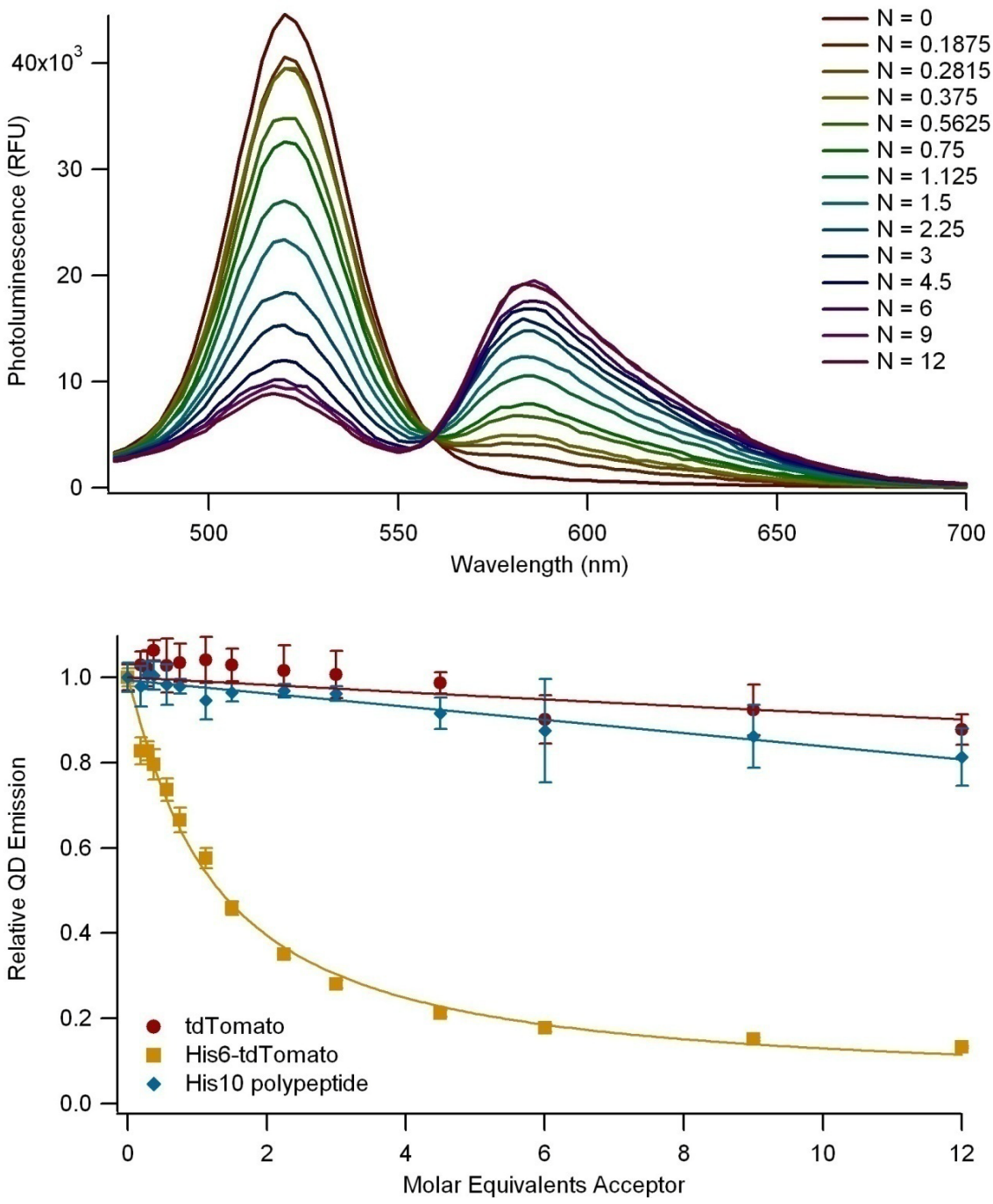

Figure 6.8: FRET between 520 nm EviTags and tdTomato.
Top: Emission spectra of 520 nm T2-MP carboxyl-functionalized EviTags incubated with His6-tdTomato, showing a dose-dependent decrease in QD emission and concomitant increase in the sensitized emission of tdTomato.
Bottom: Plot of the relative QD emission *versus* the number of acceptor molecules per QD. Points represent mean ± standard deviation of $n = 3$.

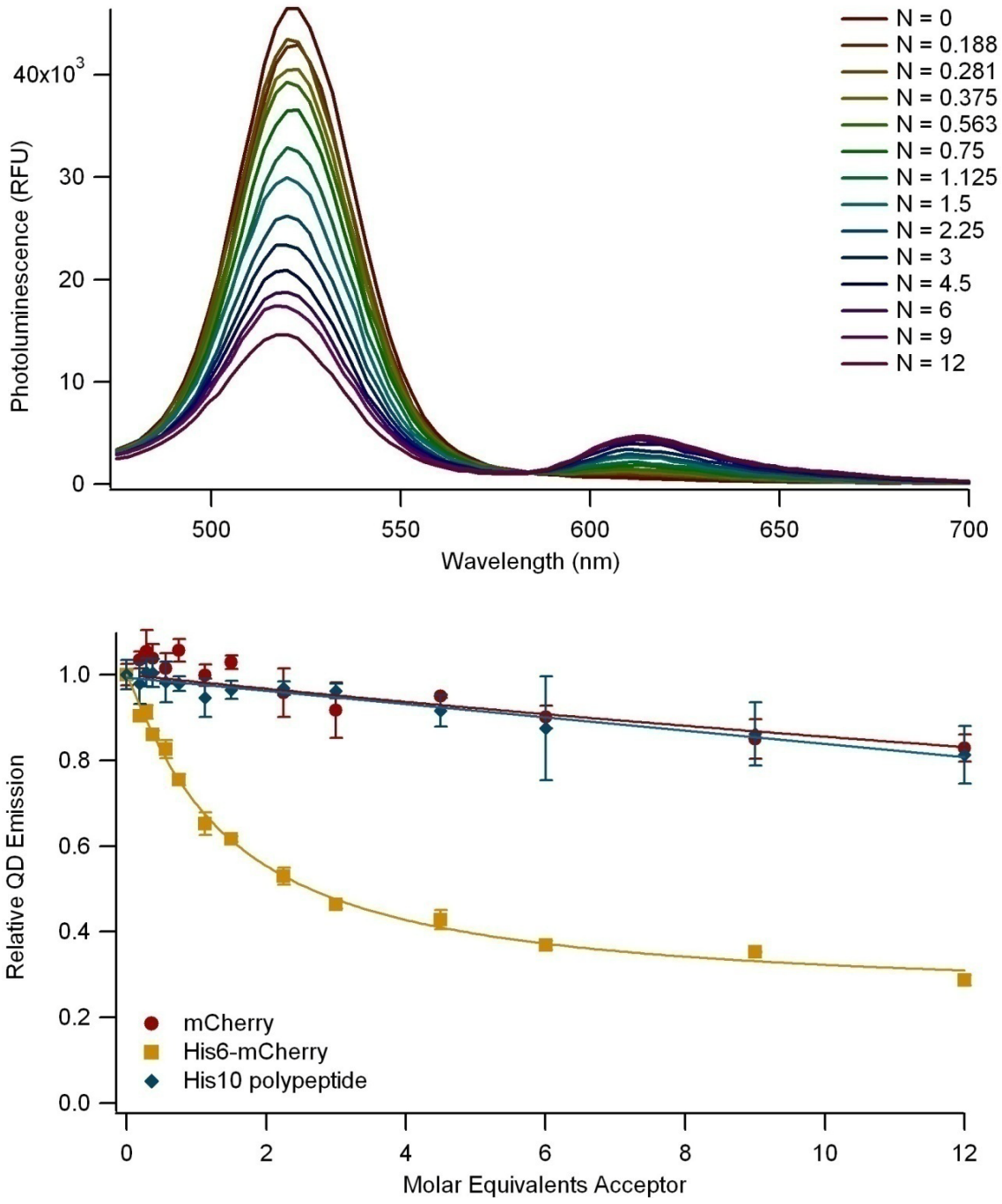

Figure 6.9: FRET between 520 nm EviTags and mCherry.
Top: Emission spectra of 520 nm T2-MP carboxyl-functionalized EviTags incubated with His6-tdTomato, showing a dose-dependent decrease in QD emission and concomitant increase in the sensitized emission of tdTomato.
Bottom: Plot of the relative QD emission *versus* the number of acceptor molecules per QD. Points represent mean ± standard deviation of $n = 3$.

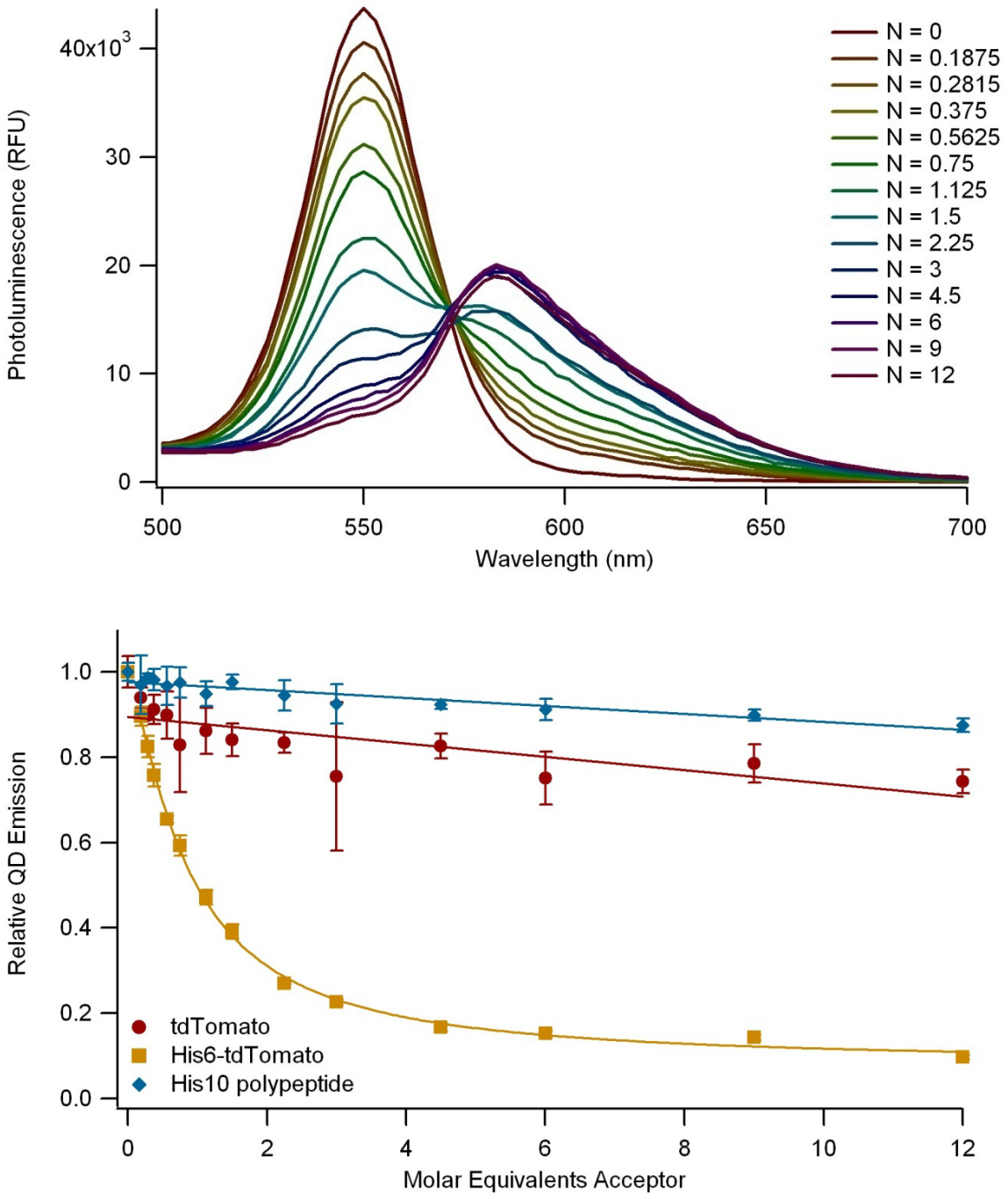

Figure 6.10: FRET between 540 nm EviTags and tdTomato.
Top: Emission spectra of 520 nm T2-MP carboxyl-functionalized EviTags incubated with His6-tdTomato, showing a dose-dependent decrease in QD emission and concomitant increase in the sensitized emission of tdTomato.
Bottom: Plot of the relative QD emission *versus* the number of acceptor molecules per QD. Points represent mean ± standard deviation of $n = 3$.

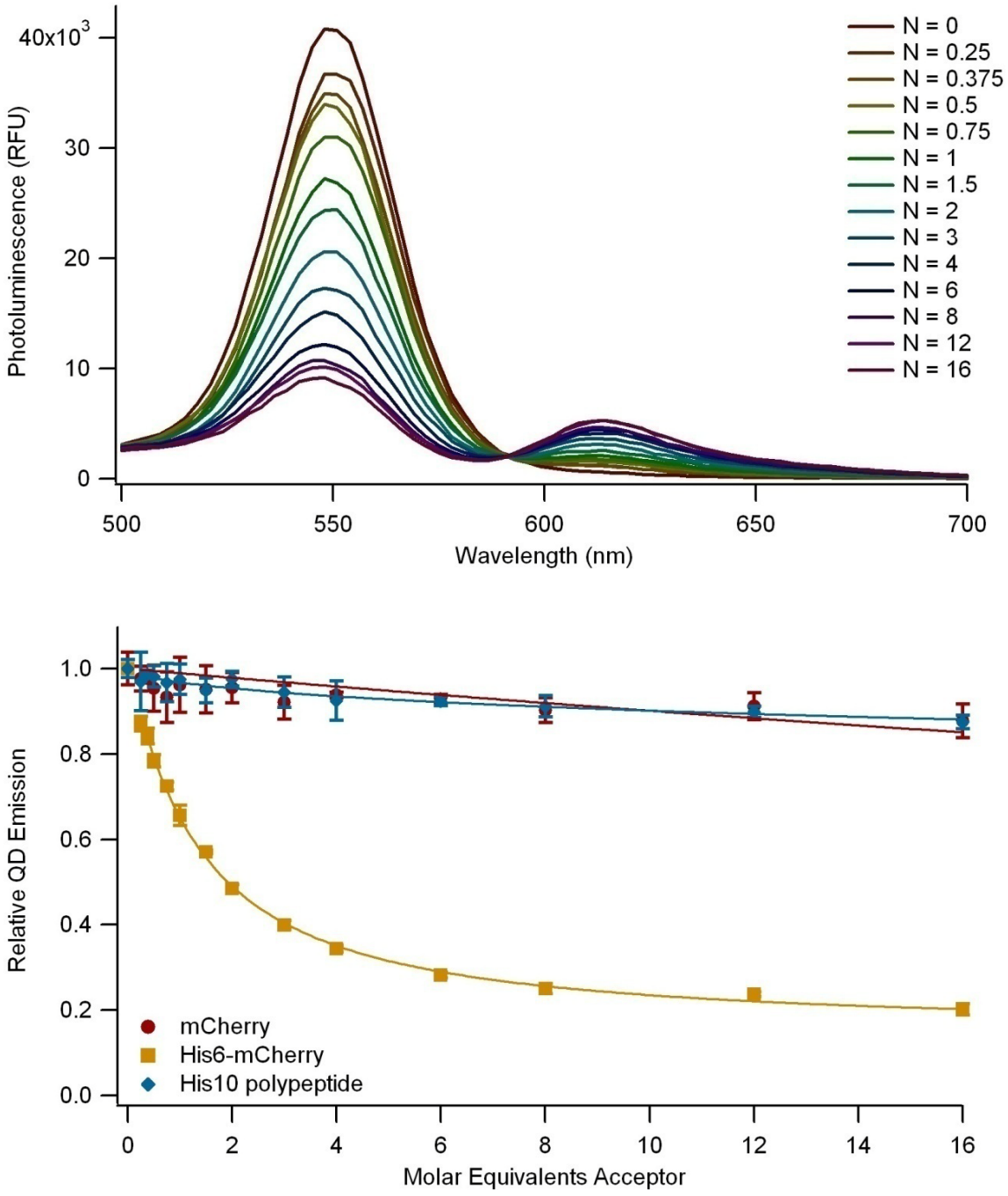

Figure 6.11: FRET between 540nm EviTag and mCherry.
Top: Emission spectra of 520 nm T2-MP carboxyl-functionalized EviTags incubated with His6-mCherry, showing a dose-dependent decrease in QD emission and concomitant increase in the sensitized emission of mCherry.
Bottom: Plot of the relative QD emission *versus* the number of acceptor molecules per QD.Points represent mean ± standard deviation of $n = 3$.

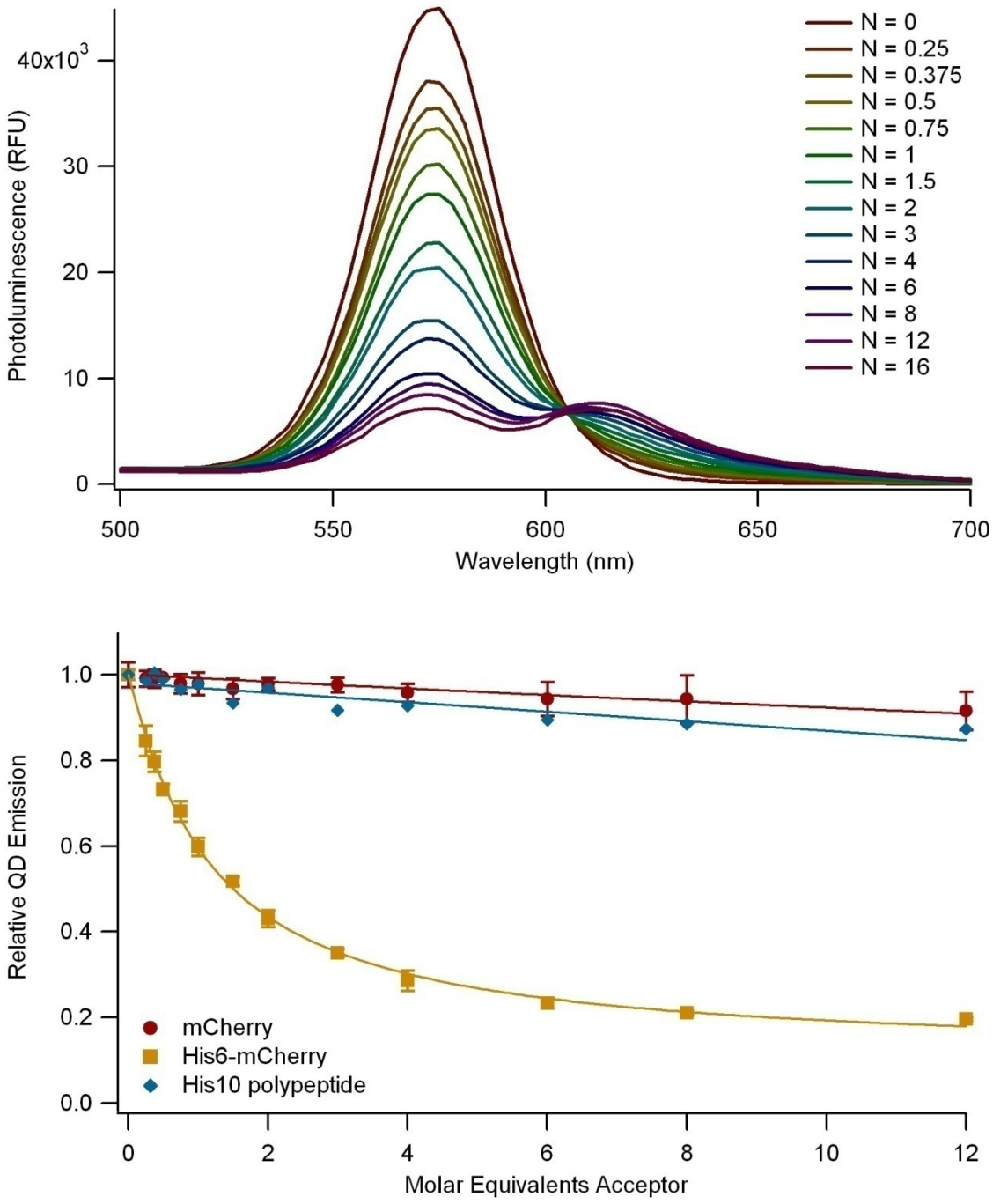

Figure 6.12: FRET between 560 nm EviTags and mCherry.
Top: Emission spectra of 520 nm T2-MP carboxyl-functionalized EviTags incubated with His6-tdTomato, showing a dose-dependent decrease in QD emission and concomitant increase in the sensitized emission of tdTomato.
Bottom: Plot of the relative QD emission *versus* the number of acceptor molecules per QD. Points represent mean ± standard deviation of $n = 3$.

FRET Analysis. Although the direct excitation of the FPs was minimal, the background emission was subtracted from each of the FRET spectra at the same FP concentration at the beginning of the analysis. Each background–subtracted spectrum was then deconvolved as described in the Methods (page 47), and the areas under the QD peaks with FRET were normalized to the area under the QD spectrum in the absence of FP. The resulting normalized QD emission intensities were plotted *versus* the acceptor concentrations in Figure 6.7 to Figure 6.12. The non-His-tagged FP results were fitted to the Stern-Vollmer equation (Equation (6), page 48), which describes collisional quenching (*4*). To estimate the strength of binding between the EviTags and the His-tagged proteins under steady-state conditions, the His6-FP data were fitted to the modified Hill equation (Equation (8), page 49) derived in the Methods (page 48):

$$\frac{F_{DA}}{F_D} = 1 - E_{\max}\left[\frac{1}{1+\left(\frac{K_D}{c}\right)^h}\right], \qquad (8)$$

where F_{DA} is the fluorescence of the donor in the presence of the acceptor, F_D is the fluorescence of the donor in the absence of the acceptor, $E_{\max}$ is the maximum FRET efficiency, c is the concentration of the acceptor, h is the Hill coefficient, and K_D is a nominal dissociation constant defined as the acceptor concentration at which there is 50% quenching of the QDs (*106*). Note that the nominal K_D is not the concentration at which there is 50% binding, but rather the concentration at which there is 50% quenching of the QD. The two are distinct because the fluorescent quenching is not linearly related to the number of acceptors bound (*4*, *10*). All of the curvefit coefficients, including the nominal K_Ds for each FRET pair, are listed in Table 6.4.

Table 6.4: Summary of curve-fit coefficients.

	Coefficients from fitting the His6-FP/QD data (relative QD emission) to a modified Hill equation			Stern-Volmer coefficient from FP/QD data
Donor-Acceptor Pair	E_{max}	K_D (nM)	h	K_{SV}
QD520-mOrange	0.827 ± 0.037	92.7 ± 9.6	1.256 ± 0.103	0.0129 ± 0.0012
QD520-tdTomato	0.960 ± 0.040	61.2 ± 6.6	1.085 ± 0.090	0.0097 ± 0.0022
QD540-tdTomato	0.920 ± 0.011	43.2 ± 1.3	1.301 ± 0.044	0.0392 ± 0.0068
QD520-mCherry	0.755 ± 0.028	72.0 ± 6.7	1.115 ± 0.077	0.0174 ± 0.0021
QD540-mCherry	0.852 ± 0.014	69.7 ± 3.0	1.101 ± 0.040	0.0104 ± 0.0015
QD560-mCherry	0.892 ± 0.016	59.8 ± 2.9	1.059 ± 0.044	0.0083 ± 0.0004

The donor-acceptor distance was calculated for each pair at each concentration using Equation (11) (page 50) and the average and standard deviation is presented in Table 6.3. All of the donor-acceptor pairs displayed a separation distance of 5-6 nm. While compared with the relatively small differences in the QD sizes the standard deviations on these values are too large to allow for correlations to be drawn between the QD core-shell radius and the distance between the donor and acceptor, all of the values are consistent with the fluorescent protein binding to the QD core-shell surface.

Ratiometric analysis. To highlight differences in the carious FP acceptors, the FRET data were also analyzed using a ratiometric method, where the emission of the acceptor was divided by the emission from the donor and plotted as a function of the number of proteins per QD (Figure 6.13, top). While all three of the FPS were shown to be effective quenchers of the QD emission, this ratiometric analysis demonstrates the contrast between the emissions of the three proteins. For example, the three FRET pairs containing mCherry showed only a small increase in F_A/F_D due to the low quantum yield of the FP, while the FRET pairs containing tdTomato demonstrated a dramatic increase because of the exceptional brightness of tdTomato. mOrange fell between the two in the

increase of F_A/F_D as it possesses a quantum yield as high as that of tdTomato, but like mCherry, it has only half the molar extinction coefficient as that of tdTomato due to its monomeric form. The distinction between different FPs based on their emission properties was further demonstrated in Figure 6.13 (bottom) by plotting the log of F_A/F_D as a function of the FRET efficiency. When the effect of the absorption characteristics of the FPs is eliminated, the six QD-FP pairs split into two groups: those containing the more efficient emitters mOrange or tdTomato and those containing mCherry. Not that tdTomato and mOrange converged almost completely because both have quantum yields of 0.69 (Table 6.1).

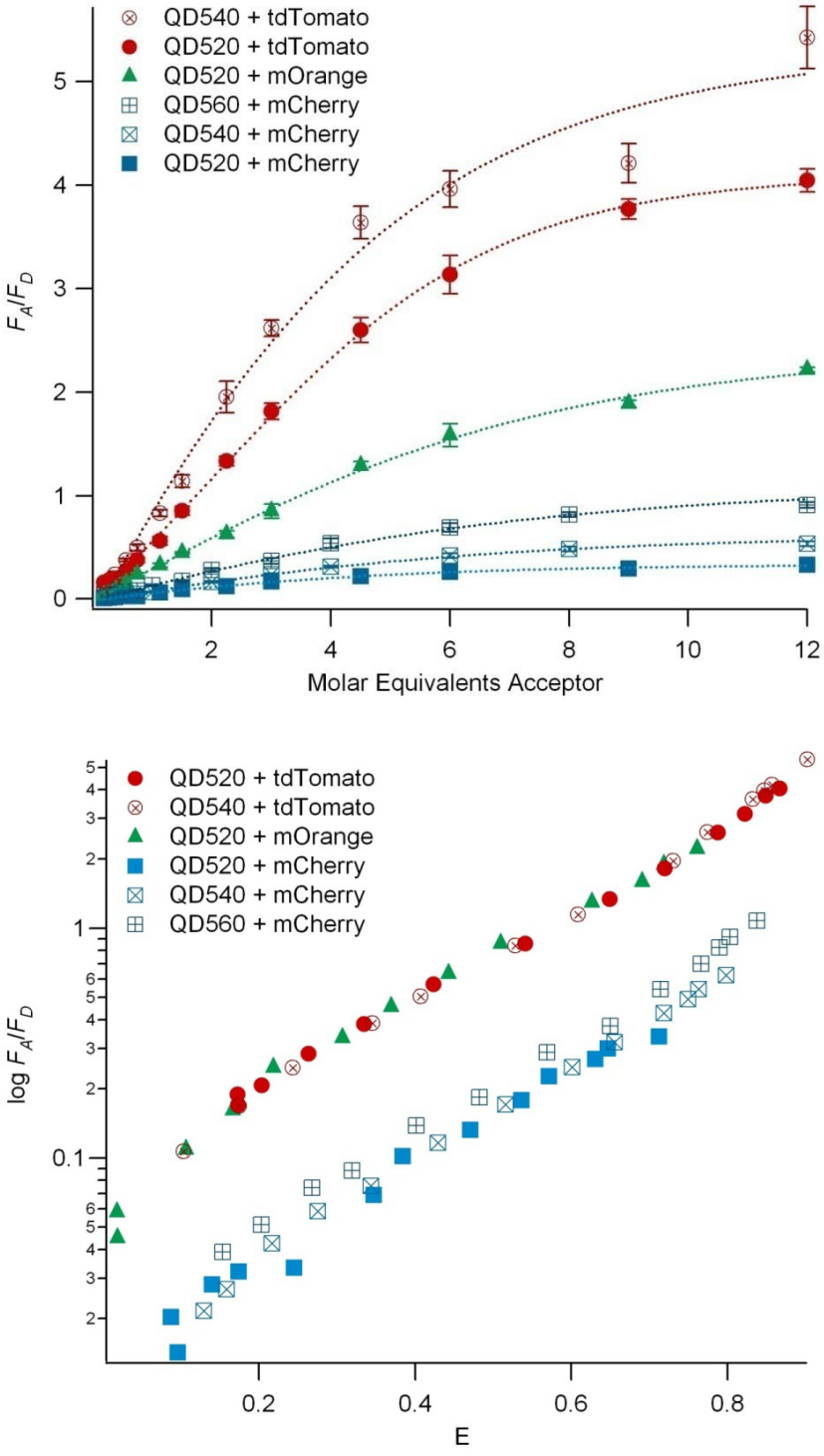

Figure 6.13: Ratiometric analysis of FRET assays.
Top: The acceptor emission to donor emission ratio as a function of acceptor concentration. Data are represented as a mean ± standard deviation of $n = 3$.
Bottom: The log of the acceptor emission/donor emission as a function of FRET efficiency. Each point is the mean of data taken in triplicate.

DISCUSSION

All six of the QD-FP FRET pairs demonstrated a significant level of energy transfer with 26-50% QD quenching at a 1:1 FP:QD ratio and up to 90% quenching at higher FP:QD ratios. The non-His-tagged and His10 controls produced minimal quenching of the EviTags, demonstrating that the effect was neither due to contact quenching nor due to the presence of freely dispersed fluorescent protein, but rather the presence of both the polyhistidine and the fluorescent protein was necessary for effective quenching.

The binding of the His-tagged proteins to the EviTags had a nominal K_D between 40 and 100 nM, which is in the range of dissociation constants described for antigen-antibody binding (*114*). This binding strength indicates that the His-tag conjugation to the commercially-available EviTags should be sufficient for use in *in vitro* assays. FPs containing a His10 N-terminal insertion were also tested in the FRET assay with the hypothesis that the longer polyhistidine-tag may increase the binding affinity, as is seen in IMAC (*115*). No significant difference between the nominal K_Ds of the His6-FPs and His10-FPs was observed (data not shown), however, which is consistent with what reported in the literature (*78*).

All three of the fluorescent proteins tested were effective QD quenchers, but their capacity for sensitized emission varied significantly. mOrange and, in particular, tdTomato each emitted strongly due to FRET, emitting more strongly than the QD donor at high acceptor to donor ratios. In contrast, mCherry emitted relatively weakly, although the FRET measured FRET efficiencies were higher than those for mOrange because mCherry still absorbed the energy very effectively.

While the increased molar extinction coefficient of tdTomato did make it a more effective quencher than the monomeric mOrange and mCherry, the difference was not dramatic enough for one to choose tdTomato over mCherry when probe size is a concern. In the ratiometric analysis, however, the differences due to the FP properties was clear. Thus, the difference between the FPs can be exploited in probe design: using the quencher-like mCherry allows one to neglect the acceptor emission for a more straightforward data analysis, whereas tdTomato is preferred when the ratiometric method could be used in data analysis to extend the dynamic range of an assay or to minimize the effects of well-to-well variation.

CONCLUSION

This study characterized six QD-FP FRET pairs and demonstrated that mOrange, mCherry, and tdTomato are efficient FRET acceptors when paired with a quantum dot donor. The up to 90% quenching of QD photoluminescence seen here indicates that, under the right conditions, QD emission could be modulated in a fashion conducive to highly sensitive sensor applications. The large variation of fluorescent protein properties that can be achieved through genetic engineering guarantees a wide variety of FRET pairs can be constructed, each designed to suit various applications. These findings have significant implications for the development of versatile and easily accessible QD-based FRET probes for biomedical applications.

CHAPTER 7

APPLICATION OF THE QUANTUM DOT-FLUORESCENT PROTEIN PAIR AS A RATIOMETRIC pH SENSOR[*]

INTRODUCTION

Intracellular pH is an important modulator of cell function. Even very small changes in pH can trigger dramatic cellular responses, and a number of mechanisms finely regulate the pH of various sub-cellular domains (*116*). Imaging intracellular pH with high spatial resolution could extend our insight into many physiological or pathogenic processes taking place within cells. Fluorescent indicators, most commonly fluorescein and its many derivatives, can be used to measure intracellular pH, but are typically not suited for precise quantification because single wavelength emitters provide no internal control for concentration. Thus, it is unclear whether a change in the brightness of the indicator is due to a change in local concentration, which is frequently exasperated by the leakage of the dyes, or is truly a result of a pH fluctuation (*117*). In contrast, such an internal control is inherent in ratiometric pH indicators, facilitating quantification. In addition, traditional fluorophores often exhibit significant photbleaching, hindering their usage for monitoring changes in pH over time. Designing pH-sensitive imaging agents based on highly photostable components, such as semiconductor quantum dots (QDs), could facilitate time-lapse fluorescence microscopy studies that could deepen our understanding of elusive intracellular processes.

[*] Modified from Dennis AM, Rhee WJ, Sotto D, and G Bao. Quantum Dot-Fluorescent Protein Hybrid pH Sensor for Intracellular Imaging, in preparation.

With these goals in mind, QDs were used to design a pH-sensitive fluorescence resonance energy transfer (FRET) probe. A very few examples of QD-based pH sensors have been described in the literature. In fact, the only example of imaging intracellular pH with QDs simply relies on the inherent pH instability of minimally passivated QDs. As the QDs described were brighter at alkaline pHs than at acidic pHs, the authors suggested that they could be used as intracellular pH sensors (*118*), but because just the

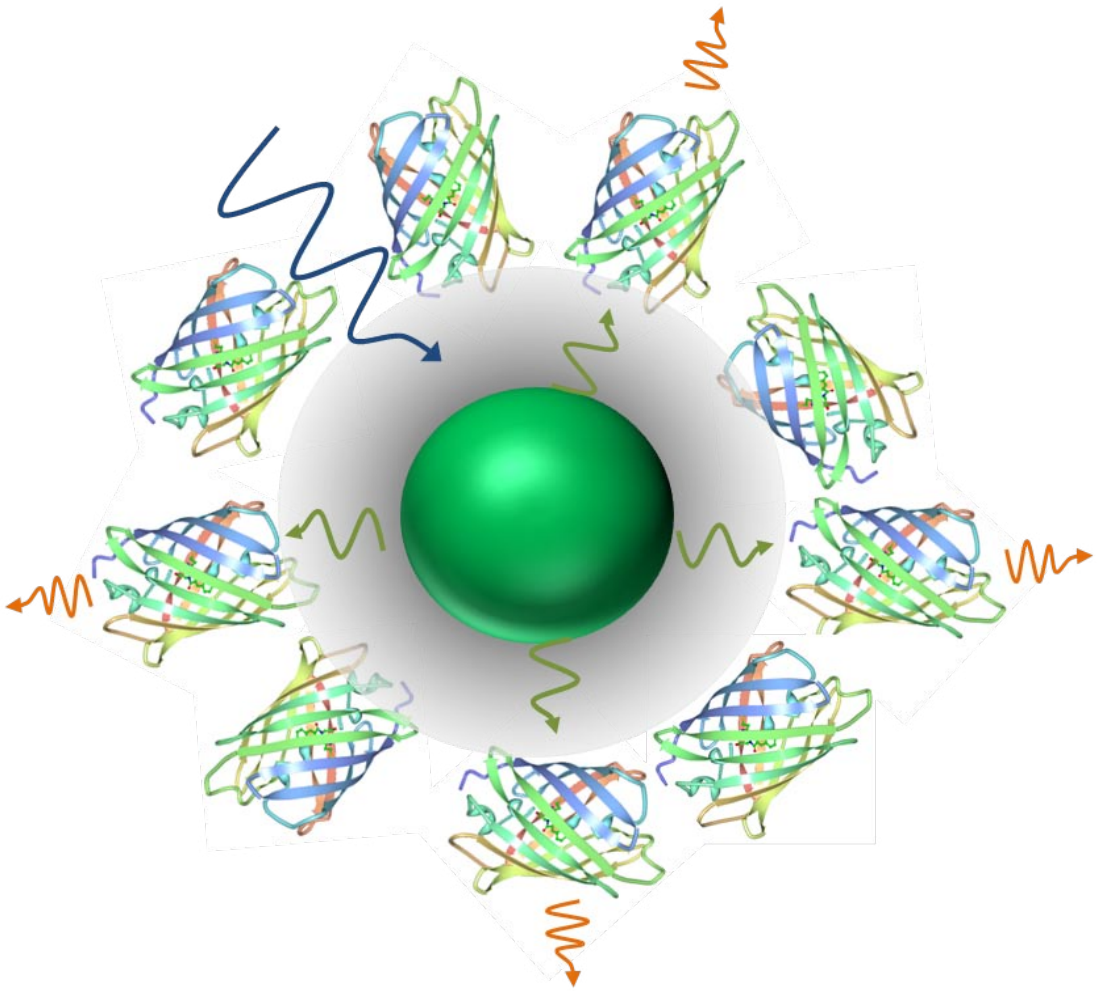

Figure 7.1: Schematic of QD-FP FRET-based pH sensor.
Numerous GFP-like fluorescent proteins are covalently conjugated to the outer polymer layer of 525 nm ITK carboxyl Qdots. When the QD is excited with UV illumination, some of this energy is transferred to the protein, resulting in sensitized emission of the protein. The efficiency of this energy transfer varies with the protein spectral properties, which are pH dependent, resulting in an optical FRET-based pH sensor.

emission intensity of the QD is modulated, it would be very difficult to use this as an independent indicator. In another example, an organic ligand, [1,3]oxazine, is used as either a quencher or an electron donor to the QD based on its protonation state (*16*). This probe design results in the gradual change in QD photoluminescence over a range of pH 3-11. Both because of a lack of sensitivity in physiological pHs and the absence of a control for concentration, this probe is not proposed for intracellular imaging.

Two FRET-based, ratiometric pH sensors utilizing a QD donor to a pH sensitive dye have been described (*17, 18*). The first uses the a pH sensitive squarine dye as the acceptor, whose molar extinction coefficient decreases as the pH increases with a pK_a ~8.5, (*17*). While this probe exhibits a pH-dependent shift in the conjugate emission spectra, the high pK_a does not recommend it for intracellular imaging. The second uses a fluoroscien derivative as the FRET acceptor (*18*). Although this conjugate is poorly characterized, it is described as having sensing capabilities over a range of ~pH 5.5 to 8.5 with a region of insensitivity from 7.0-7.5, precisely where sensitivity is needed for intracellular imaging. More successful nanoparticle pH sensors for intracellular imaging have been based on using dye-loaded polymer spheres (*119, 120*).

As was shown in Chapter 5 and Chapter 6, GFP-like fluorescent proteins have been paired with QDs to form FRET probes (*15, 84*). The high efficiency of energy transfer indicates that these FRET pairings could be used effectively in various sensing applications. In fact, one QD-FP biosensor has already been developed for monitoring protease activity (*84*). Here we utilize the intrinsic pH sensitivity of mOrange in a new QD-FP FRET-based sensor: a pH sensor with properties appropriate for intracellular imaging.

RESULTS

Protein Properties

The optical properties of two different GFP-like fluorescent proteins were evaluated, particularly for their pH sensitivity. The absorbance spectra of mOrange and a single point mutation thereof, mOrange M163K, were measured as the pH was titrated with 1 N HCl. All titrations were performed in 20 mM PBS supplemented with 1% (w/v) bovine serum albumin (BSA) to minimize adsorption of the protein or probe to the cuvette walls. The absorption spectra of mOrange show a decrease in the primary absorption peak at 547 nm and the development of a secondary peak at 400 nm at low pHs (Figure 7.2, top). The lack of isosbestic point indicates that this is not a transition between two discrete protein states, but rather is more likely a cooperative effect. The molar extinction coefficient of mOrange at 547nm changes with pH, as shown in Figure 7.2 (bottom). The change in molar extinction coefficient with pH is dramatic and relatively sharp with a pK_a of 6.9.

The mutant mOrange M163K similarly shows a decrease in absorption at 547 nm and a concomitant increase at 400 nm, but this transition is even more complicated than that of mOrange, making clear that this is not a simple phase transition between two discrete states (Figure 7.3, top). The molar extinction coefficient at 547 nm shows a similarly smooth, if more gradual, transition as that of mOrange with a pK_a pf 7.9 (Figure 7.3, bottom). After titrating with HCl, 1 N NaOH was added to all of the test solutions to demonstrate that the change in the spectral profile is reversible. Although in many cases the pH of the solution was not brought back to the extreme upper end of the pH range tested here (pH 10.0), the intermediate pH shown by the “recovered” spectra on the

spectral plots demonstrates that the trace mimics other spectra from the more alkaline pH ranges, indicating reversibility.

Although the irregular absorption spectra of the pH-sensitive proteins, particularly mOrange M163K, raised concerns about the predictability of the protein emission with respect to pH, the relative regularity of the excitation spectra of each of the proteins allayed those concerns. In fact, the excitation spectra of the two protein variants are very similar and show that there is no excitation of the fluorophore from the higher energy wavelengths that were absorbing at acidic pHs (Figure 7.4 and Figure 7.5). The emission spectra of the two proteins also vary in intensity with the pH, but this is not due to a change in the FP quantum yield (QY), but rather directly correlates to the amount of light being absorbed due to the changing molar extinction coefficient.

Circular dichroism (CD) spectroscopy was used to ensure that the changes in the protein optical properties were not a result of significant changes in the characteristic barrel structure of the GFP-like fluorescent proteins. As with the optical spectra, the protein was diluted in 20 mM PBS, pH 10.0 (although without the BSA supplementation) and was titrated with 1 N HCl. The mean residue ellipticity (MRE) of the His6-mOrange M163K mutant did not vary significantly with pH (Figure 7.6, bottom). His6-mOrange, in contrast, showed a clear pH-dependent decrease in the negative peak at 218 nm (Figure 7.6, top). The plot of the magnitude of the MRE at 218 nm with respect to pH (Figure 7.6, top inset) shows a clear similarity to the plots of other pH-dependent characteristics of mOrange like absorbance (Figure 7.2, bottom).

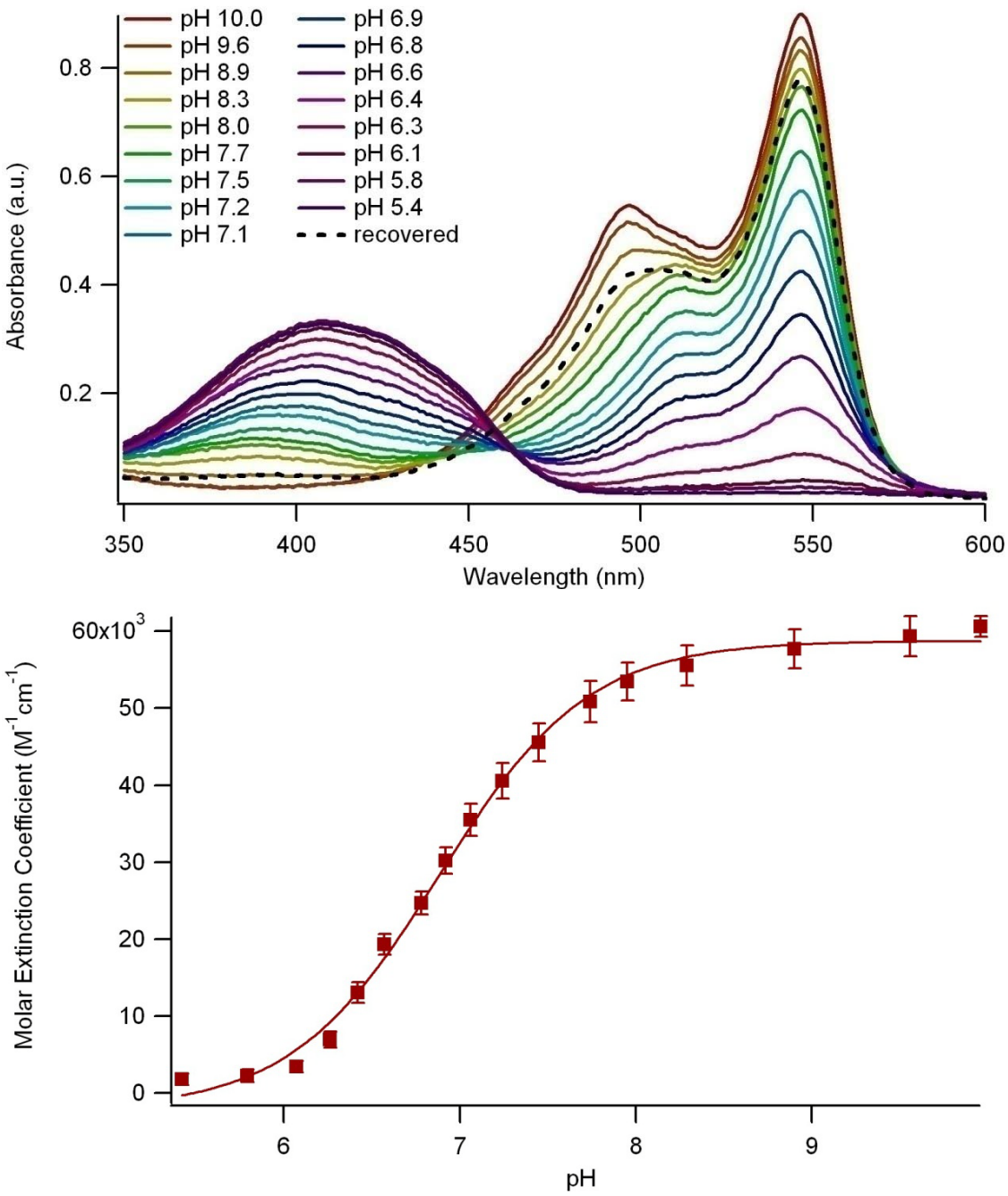

Figure 7.2: Absorbance of mOrange with respect to pH.
The absorbance spectra of mOrange changes in both magnitude and shape with pH (top), which is reflected in the change in the molar extinction coefficient at 547 nm with pH (bottom). All measurements started in alkaline buffer and were titrated with 1 N HCl. "Recovered" spectrum measured after adding a bolus of 1 N NaOH to acidified solution to show reversibility of transition (Note: pH not returned to maximum pH 10.0). Points in lower plot are mean ± standard deviation of three separate titrations.

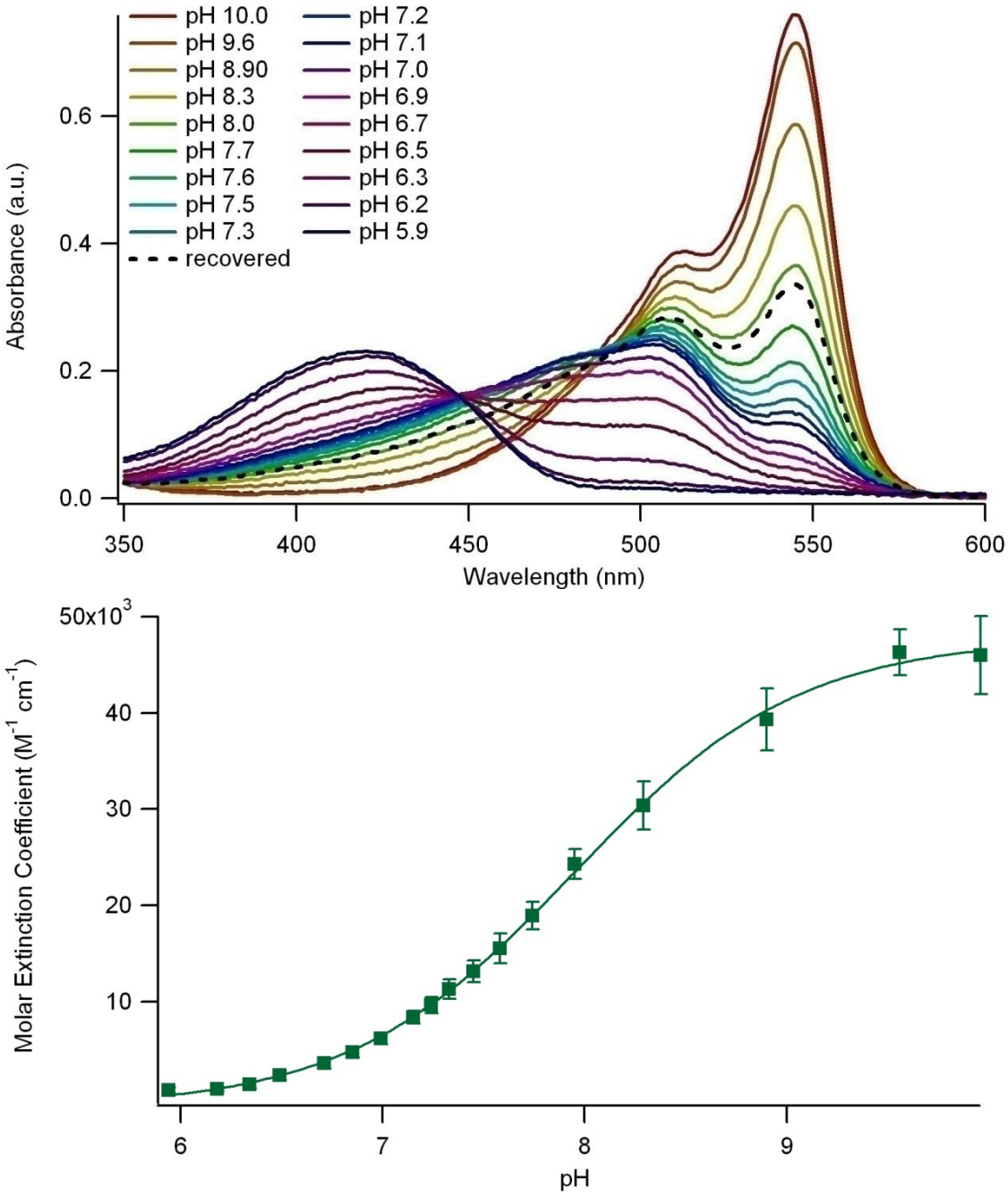

Figure 7.3: Absorbance of mOrange M163K with respect to pH.
The absorbance spectra of mOrange M163K changes in both magnitude and shape with pH (top), which is reflected in the change in the molar extinction coefficient at 547 nm with pH (bottom). All measurements started in alkaline buffer and were titrated with 1 N HCl. "Recovered" spectrum measured after adding a bolus of 1 N NaOH to acidified solution to show reversibility of transition (Note: pH not returned to maximum pH 10.0). Points in lower plot are mean ± standard deviation of three separate titrations.

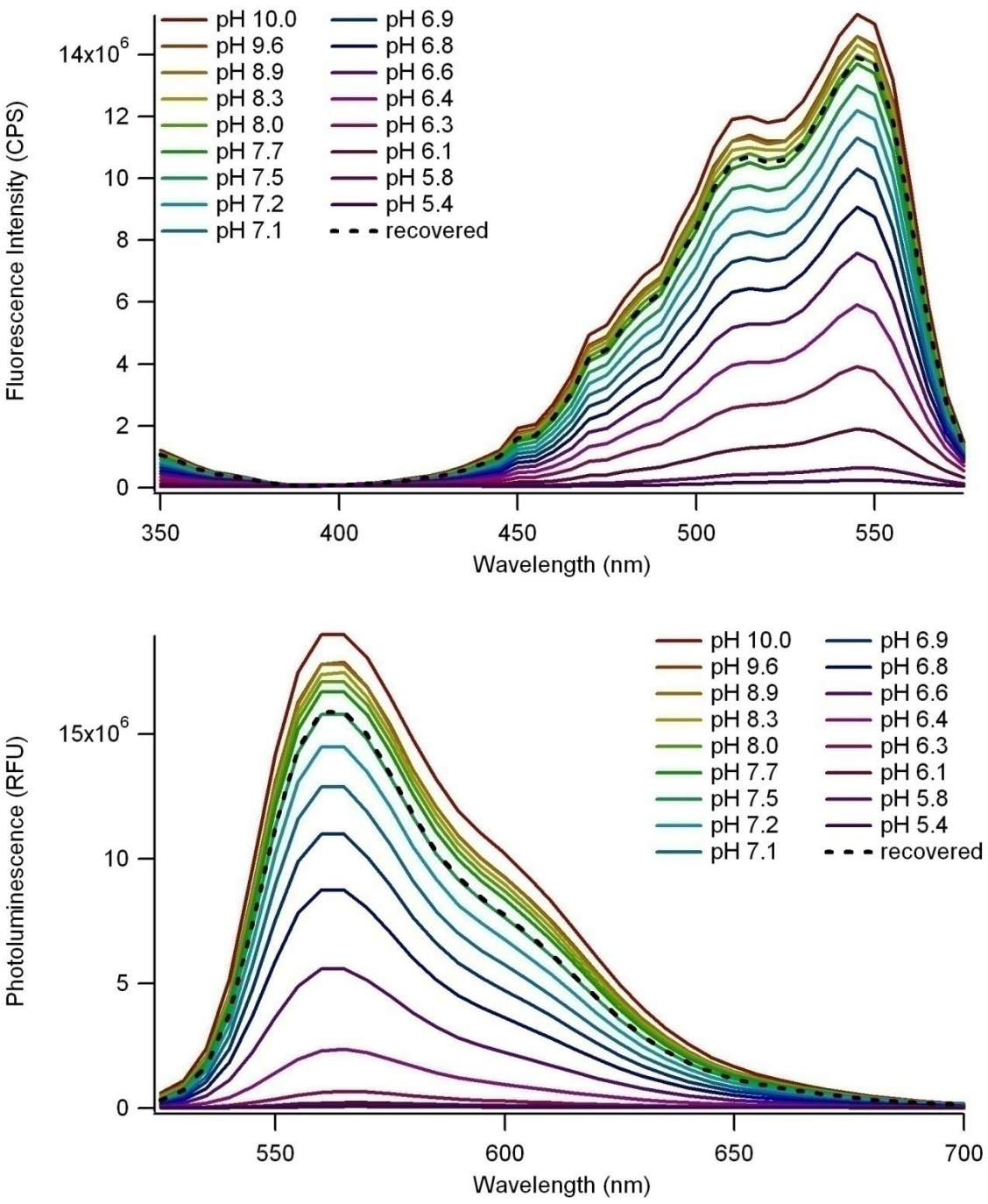

Figure 7.4: Fluorescence spectra of mOrange with respect to pH.
Excitation (top) and emission (bottom) spectra of mOrange with titration with 1 N HCl. The excitation spectra were measured with a fixed 585 nm emission wavelength, while the emission spectra were measured with excitation at 515 nm. "Recovered" spectra measured after addition of 1 N NaOH demonstrates reversibility of spectral changes.

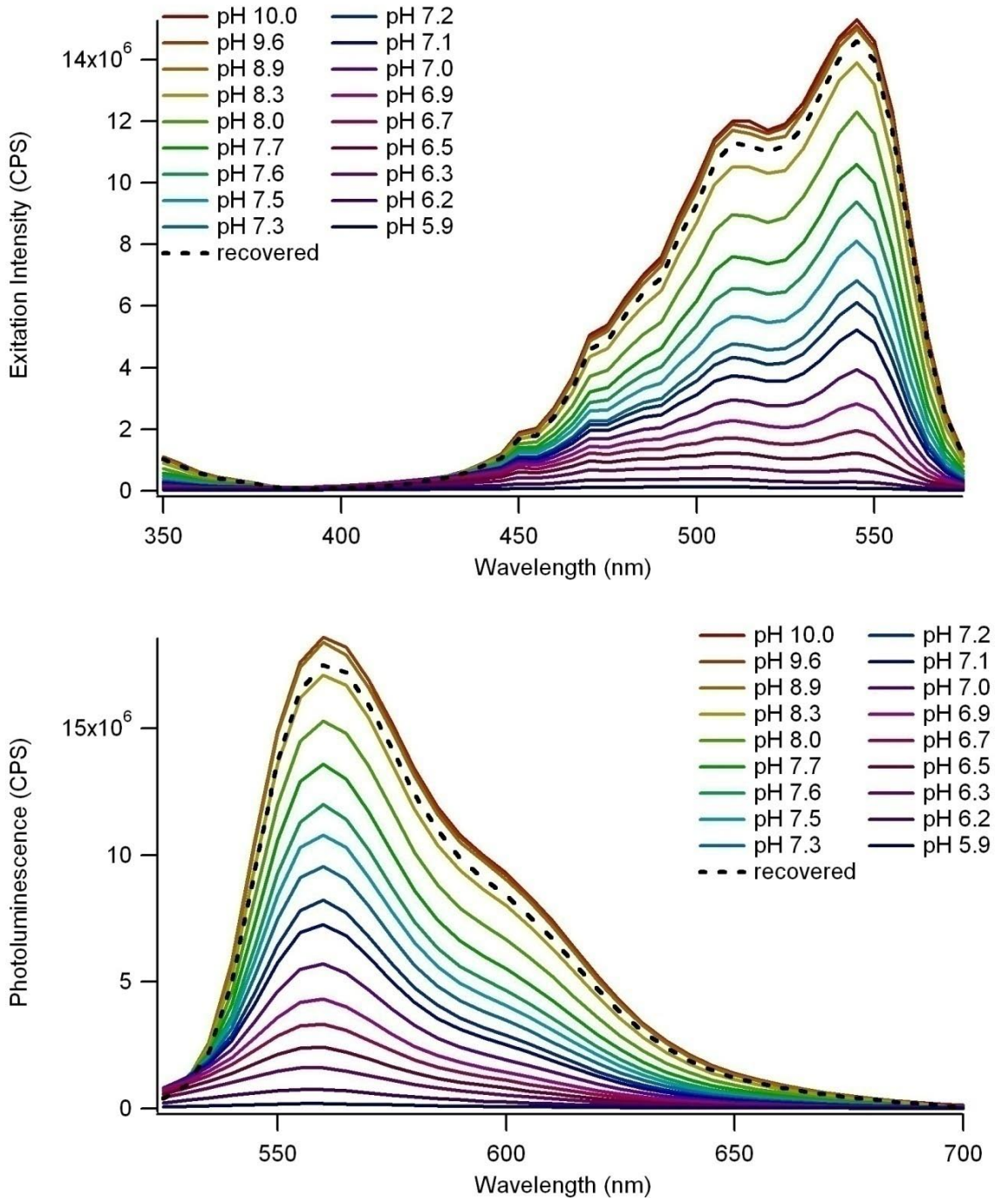

Figure 7.5: Fluorescence spectra of mOrange M163K with respect to pH.
Excitation (top) and emission (bottom) spectra of mOrange M163K with titration with 1 N HCl. The excitation spectra were measured with a fixed 585 nm emission wavelength, while the emission spectra were measured with excitation at 515 nm. "Recovered" spectra measured after addition of 1 N NaOH demonstrates reversibility of spectral changes.

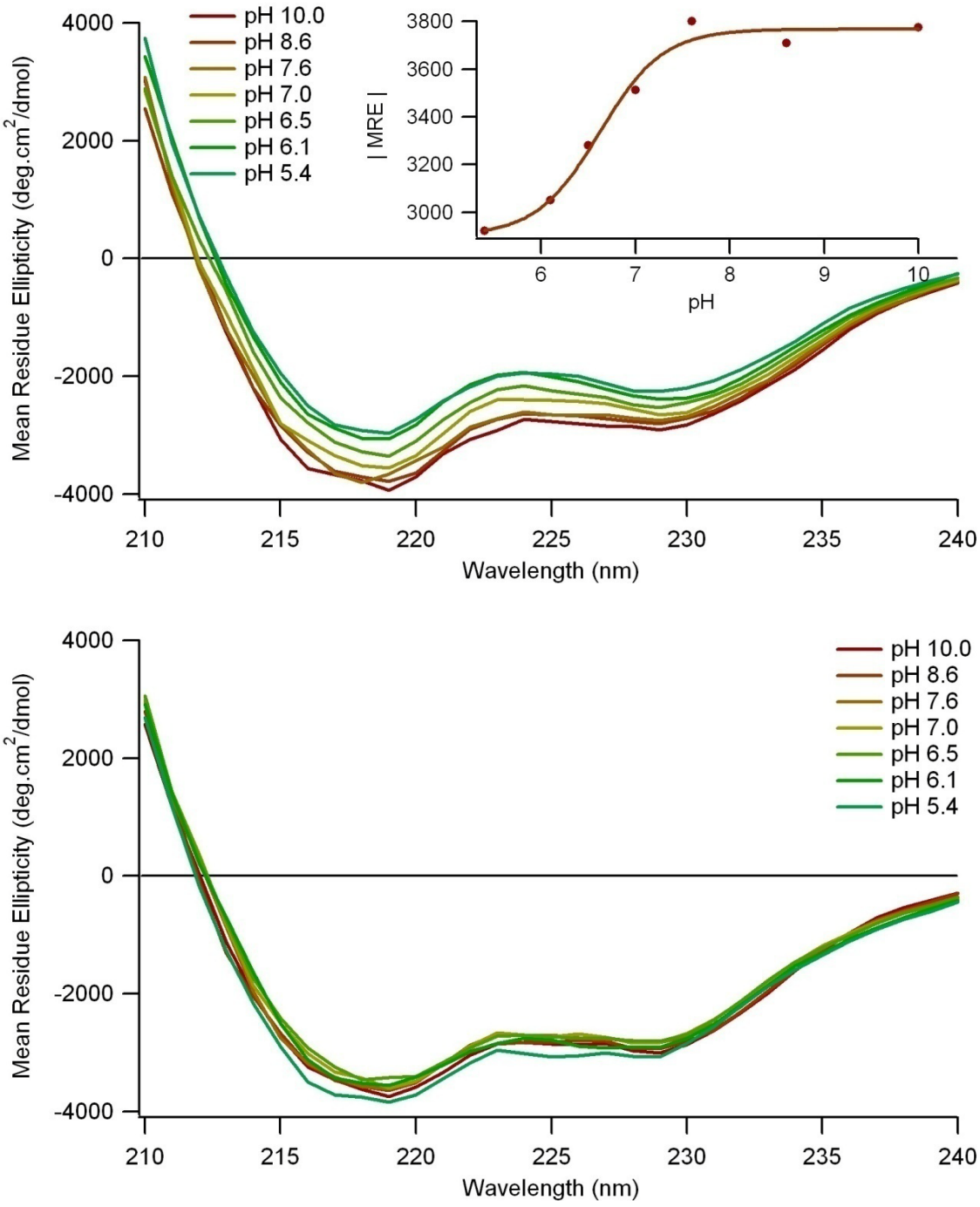

Figure 7.6: pH-dependent CD spectra of mOrange and mOrange M163K.
The CD spectra of His6-mOrange (top) and His6-mOrange M163K (bottom) were measured as the proteins were titrated with 1 N HCl. The magnitude of the mean residue ellipticity (MRE) of his6-mOrange at 218 nm is plotted against pH (top, inset).

Table 7.1: Protein and probe pK_as.

	mOrange	mOrange M163K
Molar Extinction Coefficient	6.9	7.9
Excitation	6.5	7.5
Emission	6.8	7.3
Mean Residue Ellipticity (CD)	6.6	N/A
F_A/F_D of probe	7.0	7.4

pH Stability of Qdots

The fluorescence spectra of a number of QDs with a variety of coatings were tested at various pHs and in several different buffers. In our experience, a number of the QDs showed significant variations in their PL output at different pHs, making them unsuitable as the donor for a QD-FP hybrid pH sensor (data not shown). This was true of the 525 nm ITK carboxyl Qdots as well; a decrease in QD emission was observed with decreasing pH and was accompanied by a slight red-shifting of the emission peak (Figure 7.7, top). To see if the Qdot would show similar sensitivity in the conjugated prove, a QD-FP hybrid was synthesized using the non-fluorescent GFP-like fluorescent protein mCherry-NF. While the corona of proteins that surround the Qdot on the conjugated probe appear to lessen the PL decrease as well as eliminating the red-shifting of the peak, the QD within the conjugate still demonstrates pH sensitivity that would complicate analysis of the pH sensor (Figure 7.7, bottom).

The presence of 1 % (w/v) BSA was demonstrated to greatly reduce the variation in QD PL, most likely by passivating the cuvette surface, thereby reducing nonspecific adsorption, which can vary with pH. Both the unconjugated 525 nm ITK carboxyl Qdot from Invitrogen and the QD conjugated to the non-fluorescent mCherry-NF showed minimal PL variation during titration in the buffer containing BSA.

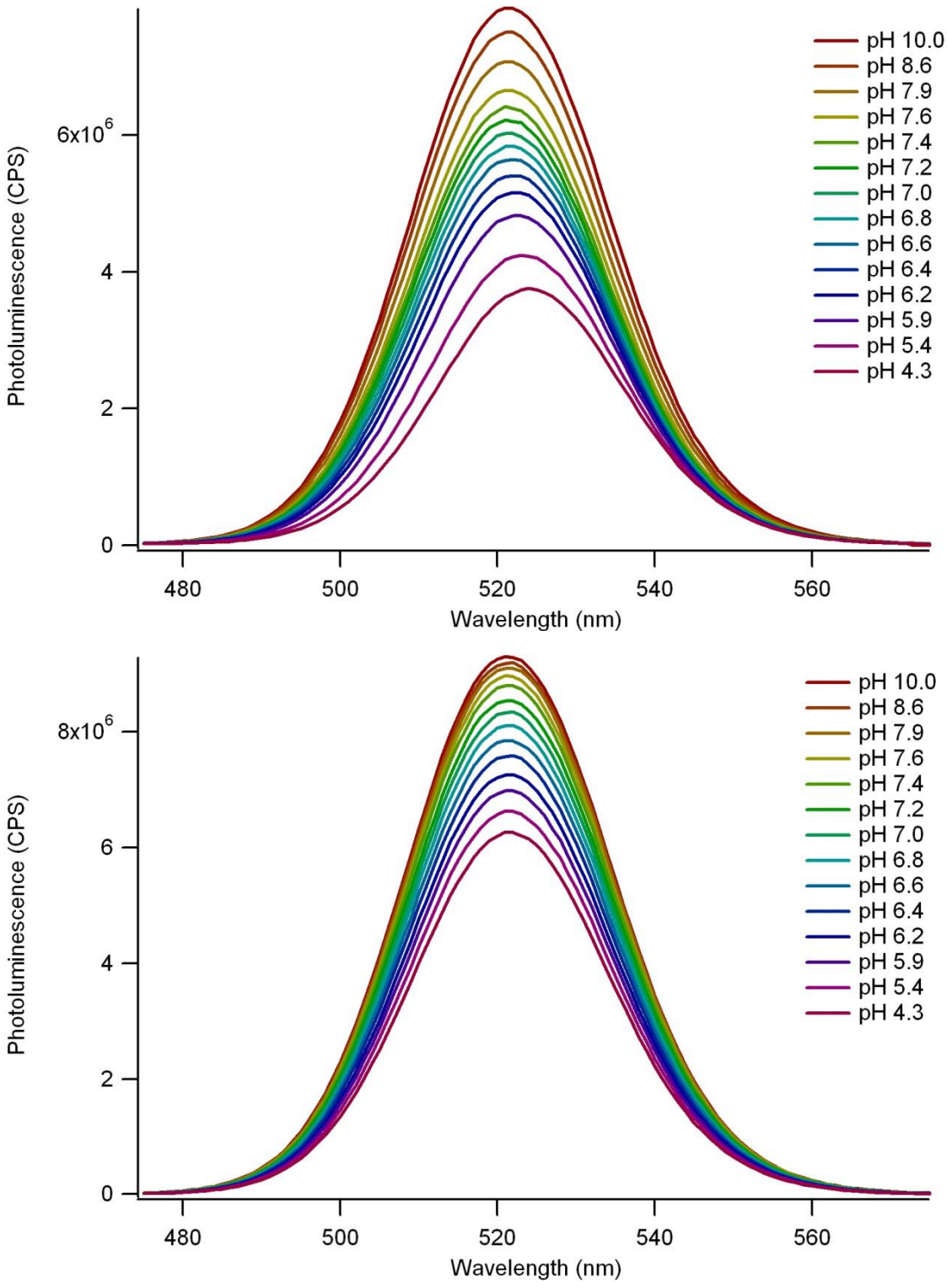

Figure 7.7: Qdots and mock probe titrated in PBS.
525 nm ITK Carboxyl Qdots (top) and Qdots conjugated to mCherry-NF titrated in 20 mM PBS.

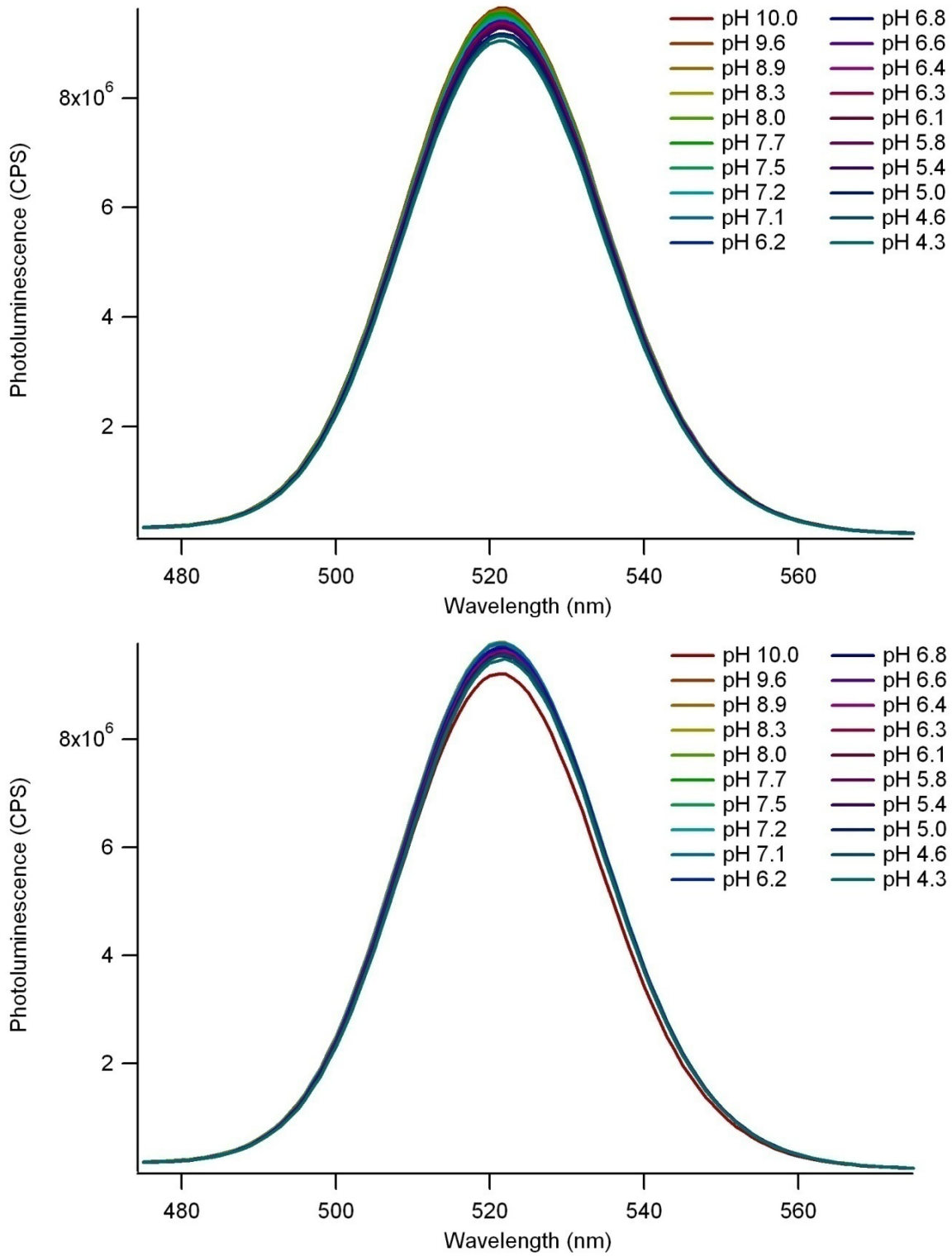

Figure 7.8: Qdots and mock probe titrated in PBS supplemented with BSA.
525 nm ITK carboxyl Qdots (top) and Qdots conjugated to mCherry-NF titrated in 20 mM PBS with 1% (w/v) BSA.

Assembly of FRET Probe

QD-FP hybrid probes were assembled using covalent chemistry. Specifically, 1-ethyl-3-(3-dimethylaminopropyl) carbodiimide (EDC) was used to activate carboxyl groups on the surface of 525 nm ITK carboxyl Qdots from Invitrogen, which then formed amide bonds with primary amines on the protein. Following reaction at 4˚C overnight, centrifugal filtration devices with a 100 kDa MW cutoff were used to remove excess EDC and unbound protein.

Absorption spectroscopy of the conjugated probe and unconjugated Qdots were used to determine the probe concentration and the average number of proteins bound to each probe. The Qdot concentration, which is equivalent to the probe concentration, was calculated using the Beer-Lambert Law and a molar extinction coefficient of 360,000 M^{-1}

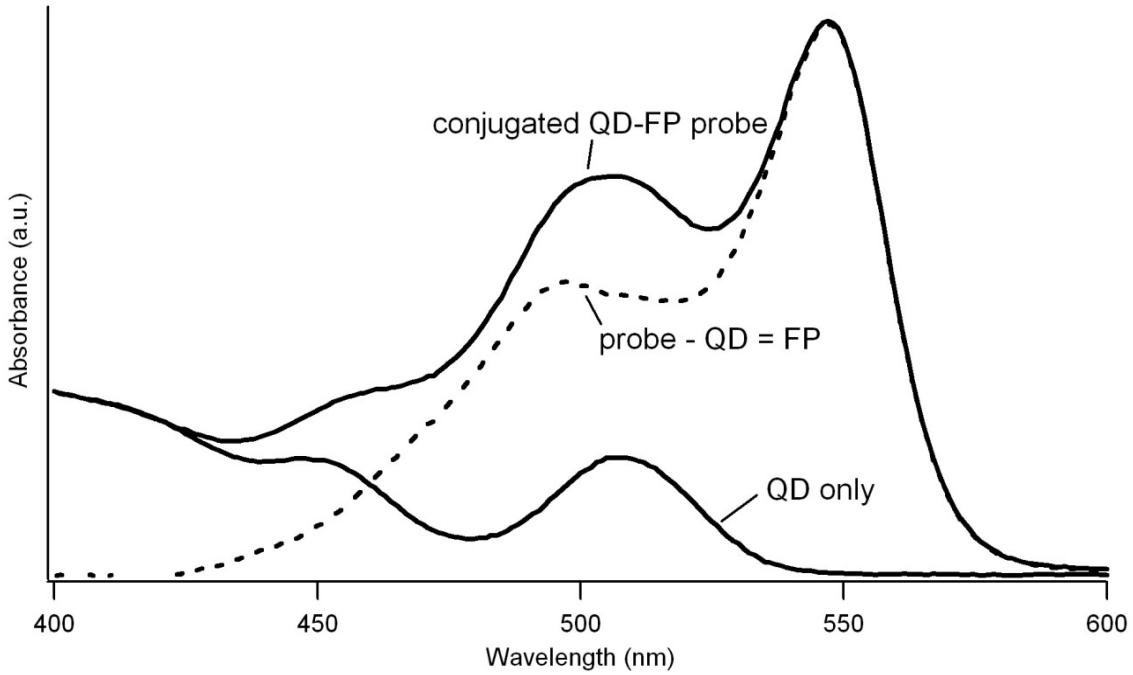

Figure 7.9: Probe concentration and composition determination.
The absorption spectra of the conjugated probe and the Qdots are normalized at 405 nm before the Qdot spectrum is subtracted from the probe spectrum, resulting in the spectrum of the conjugated protein.

cm^{-1} at 405 nm (Invitrogen product data sheet). The spectra were measured at alkaline pH to ensure that the FP was not contributing to the absorbance at this wavelength. Subtracting the normalized Qdot emission spectrum from the absorbance spectrum of the conjugated probe, both normalized to their absorbance at 405 nm, produces the absorbance spectra of the conjugated protein (Figure 7.9). Examination of the spectra shows that the Qdots do not contribute significantly to the conjugate absorbance at 547 nm. The maximum molar extinction coefficient for each of the proteins, as defined by the sigmoidal curve fits to the data in Figure 7.2 and Figure 7.3, 60,887 M^{-1} cm^{-1} and 48,797 M^{-1} cm^{-1} for mOrange and mOrange M163K, were used to calculate the protein content for each probe.

Minor batch-to-batch variation is seen for each conjugation preparation. The two probe batches used for the experiments detailed in this chapter resulted in an average of 18.4 mOrange molecules per QD and 16.5 mOrange M163K molecules per QD, respectively.

pH Sensor Characterization

The pH sensor was characterized using fluorescence spectroscopy while being titrated. Both the mOrange and mOrange M163K probes showed a characteristic double peak at strongly alkaline pHs, which correlates with efficient energy transfer from the Qdot to the fluorescent protein. As the pH decreased due to titration with 1 N HCl, the protein peak at 560 nm decreased and the QD emission at 520 nm correspondingly increased (Figure 7.10 and Figure 7.11, top). The changes in the spectral profile arise as the acidic pHs reduce the absorbance capacity of the fluorescent protein. As the protein absorbs less of the energy from the Qdot, its own sensitized emission decreases and the

emission from the Qdot increases as it is quenched less. The titration increased the volume of the sample by < 3%, which did not seem to affect the measurement significantly, based on the clear isosbestic point at 545 nm.

Following the titration, a bolus of 1 N NaOH was added to raise the pH to demonstrate the reversibility of the pH sensor. As anticipated, the protein signal was restored and the QD emission returned to the lower values originally seen at high pHs ("recovered" spectrum in Figure 7.10 and Figure 7.11, top). Both the QD and protein signals were slightly lower than observed in the original spectra, which is likely attributable to the dilution factor from the titrations.

The titrations were repeated in triplicate and the ratio of the acceptor emission to the donor emission (F_D/F_A, i.e. $F_{560\ nm}/F_{520\ nm}$) was plotted *versus* pH. The spectral and combined plots of both of the pH sensors were very similar. The mOrange M163K-based sensor showed smaller standard deviations in the averaged study, indicating a significant repeatability and clearly distinguishing one pH value from another. While the standard deviations for the mOrange-based sensor were still small, there was some overlap among the pH values tested. Both probes showed considerable change in F_D/F_A with pH. The mOrange probe showed a more than 20-fold increase overall with an 8-fold increase in the F_D/F_A between 6.1 and 8.0. The mOrange M163K probe exhibited a 16-fold increase overall and an 8-fold increase in the F_D/F_A from pH 6.3 to 8.3. Although the pH ranges of interest overlap, the pK_a of the mOrange probe was 7.0 while that of the mOrange M163K probe was 7.4.

The fluorescence emission of the Qdot mixed with, but not conjugated to mOrange was tested at the same concentrations and same conditions as the probe at pH

10. Absolutely no sensitized emission was discernable, demonstrating that the mOrange emission observed with the conjugated probe is due to sensitized emission and not direct excitation.

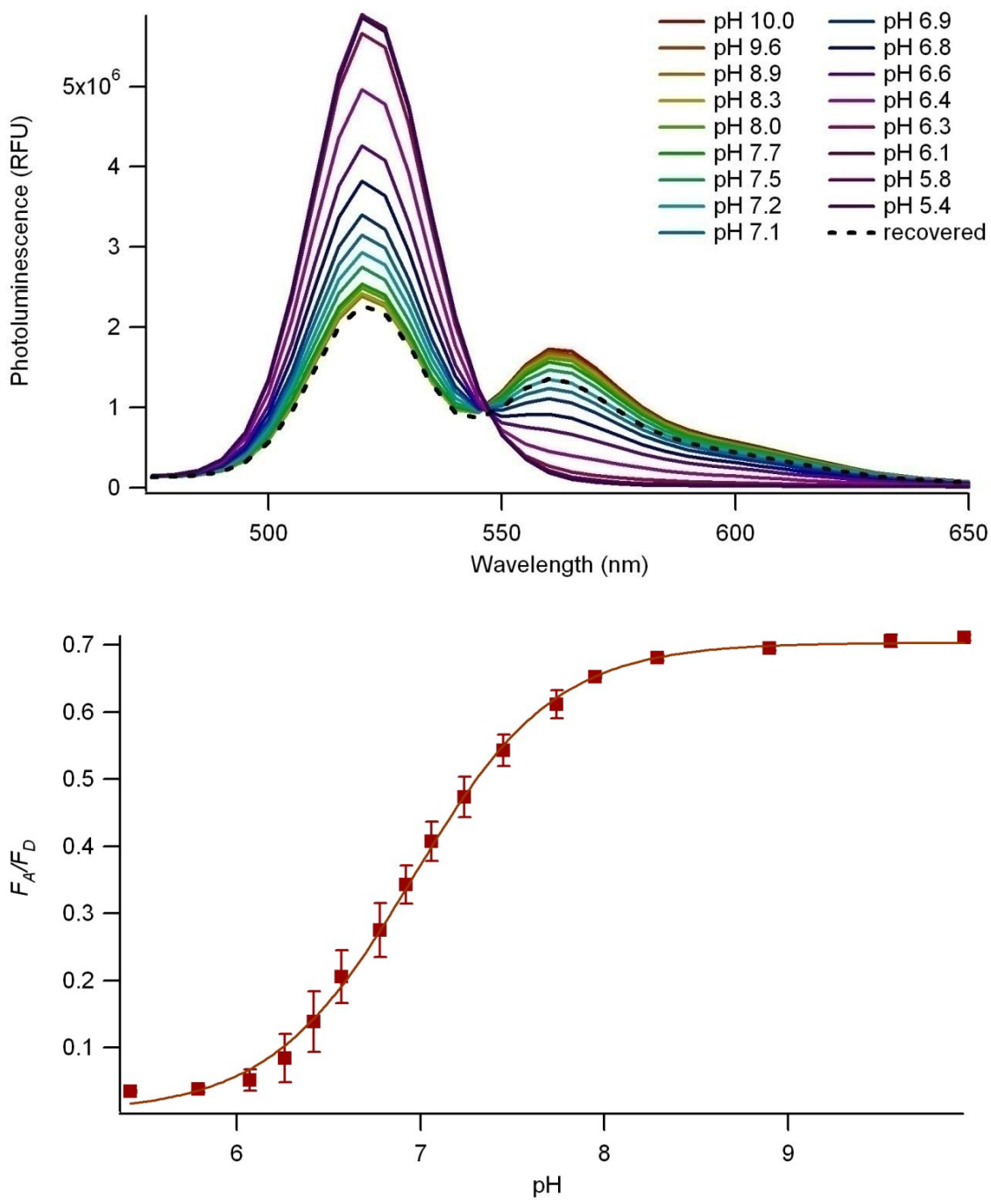

Figure 7.10: Titration of mOrange FRET probe.
Top: Emission spectra of mOrange FRET probe with respect to pH. Recovered spectrum demonstrates reversibility of pH-sensitivity.
Bottom: Acceptor emission to donor emission ratio *versus* pH. Points represent mean ± standard deviation of $n = 3$.

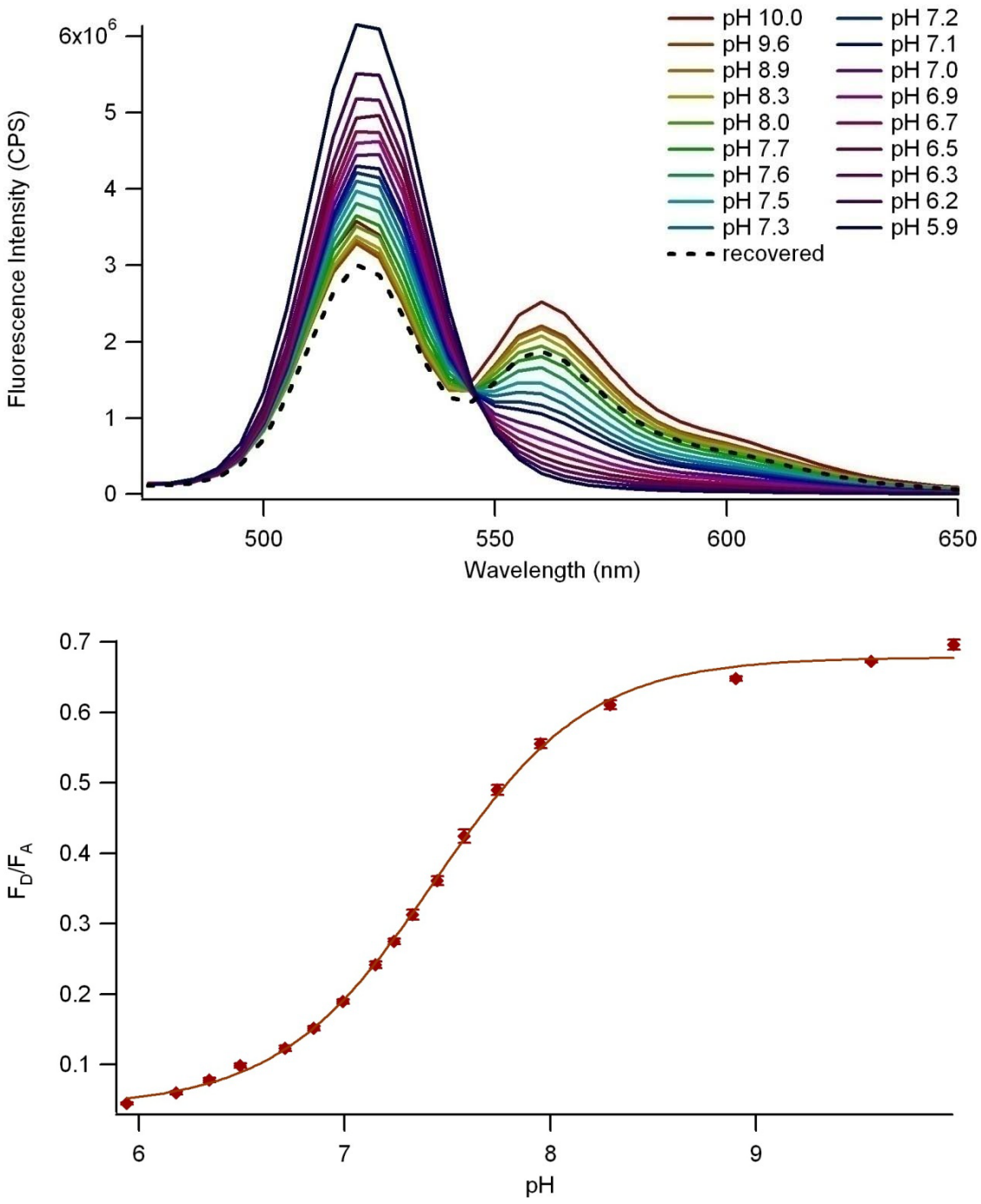

Figure 7.11: Titration of mOrange M163K FRET probe.
Top: Emission spectra of mOrange FRET probe with respect to pH. Recovered spectrum demonstrates reversibility of pH-sensitivity.
Bottom: Acceptor emission to donor emission ratio *versus* pH. Points represent mean ± standard deviation of $n = 3$.

DISCUSSION

mOrange, a member of the "Fruit Basket" family of GFP-like fluorescent proteins developed in Roger Tsien's laboratory at the University of California, San Diego (*91*), is an excellent FRET acceptor because of its high molar extinction coefficient and QY, but has not been generally applied because it is rather photolabile compared to other GFP-like fluorescent proteins and exhibits a pH sensitivity that is undesirable in many applications (*112*). The FRET probe design described here, however, exploits the pH sensitivity of mOrange to produce a pH sensor that could be used in either solution studies or intracellularly while mitigating the effects of the rapid photobleaching of mOrange by using the QD as the FRET donor. By exciting the probe at 400 nm rather than at the peak absorbance wavelength of mOrange, less light is being absorbed by the protein fluorophore, limiting the protein exposure to destructive photonic energy.

A protein variant, mOrange M163K, was described in the literature as being more photostable than mOrange and possessing an increased pK_a (*92*). We included this protein in the study as well to broaden the repertoire of pH-sensitive probes to focus on various pH points. The absorption spectra of mOrange M163K proved to have a more complicated spectral transition in response to pH titration than mOrange did, indicating that there may be a more involved structure-function relationship affecting the pH-sensitivity of this mutant. Although the absorbance spectra of both proteins shows significant blue-shifting as the pH decreases—and the emergence of a significant peak at 400 nm—these peaks are not in fact present in the excitation spectra of the proteins, thus they minimally impact the performance of the FRET probes.

CD spectra of the two titrated proteins were examined to ensure that the change in the protein optical properties was not a result of protein degradation. mOrange M163K showed negligible change in MRE as the pH was titrated down, but mOrange showed a subtle, but pH-dependent decrease in the size of its peaks. Although it is clear that the general structure of the protein remains intact, it is possible that the mOrange secondary structure relaxes somewhat in response to the change in pH. The ancestral DsRed, like mOrange M163K, contains a lysine at amino acid residue 163. Analysis of the crystal structure of DsRed indicated that the lysine forms a salt bridge with the phenolate oxygen of the chromophore (*96*). This interaction, absent in mOrange, may add the stability that prevents the mOrange M163K CD spectra from shifting in response to changes in pH.

Both the absorbance and emission spectra of the two mOrange mutants vary with pH, although the changes in the brightness of the protein appear to be a result of the change in the molar extinction coefficient and not due to a change in the quantum yield of the protein. This pH-dependence of the mOrange molar extinction coefficient makes the protein particularly useful as a FRET acceptor. As both the amount of donor quenching and the extent of the sensitized emission from the acceptor will be affected by the pH-dependent changes in mOrange's spectral properties, the change in the ratio of the acceptor and donor emissions is more dramatic, which increases the sensitivity of the probe. CdSe/ZnS core-shell QDs have been shown to have pH sensitive PL in the literature, which could have been a complicating factor in this pH sensor design (*121*), but the polymer coating appears to shield the nanoparticle from the environment, eliminating the effect of pH once precautions are taken to guard against adsorption.

The pK_as of both of the proteins are between 6 and 8, depending on the protein and specific definition of the pK_a used, which indicates that the spectral properties of the proteins will change most dramatically in a pH range that is physiologically interesting. The mOrange probe has a stronger FRET signal at cytoplasmic pHs that then decreases in acidic environments. This lends the probe to studies such as the tracking of nanoparticulates through the endocytic pathway. The mOrange M163K probe, in contrast, shows much greater variation in its ratiometric measurement at normal physiological pHs, indicating that it may be useful for seeing subtle differences in cytoplasmic pH due to cell status, such as cell growth, division, and movement.

The use of the QD-FP hybrid FRET probe has two distinct advantages over using the fluorescent protein alone. The first is that the ratiometric measurement allows one to correct for concentration. This property allows for confident comparisons between cells and sub-cellular compartments, as it ensures that differences in signal are not due to non-uniform accumulation of the probe, but are truly indications of changes in the pH. Second, by exciting the probe in the UV, far from where the protein is excited, the amount of photonic energy absorbed by the chromophore is dramatically reduced, extending the functional lifetime of the fluorescent protein. Thus, the QD-FP pH sensor could potentially be used for time-lapse imaging studies, whereas mOrange alone shows visible signs of photobleaching even as one is focusing the microscope.

The literature suggests that FRET-based biosensors can be useful in intracellular imaging applications if the change in the FRET efficiency in response to the stimulus is greater than 0.1 and the change in the donor-acceptor ratio is greater than 30% of the original ratio ($(R_{min} - R_{max})/R_{min} \geq 30\%$) (*101*). Based on those criteria, either of the

probes described here have potential as intracellular imaging probes. These probes are bright, show relatively high FRET efficiencies, and are very sensitive to their analyte, H^+. Future iterations of the probe could perform even better, however, if the donor-acceptor distance could be reduced without diminishing the QY of the QD. While the thick polymer coating on the Qdots may be necessary to prevent QD PL fluctuations in response to pH, it is also possible that QDs with thinner coatings could be buffered by the corona of proteins on the conjugated probe to maintain their stability. This will be an area of continued probe development.

CONCLUSION

This example of a functional QD-FP biosensor demonstrates how the innate sensitivity of an FP to its environment can be harnessed to modulate QD emission. As the molar extinction coefficient of mOrange decreases with pH, the QD emission increases until it is completely unquenched at acidic pHs. The sensitivity of the ratiometric measurement over a physiologically relevant pH suggests that this probe may be effective in monitoring the acidification of endosomes or other cellular processes.

CHAPTER 8

CONCLUSIONS AND FUTURE DIRECTIONS

Burgeoning progress in the field of nanobiotechnology holds great promise for improving biomedical research and disease diagnostics as biosensors become more sensitive. By investigating basic principles of inorganic-biomolecule hybrid device design and applying the knowledge gained to the implementation of a pH sensor, this thesis contributes to the advancement of the field.

First, a systematic study was undertaken to evaluate various QDs, differentiated by their organic coating, for their capacity to self-assemble with protein *via* polyhistidine coordination. Our results showed that QDs with thin or porous coatings were amenable to His-tag binding, indicating the accessibility of the surface of the semiconductor nanocrystal. The demonstration of successful binding to QDs with several coatings, including commercially available varieties, expanded the range of known options available for QD-biomolecule hybrids assembled *via* His-tag-mediated self-assembly. Furthermore, the examination of what QD parameters determined whether or not self-assembly would be successful enables the prediction of what other coating types are most likely to behave similarly.

Based on the results of the self-assembly analysis, lipid-PEG coated QDs were chosen for a study to identify viable QD-FP pairings for FRET biosensors. QDs with three emission wavelengths and three fluorescent proteins, mOrange, mCherry, and tdTomato, were evaluated for their FRET efficiency. Several effective FRET pairs were identified, including 520 nm QDs and mOrange, 540 nm QDs and tdTomato, and 560 nm

QDs and mCherry. The differences in the FP properties enabled a closer look at analytical methods, demonstrating that some FRET pairs are best scrutinized by their FRET efficiency and donor quenching, whereas ratiometric methods are highly beneficial for those FPs the exhibit high levels of sensitized emission.

Finally, we demonstrated the application of a QD-FP hybrid probe in the form of a FRET-based, ratiometric pH sensor. Two monomeric fluorescent proteins, mOrange and mOrange M163K, were evaluated for their pH-dependent optical properties and their effectiveness as FRET acceptors to a QD donor. With an up to 20-fold change in the acceptor emission to donor emission ratio over a pH range that is physiologically interesting, these probes have promise as intracellular imaging agents. Potential applications include endosomal tracking or the elucidation of delivery pathways used by various cell-penetrating peptides for model nanoparticle-protein drug delivery devices.

The specific experiments described in this thesis lead to a number of conclusions regarding the affect that QD organic coatings have on polyhistidine-mediated self-assembly, the various QD-FP pairings available for device design, and the design aspects that affect the performance of the pH sensor. Moreover, these results invite a variety of future studies that improve on device design and expand the applications of QD-FP FRET biosensors. Several of these potential studies are described below.

IMPROVING THE QD-FP FRET PROBE PERFORMANCE

QD Donors

While the QD is undoubtedly a successful FRET donor, as demonstrated by the studies in this thesis as well as other studies in the field, several improvements in the QDs available for use in the FRET probes could have a dramatic impact on the FRET

efficiency of the probes. As discussed in Chapter 3, the FRET efficiency of a system is primarily influenced by three variables: the spectral overlap of the donor and acceptor, the quantum yield of the donor, and, most dramatically, the donor-acceptor distance. The tunability of QD emissions already guarantees that high levels of spectral overlap between the donor and acceptor can be assured by choosing the right donor for the desired acceptor. Improvements could be made, however, in the QD quantum yield and donor-acceptor distance. While water-soluble QDs with high QYs have been available, even commercially, for several years now, the QDs that have the highest QYs are also typically larger, owing to ZnS capping layers to improve the nanocrystal QY (*25, 26*) and typically thicker organic coating layers that maintain the higher QYs by not disrupting the hydrophobic surfactant layer left on the particle surface following the inorganic synthesis. This larger QD size contributes to expanded donor-acceptor distances, thereby mitigating the effects of the improvements in FRET efficiency that could have been seen with the higher QY. Several improvements in QD core-shell synthesis protocols and in coating procedures indicate that convenient access to small, high QY QDs with thin organic coatings that are appropriate FRET donors is on the horizon. Approaches include implementing alternative nanocrystal compositions, such as CdTeSe alloys or lattice mismatched core-shell structures that produce bright nanocrystals with small inorganic diameters (*33, 34*). Additionally, gentler ligand exchange coating protocols claim to maintain QD QYs while conferring water-solubility with minimal coatings (*50, 51*), and multi-dentate coatings have the potential for increased colloidal stability despite the small size (*52*). When these incremental changes are taken together, the improvements to FRET efficiency and, therefore, probe sensitivity could be dramatic.

Fluorescent Protein Acceptors

Developments in FP engineering have resulted in a wide range of FPs to choose from when designing QD-FP hybrid probes. The range of colors and spectral properties is astonishing, but further developments will improve the repertoire even further. Biosensor design will improve as FPs with improved photostability, increased brightness, and narrower spectral peak profiles emerge. Furthermore, FPs with absorption and emission in the near-infrared (NIR; 650-900 nm) would pair nicely with existing and future QDs. NIR-based FRET probes would be of key interest for *in vivo* studies, as tissue is most transparent at these wavelengths, with penetration depths extending into centimeters (*122*).

In addition to using fluorescent proteins as protein acceptors, non-fluorescent chromoproteins could be alternative FRET acceptors. The use of such "protein quenchers" could allow for the multiplexing of QD-FP FRET-based sensors as the emission from the FP would not interfere with the multiplexing advantages of the QDs. One such protein, REACh1, is a dark YFP variant that has been used as a FRET acceptor for GFP. A single point mutation to EYFP, Y145W, reduced the fluorescence emission from the protein by 98%, while the absorbance profile and molar extinction coefficient was maintained (*123*). The absorbance spectra of REACh1 makes it an appropriate FRET acceptor for blue-emitting QDs. As another study has identified mutations to the tetrameric protein DsRed, the ancestor of the Fruit Basket proteins, that produced a non-fluorescent chromophore named DsRed-NF (*124*), it is highly likely that mutations to the stably monomeric mFruit proteins could result in a series of monomeric, non-fluorescent chromoproteins with a range of absorbance spectra peaks. Such proteins could be used to

quench QD emission to create a series of biosensors that could be multiplexed for efficient multiparameter sensing. In particular, probes containing protein quenchers as the FRET acceptor could be used in fluorescence lifetime imaging (FLIM) to provide an alternative to ratiometric sensing that is more amenable to multiplexing (*6*). Like ratiometric methods, FRET-FLIM is inherently quantitative and concentration independent (*125*), but as only the QD emission would be of consequence, many more sensors could be spectrally accommodated.

OTHER APPLICATIONS OF QD-FP BIOSENSORS

Sensing by Modulating the FP Properties

Similarly to the mOrange pH sensor, other biosensors could be developed that take advantage of natural modulation of FP spectral properties based on environmental cues. Examples include the copper-sensitivity of DsRed (*126*) and the sensitivity of various YFP mutants to chloride (*127, 128*). As was discussed for the pH sensor, using the FP in tandem with the QD improves upon just using the FP alone because it controls for changes in probe concentration, extends the lifetime of the probe by reducing the photobleaching of the protein, and enables fluorescence lifetime measurements, expanding on the analytical options. Genetic screens on mutants could be performed to select for sensitivity to other small-molecule analytes of interest.

Genetic engineering of binding pockets into the proteins could further expand the range of QD-FP FRET-based biosensors that are modulated by changes in the spectral changes of the GFP-like protein. In one instance, for example, the emission of a modified EGFP was quenched upon the binding of bacterial endotoxin (or lipopolysaccharide, LPS) to a binding region engineered into the barrel structure of the FP (*129*). Any such

existing GFP-like protein-based sensor could be adapted to the QD-FP FRET system by conjugating it to a QD. Such adaptations could improve the biosensors in all of the ways previously discussed—i.e. controlling for concentration fluctuations, reduced photobleaching of the FP, possibility of FRET-FLIM imaging—but eliminates one advantage of the protein biosensors: the genetically encoded probes can be expressed by cells following transfection; there is no need for more strenuous probe delivery protocols.

Sensing by Modulating Donor-Acceptor Distance

As demonstrated in Figure 3.7, a number of FRET-based biosensor designs center around changing the donor-acceptor distance, rather than modulating the optical properties of the acceptor. Theoretically, any of these sensing designs could be applied to QD-FP biosensors as well. In fact, one recent publication demonstrates the utility of a QD-FP FRET-based probe for protease activity (Figure 8.1) (*84*). Any of the FP-to-FP FRET-based biosensors whose research value could be improved by enhancing the signal output, reducing crosstalk, and reducing photobleaching could be adapted to this QD-FP

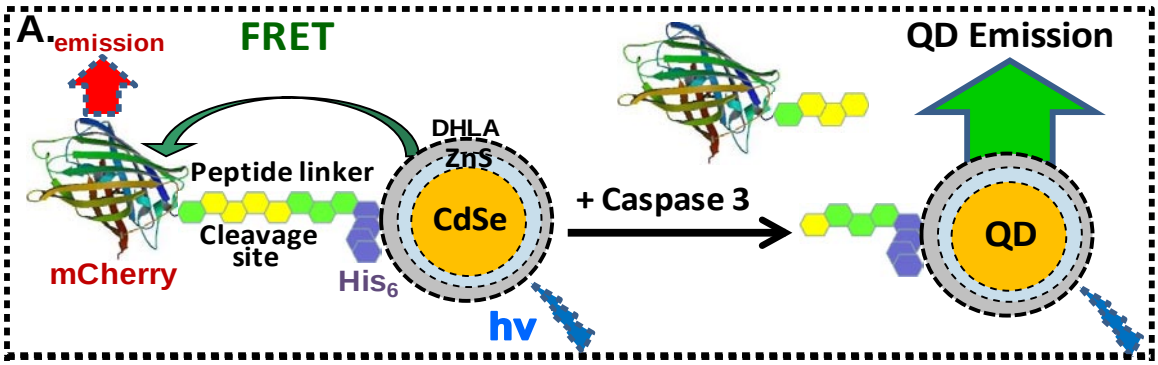

Figure 8.1: QD-FP FRET-based assay for proteolytic activity.
mCherry bound to the CdSe/ZnS QD *via* a polyhistidine tag quenches the QD until the linker between the FP and the his-tag is enzymatically cleaved, releasing the protein from the QD surface. In the absence of the bound FP, the QD emission is restored. Reprinted with permission (*84*).

sensor format. QD-FP sensors are not, however, genetically encodable as the FP-FP biosensors are, so probe delivery will have to be addressed for intracellular imaging applications.

INTRACELLULAR IMAGING OF QD-FP FRET PROBES

The literature suggests that FRET-based biosensors can be useful in intracellular imaging applications if the change in the FRET efficiency in response to the stimulus is greater than 0.1 and the change in the donor-acceptor ratio is greater than 30% of the original ratio ($(R_{min} - R_{max})/R_{min} \geq 30\%$) (*101*). The pH sensor described in Chapter 7 certainly clears this hurdle, making it a prime candidate for live-cell imaging.

The first concern for any intracellular imaging application with QD-based probes is the delivery of the probe into the cell. As some success has been had using cell penetrating peptides to deliver a QD and its protein cargo *via* endocytosis (*110*), we have engineered an mOrange variant that includes nine arginines at the C-terminus. Preliminary experiments have been conducted to evaluate this QD-mOrange-Arg9 probe for fluorescence microscopy. While our initial impressions, both of delivery and of probe function, are promising, much work remains to convincingly demonstrate the probe function intracellularly.

In conclusion, the projects contained in this thesis describe a new biosensing platform that combines the unique optical properties of QDs with the intrinsic bioresponsive elements of FPs. While issues of probe design and development are investigated and a functional biosensor described, examination of this new type of hybrid probe has only just begun. Many opportunities exist for future projects, whether that be in

improving on the current design of the pH sensor, applying the sensor to intracellular assays, or developing QD-FP biosensors for other applications.

REFERENCES

(1) Zhong, W. W. (2009) Nanomaterials in fluorescence-based biosensing. *Analytical and Bioanalytical Chemistry 394*, 47-59.

(2) Medintz, I. L., and Mattoussi, H. (2009) Quantum dot-based resonance energy transfer and its growing application in biology. *Physical Chemistry Chemical Physics 11*, 17-45.

(3) Li, I. T., Pham, E., and Truong, K. (2006) Protein biosensors based on the principle of fluorescence resonance energy transfer for monitoring cellular dynamics. *Biotechnology Letters 28*, 1971-1982.

(4) Lakowicz, J. R. (2006) *Principles of Fluorescence Spectroscopy*, 3rd ed., Springer, New York.

(5) Medintz, I. L., Mattoussi, H., and Clapp, A. R. (2008) Potential clinical applications of quantum dots. *International Journal of Nanomedicine 3*, 151-167.

(6) Carlson, H. J., and Campbell, R. E. (2009) Genetically encoded FRET-based biosensors for multiparameter fluorescence imaging. *Current Opinion in Biotechnology 20*, 19-27.

(7) Chalfie, M., Tu, Y., Euskirchen, G., Ward, W. W., and Prasher, D. C. (1994) Green Fluorescent Protein as a Marker for Gene-Expression. *Science 263*, 802-805.

(8) Chalfie, M. (2009) GFP: Lighting Up Life (Nobel Lecture). *Angewandte Chemie-International Edition 48*, 5603-5611.

(9) Tsien, R. Y. (2009) Constructing and Exploiting the Fluorescent Protein Paintbox (Nobel Lecture). *Angewandte Chemie-International Edition 48*, 5612-5626.

(10) Medintz, I. L., Clapp, A. R., Mattoussi, H., Goldman, E. R., Fisher, B., and Mauro, J. M. (2003) Self-assembled nanoscale biosensors based on quantum dot FRET donors. *Nature Materials 2*, 630-8.

(11) Clapp, A. R., Medintz, I. L., Mauro, J. M., Fisher, B. R., Bawendi, M. G., and Mattoussi, H. (2004) Fluorescence resonance energy transfer between quantum dot donors and dye-labeled protein acceptors. *Journal of the American Chemical Society 126*, 301-310.

(12) Chang, E., Miller, J. S., Sun, J., Yu, W. W., Colvin, V. L., Drezek, R., and West, J. L. (2005) Protease-activated quantum dot probes. *Biochemical and Biophysical Research Communications 334*, 1317-21.

(13) Xu, C., Xing, B., and Rao, J. (2006) A self-assembled quantum dot probe for detecting beta-lactamase activity. *Biochemical and Biophysical Research Communications 344*, 931-5.

(14) Medintz, I. L., Clapp, A. R., Brunel, F. M., Tiefenbrunn, T., Uyeda, H. T., Chang, E. L., Deschamps, J. R., Dawson, P. E., and Mattoussi, H. (2006) Proteolytic activity monitored by fluorescence resonance energy transfer through quantum-dot-peptide conjugates. *Nature Materials 5*, 581-9.

(15) Dennis, A. M., and Bao, G. (2008) Quantum dot-fluorescent protein pairs as novel fluorescence resonance energy transfer probes. *Nano Letters 8*, 1439-45.

(16) Tomasulo, M., Yildiz, I., Kaanumalle, S. L., and Raymo, F. M. (2006) pH-sensitive ligand for luminescent quantum dots. *Langmuir 22*, 10284-10290.

(17) Snee, P. T., Somers, R. C., Nair, G., Zimmer, J. P., Bawendi, M. G., and Nocera, D. G. (2006) A ratiometric CdSe/ZnS nanocrystal pH sensor. *Journal of the American Chemical Society 128*, 13320-13321.

(18) Suzuki, M., Husimi, Y., Komatsu, H., Suzuki, K., and Douglas, K. T. (2008) Quantum dot FRET Biosensors that respond to pH, to proteolytic or nucleolytic cleavage, to DNA synthesis, or to a multiplexing combination. *Journal of the American Chemical Society 130*, 5720-5725.

(19) Berger, W., Prinz, H., Striessnig, J., Kang, H. C., Haugland, R., and Glossmann, H. (1994) Complex molecular mechanism for dihydropyridine binding to L-type Ca(2+)-channels as revealed by fluorescence resonance energy transfer. *Biochemistry 33*, 11875-83.

(20) Sato, M., Ozawa, T., Inukai, K., Asano, T., and Umezawa, Y. (2002) Fluorescent indicators for imaging protein phosphorylation in single living cells. *Nature Biotechnology 20*, 287-94.

(21) Matayoshi, E. D., Wang, G. T., Krafft, G. A., and Erickson, J. (1990) Novel fluorogenic substrates for assaying retroviral proteases by resonance energy transfer. *Science 247*, 954-8.

(22) Tyagi, S., and Kramer, F. R. (1996) Molecular beacons: probes that fluoresce upon hybridization. *Nature Biotechnology 14*, 303-8.

(23) Kairdolf, B. A., Smith, A. M., and Nie, S. (2008) One-pot synthesis, encapsulation, and solubilization of size-tuned quantum dots with amphiphilic multidentate ligands. *Journal of the American Chemical Society 130*, 12866-+.

(24) Chan, W. C. W., Maxwell, D. J., Gao, X. H., Bailey, R. E., Han, M. Y., and Nie, S. M. (2002) Luminescent quantum dots for multiplexed biological detection and imaging. *Current Opinion in Biotechnology 13*, 40-46.

(25) Hines, M. A., and Guyot-Sionnest, P. (1996) Synthesis and characterization of strongly luminescing ZnS-Capped CdSe nanocrystals. *Journal of Physical Chemistry 100*, 468-471.

(26) Dabbousi, B. O., RodriguezViejo, J., Mikulec, F. V., Heine, J. R., Mattoussi, H., Ober, R., Jensen, K. F., and Bawendi, M. G. (1997) (CdSe)ZnS core-shell quantum dots: Synthesis and characterization of a size series of highly luminescent nanocrystallites. *Journal of Physical Chemistry B 101*, 9463-9475.

(27) Peng, Z. A., and Peng, X. G. (2001) Formation of high-quality CdTe, CdSe, and CdS nanocrystals using CdO as precursor. *Journal of the American Chemical Society 123*, 183-184.

(28) Murray, C. B., Norris, D. J., and Bawendi, M. G. (1993) Synthesis and Characterization of Nearly Monodisperse Cde (E = S, Se, Te) Semiconductor Nanocrystallites. *Journal of the American Chemical Society 115*, 8706-8715.

(29) Grecco, H. E., Lidke, K. A., Heintzmann, R., Lidke, D. S., Spagnuolo, C., Martinez, O. E., Jares-Erijman, E. A., and Jovin, T. M. (2004) Ensemble and single particle photophysical proper-ties (Two-Photon excitation, anisotropy,

FRET, lifetime, spectral conversion) of commercial quantum dots in solution and in live cells. *Microscopy Research and Technique 65*, 169-179.

(30) Denk, W., and Svoboda, K. (1997) Photon upmanship: Why multiphoton imaging is more than a gimmick. *Neuron 18*, 351-357.

(31) Squirrell, J. M., Wokosin, D. L., White, J. G., and Bavister, B. D. (1999) Long-term two-photon fluorescence imaging of mammalian embryos without compromising viability. *Nature Biotechnology 17*, 763-767.

(32) Qu, L., and Peng, X. (2002) Control of photoluminescence properties of CdSe nanocrystals in growth. *Journal of the American Chemical Society 124*, 2049-55.

(33) Bailey, R. E., and Nie, S. M. (2003) Alloyed semiconductor quantum dots: Tuning the optical properties without changing the particle size. *Journal of the American Chemical Society 125*, 7100-7106.

(34) Smith, A. M., Mohs, A. M., and Nie, S. (2009) Tuning the optical and electronic properties of colloidal nanocrystals by lattice strain. *Nature Nanotechnology 4*, 56-63.

(35) Han, M. Y., Gao, X. H., Su, J. Z., and Nie, S. (2001) Quantum-dot-tagged microbeads for multiplexed optical coding of biomolecules. *Nature Biotechnology 19*, 631-635.

(36) Hama, Y., Koyama, Y., Urano, Y., Choyke, P. L., and Kobayashi, H. (2007) Simultaneous two-color spectral fluorescence lymphangiography with near infrared quantum dots to map two lymphatic flows from the breast and the upper extremity. *Breast Cancer Research and Treatment 103*, 23-8.

(37) Gao, X., Cui, Y., Levenson, R. M., Chung, L. W., and Nie, S. (2004) In vivo cancer targeting and imaging with semiconductor quantum dots. *Nature Biotechnology 22*, 969-76.

(38) Sapsford, K. E., Pons, T., Medintz, I. L., and Mattoussi, H. (2006) Biosensing with luminescent semiconductor quantum dots. *Sensors 6*, 925-953.

(39) Striolo, A., Ward, J., Prausnitz, J. M., Parak, W. J., Zanchet, D., Gerion, D., Milliron, D., and Alivisatos, A. P. (2002) Molecular weight, osmotic second virial

coefficient, and extinction coefficient of colloidal CdSe nanocrystals. *Journal of Physical Chemistry B 106*, 5500-5505.

(40) Medintz, I. L., Uyeda, H. T., Goldman, E. R., and Mattoussi, H. (2005) Quantum dot bioconjugates for imaging, labelling and sensing. *Nature Materials 4*, 435-46.

(41) Chan, W. C., and Nie, S. (1998) Quantum dot bioconjugates for ultrasensitive nonisotopic detection. *Science 281*, 2016-8.

(42) Aldana, J., Lavelle, N., Wang, Y. J., and Peng, X. G. (2005) Size-dependent dissociation pH of thiolate ligands from cadmium chalcogenide nanocrystals. *Journal of the American Chemical Society 127*, 2496-2504.

(43) Aldana, J., Wang, Y. A., and Peng, X. G. (2001) Photochemical instability of CdSe nanocrystals coated by hydrophilic thiols. *Journal of the American Chemical Society 123*, 8844-8850.

(44) Mattoussi, H., Mauro, J. M., Goldman, E. R., Anderson, G. P., Sundar, V. C., Mikulec, F. V., and Bawendi, M. G. (2000) Self-assembly of CdSe-ZnS quantum dot bioconjugates using an engineered recombinant protein. *Journal of the American Chemical Society 122*, 12142-12150.

(45) Uyeda, H. T., Medintz, I. L., Jaiswal, J. K., Simon, S. M., and Mattoussi, H. (2005) Synthesis of compact multidentate ligands to prepare stable hydrophilic quantum dot fluorophores. *Journal of the American Chemical Society 127*, 3870-8.

(46) Mattoussi, H., Mauro, J. M., Goldman, E. R., Green, T. M., Anderson, G. P., Sundar, V. C., and Bawendi, M. G. (2001) Bioconjugation of highly luminescent colloidal CdSe-ZnS quantum dots with an engineered two-domain recombinant protein. *Physica Status Solidi B-Basic Research 224*, 277-283.

(47) Mei, B. C., Susumu, K., Medintz, I. L., Delehanty, J. B., Mountziaris, T. J., and Mattoussi, H. (2008) Modular poly(ethylene glycol) ligands for biocompatible semiconductor and gold nanocrystals with extended pH and ionic stability. *Journal of Materials Chemistry 18*, 4949-4958.

(48) Mei, B. C., Susumu, K., Medintz, I. L., and Mattoussi, H. (2009) Polyethylene glycol-based bidentate ligands to enhance quantum dot and gold nanoparticle stability in biological media. *Nature Protocols 4*, 412-23.

(49) Susumu, K., Mei, B. C., and Mattoussi, H. (2009) Multifunctional ligands based on dihydrolipoic acid and polyethylene glycol to promote biocompatibility of quantum dots. *Nature Protocols 4*, 424-36.

(50) Pong, B. K., Trout, B. L., and Lee, J. Y. (2008) Modified ligand-exchange for efficient solubilization of CdSe/ZnS quantum dots in water: A procedure guided by computational studies. *Langmuir 24*, 5270-5276.

(51) Iyer, G., Pinaud, F., Tsay, J., and Weiss, S. (2007) Solubilization of quantum dots with a recombinant peptide from Escherichia coli. *Small 3*, 793-798.

(52) Smith, A. M., and Nie, S. (2008) Minimizing the hydrodynamic size of quantum dots with multifunctional multidentate polymer ligands. *Journal of the American Chemical Society 130*, 11278-+.

(53) Pellegrino, T., Manna, L., Kudera, S., Liedl, T., Koktysh, D., Rogach, A. L., Keller, S., Radler, J., Natile, G., and Parak, W. J. (2004) Hydrophobic nanocrystals coated with an amphiphilic polymer shell: A general route to water soluble nanocrystals. *Nano Letters 4*, 703-707.

(54) Wu, X. Y., Liu, H. J., Liu, J. Q., Haley, K. N., Treadway, J. A., Larson, J. P., Ge, N. F., Peale, F., and Bruchez, M. P. (2003) Immunofluorescent labeling of cancer marker Her2 and other cellular targets with semiconductor quantum dots. *Nature Biotechnology 21*, 41-46.

(55) Smith, A. M., Duan, H. W., Rhyner, M. N., Ruan, G., and Nie, S. M. (2006) A systematic examination of surface coatings on the optical and chemical properties of semiconductor quantum dots. *Physical Chemistry Chemical Physics 8*, 3895-3903.

(56) Dubertret, B., Skourides, P., Norris, D. J., Noireaux, V., Brivanlou, A. H., and Libchaber, A. (2002) In vivo imaging of quantum dots encapsulated in phospholipid micelles. *Science 298*, 1759-1762.

(57) Bentzen, E. L., Tomlinson, I. D., Mason, J., Gresch, P., Warnement, M. R., Wright, D., Sanders-Bush, E., Blakely, R., and Rosenthal, S. J. (2005) Surface modification to reduce nonspecific binding of quantum dots in live cell assays. *Bioconjugate Chemistry 16*, 1488-1494.

(58) Kim, J. H., Morikis, D., and Ozkan, M. (2004) Adaptation of inorganic quantum dots for stable molecular beacons. *Sensors and Actuators B-Chemical 102*, 315-319.

(59) Gill, R., Willner, I., Shweky, I., and Banin, U. (2005) Fluorescence resonance energy transfer in CdSe/ZnS-DNA conjugates: Probing hybridization and DNA cleavage. *Journal of Physical Chemistry B 109*, 23715-23719.

(60) Shi, L. F., De Paoli, V., Rosenzweig, N., and Rosenzweig, Z. (2006) Synthesis and application of quantum dots FRET-based protease sensors. *Journal of the American Chemical Society 128*, 10378-10379.

(61) Hermanson, G. T. (2008) *Bioconjugate Techniques*, 2nd Ed. ed., Academic Press, San Diego.

(62) Susumu, K., Uyeda, H. T., Medintz, I. L., Pons, T., Delehanty, J. B., and Mattoussi, H. (2007) Enhancing the stability and biological functionalities of quantum dots via compact multifunctional ligands. *Journal of the American Chemical Society 129*, 13987-96.

(63) Hua, X. F., Liu, T. C., Cao, Y. C., Liu, B., Wang, H. Q., Wang, J. H., Huang, Z. L., and Zhao, Y. D. (2006) Characterization of the coupling of quantum dots and immunoglobulin antibodies. *Analytical and Bioanalytical Chemistry 386*, 1665-1671.

(64) So, M. K., Xu, C. J., Loening, A. M., Gambhir, S. S., and Rao, J. H. (2006) Self-illuminating quantum dot conjugates for in vivo imaging. *Nature Biotechnology 24*, 339-343.

(65) Nakajima, N., and Ikada, Y. (1995) Mechanism of amide formation by carbodiimide for bioconjugation in aqueous-media. *Bioconjugate Chemistry 6*, 123-130.

(66) Ybo, J., Kambara, T., Gonda, K., and Higuchi, H. (2008) Intracellular imaging of targeted proteins labeled with quantum dots. *Experimental Cell Research 314*, 3563-3569.

(67) Diagaradjane, P., Orenstein-Cardona, J. M., Colon-Casasnovas, N. E., Deorukhkar, A., Shentu, S., Kuno, N., Schwartz, D. L., Gelovani, J. G., and Krishnan, S. (2008) Imaging epidermal growth factor receptor expression in vivo:

Pharmacokinetic and biodistribution characterization of a bioconjugated quantum dot nanoprobe. *Clinical Cancer Research 14*, 731-741.

(68) Green, N. M. (1990) Avidin and streptavidin. *Methods in Enzymology 184*, 51-67.

(69) Srisa-Art, M., Dyson, E. C., Demello, A. J., and Edel, J. B. (2008) Monitoring of real-time streptavidin-biotin binding kinetics using droplet microfluidics. *Analytical Chemistry 80*, 7063-7067.

(70) Pinaud, F., King, D., Moore, H. P., and Weiss, S. (2004) Bioactivation and cell targeting of semiconductor CdSe/ZnS nanocrystals with phytochelatin-related peptides. *Journal of the American Chemical Society 126*, 6115-23.

(71) Howarth, M., Takao, K., Hayashi, Y., and Ting, A. Y. (2005) Targeting quantum dots to surface proteins in living cells with biotin ligase. *Proceedings of the National Academy of Sciences U S A 102*, 7583-8.

(72) Garon, E. B., Marcu, L., Luong, Q., Tcherniantchouk, O., Crooks, G. M., and Koeffler, H. P. (2007) Quantum dot labeling and tracking of human leukemic, bone marrow and cord blood cells. *Leukemia Research 31*, 643-51.

(73) Howarth, M., Chinnapen, D. J. F., Gerrow, K., Dorrestein, P. C., Grandy, M. R., Kelleher, N. L., El-Husseini, A., and Ting, A. Y. (2006) A monovalent streptavidin with a single femtomolar biotin binding site. *Nature Methods 3*, 267-273.

(74) Howarth, M., Liu, W. H., Puthenveetil, S., Zheng, Y., Marshall, L. F., Schmidt, M. M., Wittrup, K. D., Bawendi, M. G., and Ting, A. Y. (2008) Monovalent, reduced-size quantum dots for imaging receptors on living cells. *Nature Methods 5*, 397-399.

(75) Whaley, S. R., English, D. S., Hu, E. L., Barbara, P. F., and Belcher, A. M. (2000) Selection of peptides with semiconductor binding specificity for directed nanocrystal assembly. *Nature 405*, 665-668.

(76) Peelle, B. R., Krauland, E. M., Wittrup, K. D., and Belcher, A. M. (2005) Design criteria for engineering inorganic material-specific peptides. *Langmuir 21*, 6929-6933.

(77) Peelle, B. R., Krauland, E. M., Wittrup, K. D., and Belcher, A. M. (2005) Probing the interface between biomolecules and inorganic materials using yeast surface display and genetic engineering. *Acta Biomaterialia 1*, 145-154.

(78) Sapsford, K. E., Pons, T., Medintz, I. L., Higashiya, S., Brunel, F. M., Dawson, P. E., and Mattoussi, H. (2007) Kinetics of metal-affinity driven self-assembly between proteins or peptides and CdSe-ZnS quantum dots. *Journal of Physical Chemistry C 111*, 11528-11538.

(79) Sulkowski, E. (1985) Purification of Proteins by Imac. *Trends in Biotechnology 3*, 1-7.

(80) Liu, W., Howarth, M., Greytak, A. B., Zheng, Y., Nocera, D. G., Ting, A. Y., and Bawendi, M. G. (2008) Compact biocompatible quantum dots functionalized for cellular imaging. *Journal of the American Chemical Society 130*, 1274-1284.

(81) Lu, H., Schops, O., Woggon, U., and Niemeyer, C. M. (2008) Self-assembled donor comprising quantum dots and fluorescent proteins for long-range fluorescence resonance energy transfer. *Journal of the American Chemical Society 130*, 4815-4827.

(82) Medintz, I. L., Berti, L., Pons, T., Grimes, A. F., English, D. S., Alessandrini, A., Facci, P., and Mattoussi, H. (2007) A reactive peptidic linker for self-assembling hybrid quantum dot-DNA bioconjugates. *Nano Letters 7*, 1741-8.

(83) Dennis, A. M., and Bao, G. (2008) Förster Resonance Energy Transfer (FRET) between a fluorescent protein and commercially available quantum dots: a comparison. *Proceedings of SPIE 6866*, 1-11.

(84) Boeneman, K., Mei, B. C., Dennis, A. M., Bao, G., Deschamps, J. R., Mattoussi, H., and Medintz, I. L. (2009) Sensing caspase 3 activity with quantum dot-fluorescent protein assemblies. *Journal of the American Chemical Society 131*, 3828-9.

(85) Yao, H., Zhang, Y., Xiao, F., Xia, Z., and Rao, J. (2007) Quantum dot/bioluminescence resonance energy transfer based highly sensitive detection of proteases. *Angewandte Chemie International Edition 46*, 4346-4349.

(86) Xia, Z. Y., Xing, Y., So, M. K., Koh, A. L., Sinclair, R., and Rao, J. H. (2008) Multiplex Detection of Protease Activity with Quantum Dot Nanosensors

Prepared by Intein-Mediated Specific Bioconjugation. *Analytical Chemistry 80*, 8649-8655.

(87) Tsien, R. Y. (1998) The green fluorescent protein. *Annual Review of Biochemistry 67*, 509-44.

(88) Prasher, D. C., Eckenrode, V. K., Ward, W. W., Prendergast, F. G., and Cormier, M. J. (1992) Primary Structure of the Aequorea-Victoria Green-Fluorescent Protein. *Gene 111*, 229-233.

(89) Matz, M. V., Fradkov, A. F., Labas, Y. A., Savitsky, A. P., Zaraisky, A. G., Markelov, M. L., and Lukyanov, S. A. (1999) Fluorescent proteins from nonbioluminescent Anthozoa species. *Nature Biotechnology 17*, 969-973.

(90) Baird, G. S., Zacharias, D. A., and Tsien, R. Y. (2000) Biochemistry, mutagenesis, and oligomerization of DsRed, a red fluorescent protein from coral. *Proceedings of the National Academy of Sciences of the United States of America 97*, 11984-11989.

(91) Shaner, N. C., Campbell, R. E., Steinbach, P. A., Giepmans, B. N., Palmer, A. E., and Tsien, R. Y. (2004) Improved monomeric red, orange and yellow fluorescent proteins derived from Discosoma sp. red fluorescent protein. *Nature Biotechnology 22*, 1567-72.

(92) Shaner, N. C., Lin, M. Z., McKeown, M. R., Steinbach, P. A., Hazelwood, K. L., Davidson, M. W., and Tsien, R. Y. (2008) Improving the photostability of bright monomeric orange and red fluorescent proteins. *Nature Methods 5*, 545-551.

(93) Ormo, M., Cubitt, A. B., Kallio, K., Gross, L. A., Tsien, R. Y., and Remington, S. J. (1996) Crystal structure of the Aequorea victoria green fluorescent protein. *Science 273*, 1392-1395.

(94) Patterson, G. H., Knobel, S. M., Sharif, W. D., Kain, S. R., and Piston, D. W. (1997) Use of the green fluorescent protein and its mutants in quantitative fluorescence microscopy. *Biophysical Journal 73*, 2782-2790.

(95) Niwa, H., Inouye, S., Hirano, T., Matsuno, T., Kojima, S., Kubota, M., Ohashi, M., and Tsuji, F. I. (1996) Chemical nature of the light emitter of the Aequorea green fluorescent protein. *Proceedings of the National Academy of Sciences of the United States of America 93*, 13617-13622.

(96) Yarbrough, D., Wachter, R. M., Kallio, K., Matz, M. V., and Remington, S. J. (2001) Refined crystal structure of DsRed, a red fluorescent protein from coral, at 2.0-angstrom resolution. *Proceedings of the National Academy of Sciences of the United States of America 98*, 462-467.

(97) Vrzheshch, P. V., Akovbian, N. A., Varfolomeyev, S. D., and Verkhusha, V. V. (2000) Denaturation and partial renaturation of a tightly tetramerized DsRed protein under mildly acidic conditions. *FEBS Letters 487*, 203-8.

(98) Lissandron, V., Terrin, A., Collini, M., D'Alfonso, L., Chirico, G., Pantano, S., and Zaccolo, M. (2005) Improvement of a FRET-based indicator for cAMP by linker design and stabilization of donor-acceptor interaction. *Journal of Molecular Biology 354*, 546-555.

(99) Zaccolo, M., Cesetti, T., Di Benedetto, G., Mongillo, M., Lissandron, V., Terrin, A., and Zamparo, I. (2005) Imaging the cAMP-dependent signal transduction pathway. *Biochemical Society Transactions 33*, 1323-1326.

(100) Luo, K. Q., Yu, V. C., Pu, Y. M., and Chang, D. C. (2003) Measuring dynamics of caspase-8 activation in a single living HeLa cell during TNF alpha-induced apoptosis. *Biochemical and Biophysical Research Communications 304*, 217-222.

(101) Campbell, R. E. (2009) Fluorescent-Protein-Based Biosensors: Modulation of Energy Transfer as a Design Principle. *Analytical Chemistry 81*, 5972-5979.

(102) Piston, D. W., and Kremers, G. J. (2007) Fluorescent protein FRET: the good, the bad and the ugly. *Trends in Biochemical Sciences 32*, 407-414.

(103) Deng, J., Davies, D. R., Wisedchaisri, G., Wu, M., Hol, W. G., and Mehlin, C. (2004) An improved protocol for rapid freezing of protein samples for long-term storage. *Acta Crystallographica Section D: Biological Crystallography 60*, 203-4.

(104) Hink, M. A., Visser, N. V., Borst, J. W., van Hoek, A., and Visser, A. J. W. G. (2003) Practical use of corrected fluorescence excitation and emission spectra of fluorescent proteins in Forster resonance energy transfer (FRET) studies. *Journal of Fluorescence 13*, J Fluoresc.

(105) Voet, D., and Voet, J. G. (2004) *Biochemistry*, 3rd ed., J. Wiley & Sons, New York.

(106) Guignet, E. G., Hovius, R., and Vogel, H. (2004) Reversible site-selective labeling of membrane proteins in live cells. *Nature Biotechnology 22*, 440-4.

(107) Pons, T., Medintz, I. L., Wang, X., English, D. S., and Mattoussi, H. (2006) Solution-phase single quantum dot fluorescence resonance energy transfer. *Journal of the American Chemical Society 128*, 15324-31.

(108) Lingerfelt, B. M., Mattoussi, H., Goldman, E. R., Mauro, J. M., and Anderson, G. P. (2003) Preparation of quantum dot-biotin conjugates and their use in immunochromatography assays. *Analytical Chemistry 75*, 4043-4049.

(109) Sreerama, N., Venyaminov, S. Y., and Woody, R. W. (1999) Estimation of the number of alpha-helical and beta-strand segments in proteins using circular dichroism spectroscopy. *Protein Science 8*, 370-80.

(110) Medintz, I. L., Pons, T., Delehanty, J. B., Susumu, K., Brunel, F. M., Dawson, P. E., and Mattoussi, H. (2008) Intracellular delivery of quantum dot-protein cargos mediated by cell penetrating peptides. *Bioconjugate Chemistry 19*, 1785-1795.

(111) Bianco-Peled, H., Dori, Y., Schneider, J., Sung, L. P., Satija, S., and Tirrell, M. (2001) Structural study of langmuir monolayers containing lipidated poly(ethylene glycol) and peptides. *Langmuir 17*, 6931-6937.

(112) Shaner, N. C., Steinbach, P. A., and Tsien, R. Y. (2005) A guide to choosing fluorescent proteins. *Nature Methods 2*, 905-9.

(113) Moreland, J. L., Gramada, A., Buzko, O. V., Zhang, Q., and Bourne, P. E. (2005) The Molecular Biology Toolkit (MBT): a modular platform for developing molecular visualization applications. *BMC Bioinformatics 6*, 21.

(114) Harlow, E., and Lane, D. (1988) *Antibodies: a laboratory manual*, Cold Spring Harbor Laboratory, Cold Spring Harbor, NY.

(115) Hoffmann, A., and Roeder, R. G. (1991) Purification of his-tagged proteins in non-denaturing conditions suggests a convenient method for protein interaction studies. *Nucleic Acids Research 19*, 6337-8.

(116) Srivastava, J., Barber, D. L., and Jacobson, M. P. (2007) Intracellular pH sensors: design principles and functional significance. *Physiology (Bethesda) 22*, 30-9.

(117) Haworth, R. S., and Fliegel, L. (1993) Intracellular pH in Schizosaccharomyces pombe--comparison with Saccharomyces cerevisiae. *Molecular and Cellular Biochemistry 124*, 131-40.

(118) Liu, Y. S., Sun, Y. H., Vernier, P. T., Liang, C. H., Chong, S. Y. C., and Gundersen, M. A. (2007) pH-sensitive photoluminescence of CdSe/ZnSe/ZnS quantum dots in human ovarian cancer cells. *Journal of Physical Chemistry C 111*, 2872-2878.

(119) Bradley, M., Alexander, L., Duncan, K., Chennaoui, M., Jones, A. C., and Sanchez-Martin, R. M. (2008) pH sensing in living cells using fluorescent microspheres. *Bioorganic & Medicinal Chemistry Letters 18*, 313-317.

(120) Coupland, P. G., Briddon, S. J., and Aylott, J. W. (2009) Using fluorescent pH-sensitive nanosensors to report their intracellular location after Tat-mediated delivery. *Integrative Biology 1*, 318-323.

(121) Gao, X. H., Chan, W. C. W., and Nie, S. M. (2002) Quantum-dot nanocrystals for ultrasensitive biological labeling and multicolor optical encoding. *Journal of Biomedical Optics 7*, 532-537.

(122) Weissleder, R. (2001) A clearer vision for in vivo imaging. *Nature Biotechnology 19*, 316-317.

(123) Ganesan, S., Ameer-Beg, S. M., Ng, T. T., Vojnovic, B., and Wouters, F. S. (2006) A dark yellow fluorescent protein (YFP)-based Resonance Energy-Accepting Chromoprotein (REACh) for Forster resonance energy transfer with GFP. *Proceedings of the National Academy of Sciences U S A 103*, 4089-94.

(124) Bulina, M. E., Chudakov, D. M., Mudrik, N. N., and Lukyanov, K. A. (2002) Interconversion of Anthozoa GFP-like fluorescent and non-fluorescent proteins by mutagenesis. *BioMedCentral Biochemistry 3*, 7.

(125) Levitt, J. A., Matthews, D. R., Ameer-Beg, S. M., and Suhling, K. (2009) Fluorescence lifetime and polarization-resolved imaging in cell biology. *Current Opinion in Biotechnology 20*, 28-36.

(126) Rahimi, Y., Goulding, A., Shrestha, S., Mirpuri, S., and Deo, S. K. (2008) Mechanism of copper induced fluorescence quenching of red fluorescent protein, DsRed. *Biochemical and Biophysical Research Communications 370*, 57-61.

(127) Wachter, R. M., and Remington, S. J. (1999) Sensitivity of the yellow variant of green fluorescent protein to halides and nitrate. *Current Biology 9*, R628-R629.

(128) Markova, O., Mukhtarov, M., Real, E., Jacob, Y., and Bregestovski, P. (2008) Genetically encoded chloride indicator with improved sensitivity. *Journal of Neuroscience Methods 170*, 67-76.

(129) Goh, Y. Y., Frecer, V., Bow, H., and Ding, J. L. (2002) Rational design of green fluorescent protein mutants as biosensor for bacterial endotoxin. *Protein Engineering 15*, 493-502.